

ÉCOLE DOCTORALE MATIÈRE CONDENSÉE ET INTERFACE
LABORATOIRE PHYSIQUE CHIMIE DU VIVANT, INSTITUT
CURIE, UMR 168

DOCTORAT
PHYSIQUE

Bussonnier Matthias

Actin Gels mechanics
Mechanique des gels d'actine

Thèse dirigée par Timo Betz et Cécile Sykes,
Soutenue le 16 Septembre 2014

Jury

Prof. Atef Anacios , Président
Dr. Laurent Blanchoin
Dr. Guillaume Rommet-Lemonne, Rapporteur
Prof. Dr. Dr. Karsten Kruse, Rapporteur

CONTENTS

1	Background	3
1.1	Introduction	3
1.2	Living Cells	4
1.3	Oocyte	4
1.3.1	Cell Organelles	5
1.3.2	The Cytoskeleton	7
1.4	The Role And Composition Of The Cytoskeleton	7
1.4.1	Composition of cell cytoskeleton	8
1.4.2	The actin cortex	17
1.4.3	Cell Motility	18
1.4.4	Organelle Positioning	23
1.5	In vitro reconstituted actin networks	23
1.5.1	Bead motility assay	24
1.5.2	Liposomes	26
1.6	Membrane Physics	27
1.7	Actin networks as viscoelastic material	28
1.7.1	Elastics Modulus	29
1.7.2	Poisson Ratio	31
1.7.3	Viscosity	31
1.7.4	Viscoelastic	31
1.8	Optical tweezer	33
1.8.1	Determination of force and displacement on bead	34
2	Materials and methods	37
2.1	Buffers	37
2.1.1	G Buffer	37
2.1.2	Polymerisation Buffer	37
2.1.3	X Buffer with BSA	38
2.1.4	ATP Mix Buffer	38
2.2	Protein preparation	38
2.2.1	pWA	38
2.2.2	Actin	38
2.2.3	profiline	38
2.2.4	Arp2/3	39
2.2.5	Capping protein	39

2.2.6	Myosin II	39
2.3	Lipids, reagent and proteins	39
2.4	doublets preparation	40
2.5	Bead Preparation	40
2.5.1	Actin-Bead Preparation	40
2.5.2	Probe Bead Preparation	40
2.6	Force indentation experiments	41
2.6.1	Preparation of sample	41
2.6.2	QPD positioning and calibration of microscope	41
2.6.3	Initial bead trapping	41
2.6.4	Indentations	42
2.7	Time Shared Optical Trap	44
2.8	Oocyte	46
2.8.1	Oocyte obtention	46
3	Mechanical properties of a far reaching actin cloud	47
3.1	Introduction	47
3.2	Actin-Bead System	48
3.3	Probe Bead System	51
3.4	Experimental description	52
3.4.1	Approach Phase	52
3.4.2	Relaxation Phase	52
3.4.3	Retraction part	54
3.4.4	Reconstitution of Force-distance-curve	54
3.4.5	Repetitive indent	55
3.4.6	Effect of approach speed	55
3.5	Experimental observations	58
3.5.1	Approach phase modeling	60
3.5.2	Variation of parameters with Capping Protein	62
3.5.3	Determination of Young's Modulus	65
3.5.4	Mechanical properties	67
3.5.5	Interpretation	69
3.6	Relaxation phase	72
3.6.1	Retraction Phase	76
3.7	Discussion	78
4	Liposomes Doublets	81
4.1	Introduction	81
4.2	Experimental description	81
4.2.1	Formation of liposomes doublets	81
4.2.2	Formation of actin cortex on doublets	82
4.2.3	Visualisation of the interface	82
4.2.4	Geometrical parameters	82
4.3	Experimental Observations	85
4.3.1	Effect of myosin injection	85
4.3.2	Relation between the angles and tension	86
4.3.3	Contact angle dispersion	87
4.3.4	Tension of actin-shell	87

4.4	3D observation	87
4.5	Discussion	92
4.5.1	Cortical tension is homogeneous for single doublet	92
4.5.2	Relative increase in cortical tension	92
4.5.3	Cortical tension increase in doublets and in cells	92
4.5.4	Different contributions for cortical tension	93
4.5.5	Conclusion	93
4.6	3D fitting	94
4.6.1	First step: Finding a single liposome	94
4.6.2	Fitting a doublet	98
4.6.3	Discussion	104
4.6.4	Conclusion	105
5	Activity in oocyte cytoplasm	107
5.1	Introduction	107
5.2	Oocytes	107
5.3	Measure of activity	107
5.4	Conclusion	111
6	Conclusion	113
Bibliography		115

PREAMBLE

During my PhD I decided to investigate the effect of actin network on the mechanical properties of cells. Indeed, mechanical properties of cell are a key parameter that has a crucial impact on cell and organism function. Being able to detect changes in mechanical properties, and understand the mechanism that govern these changes is an important step to be able to apprehend the behavior of cells, distinguish healthy cells and tissues from cancerous ones. Understanding the mechanism as the origin of cell motion and change in shape is also a decisive step in controlling cell behavior, and being able to prevent cancer cells invasion and division without impairing healthy cells.

During the last three years, I decided to focus on biomimetic system and establish characteristic of actin network. Actin is a highly conserved component across the living domain, and it plays a major role in cells mechanics. By interacting with a number of other component of the cell, actin is able to form a various number of networks. It is on such networks, and in controlled condition that I decided to focus my research.

Along this dissertation we will mainly focus on three systems.

On the first one, we reconstitute an already observed actin network — the actin cortex — on a biomimetic system, then show that from this network emanate a second sparse actin network previously unseen, and characterize its mechanical properties. We developed the idea that the effect of this second network cannot be neglected in cell and investigate a few of the phenomenon it can be involved in.

As the effect of such a sparse actin has not been demonstrated we decided to investigate the effect of another sparse actin network on a living cell. In collaboration with College de France, we studied the mechanical properties inside mouse oocyte. We see in this system that actin related proteins have hi-impact on the structure and the mechanics both of the cell and the actin network in it.

Characterizing the dynamics of a network in a living cell by controlling the condition is complex. To characterize the dynamics and properties of actin networks on the effect of linkage between the actin-cortex and the cell membrane, we developed a new biomimetic system. This system of “doublets” allow to measure the variation of tensions generated by an acto-myosin cortex with time. The doublet system is composed by a doublet of two liposomes covered by an actin network. Imaging with Spinning disk microscopy, we are able to reconstruct changes in the acto-myosin network and deduce the changes in its properties from the change in geometry.

CHAPTER

ONE

BACKGROUND

1.1 Introduction

Cells are the basic component of living organisms. Understanding their individual behavior and the way they function is a key step to understand how they interact with their environment. One of the key components within most cells is actin, a protein which is highly conserved across the species and plays an important role for the cell mechanics, from cell migration to cell differentiation and division. It plays also a non negligible role in mechanical properties of the cell and its interactions with the environment. Under the cell membrane lies a thin actin layer which controls mechanical properties of the cell: the actin cortex. The mechanical behavior of this actin cortex is itself driven by the dynamics and interactions of the actin network it is made off. Understanding this actin network is hence a key to learn how the actin cortex behaves, leading to a better understanding of cells and tissues.

The properties of an actin network highly depend on its structure. The structure itself depends on many parameters that influenced how the network is formed. The network structure and formation is influence by physical and chemical conditions. The spatial and temporal variation of these parameters like stress and ion-concentration can determine the fate of a network. Hence it is though important to study these networks and their dynamics in order to grasp the changing structure of the cell.

Cells are complex systems that adapt their shape, mechanical properties and biochemical conditions permanently. The spatial repartition of theses properties is also variable as the cell regulates the concentration of proteins all across its cytoplasm. To well study the effect of each component independently, it is crucial to study actin networks in a controlled environment.

Biomimetic systems allow to respond to most of these concerns, they provide a controlled environment that mimic *in-vivo* phenomenon. Biochemical conditions can be well controlled, both in space and time allowing to precisely fine tune experimental conditions. Biomimetic system are also particularly adapted to be combined with optical traps which allow us to study local mechanical properties of actin networks with a high time resolution. The combination of both allows us to get insight into the variation of theses mechanical properties as a function of time and space with a high precision.

During my PhD, I have focused on the study of the mechanics of branched actin networks polymerizing on optically trapped polystyrene beads. Such networks where studied before [Kawska, Carvalho, Manzi, et al. 2012] but have been suspected to be highly inhomogeneous. Optical traps allowed to probe mechanics of parts of the network which had been unaccessible before. I further studied actin networks on other biomimetic systems constituted of liposomes, in order to better understand the effect of actin cortex polymerisation on membrane tension and characterize network dynamic over time. Finally, I participated in a collaboration in order to understand the implication such actin network in living mouse oocytes.

1.2 Living Cells

Cells are the basic building block of life, all living things are composed of cells, from unicellular to multicellular organisms like us. Unicellular organism must accomplish all the functions relative to cell life. At the other end, multicellular organism cells differentiate in order to accomplish specialised tasks often by regrouping into organs. Despite sharing the same genetic material, each cell to accomplish a different task require different mechanical properties. The variation of elasticity and other mechanical properties of cells derive from the structure they are composed of.

Cells are hence able to adapt to their environment and develop function and behavior that will depend on time. A small change of timing and/or biochemical conditions can highly injure the development of an organism : modification of the actin network at the right time of the cell cycle prevents symmetric division [Lenart, Bacher, Daigle, et al. 2005], [Vasilev, Chun, Gragnaniello, et al. 2012]. Mechanical properties of the substrate can govern the differentiation of cells : Soft substrate will favor brain-tissue cell, where stiff substrates increase the appearance of muscle cells [Engler, Sen, Sweeney, Discher, 2006].

Nonetheless, even with all these different behavior and phenotypes, cells have a common structure. The exterior of the cell is separated from the inside by a plasma membrane. The interior of the cell is filled with the cytoplasm which contain diverse structures known as organelles, genetic material, and a large number of proteins that the cell uses to accomplish its functions. To communicate with the outside, cells have a series of mechanism that allow signals and cargo to go through the membrane. This communication can be chemical, but mechanics is also known to participate in the process. To sense their mechanical environment, cells use adhesion complexes to attach to the substrate, and integrins as trans-membrane protein to transfer the force to the cell cytoskeleton situated inside the cell. Chemical signals can either cross the membrane through trans-membrane proteins, endocytosis and exocytosis are ways for the cell to import and export proteins and chemicals through its membrane.

1.3 Oocyte

A particular type of cell I was interested in during my PhD is mouse oocyte. Oocyte are female germinal cells in the process of gametogenesis. Unlike somatic cells that undergoes symmetric division via mitosis which will lead to two identical cells sharing the same genetic material, oocytes undergo a different process called meiosis. Meiosis in oocytes is a highly asymmetric process necessary for the specificity of the oocytes which are large haploid cells, containing at the end of the meiosis only one chromosome of each pair that constitutes the genetic material of a mouse. The second chromosome of each pair will be provided by the fertilisation of the oocyte by the male.

The exact process of formation of oocyte can vary among species, we will describe the main mechanisms.

The complete process of egg maturation start with Primordial germ cell which will undergo mitosis to replicate until it enter the first meiosis (Meiosis I) at which state it is now called Primary oocyte and is still diploid, that is to say still contains the two chromosomes of each pairs.

The primary oocyte will start maturation and growth, then undergo a first asymmetric division just after prophase I. This first division is asymmetric both in the genetic material separation and in the unequal size of the formed daughter cell. Indeed, the primary oocyte will divide into a secondary oocyte and a polar body. Both secondary oocyte and polar body are haploid and contain only half of the genetic material of

the primary oocyte. The secondary oocyte can go through Meiosis II in which it incur a second asymmetric division expulsion a second polar body. The polar bodies will eventually degenerate ([Fig 1.1](#)).

During meiosis, the process of cell division also differ from mitosis. Instead of separating into two identically sized cell through the formation of a cytokinetic ring, the primary oocyte will become the secondary oocyte by expulsion a polar body. The formation expulsion of the polar body require precise positioning of the cells organelles. During prophase I the nucleus of oocyte is carefully centered, undergo nuclear breakdown and formation of spindle. The first meiotic spindle will migrate toward the oocyte cortex along its major axis. Once at the cortex half of the genetic material of the spindle will be exposed through the membrane forming the first polar body of much smaller size than second oocyte.

Mouse oocyte are good model system for study of mechanical properties inside cells, indeed, they form big spherical cells with a diameter of around 80 μm which allows study of mechanical properties of cell at different location in the cytoplasm.

In the third part of my PhD I participated in a collaboration with Marie-Hélène Verhlauc and Maria Almonacid at Collège de France who are interested of the effect of actin dynamics in oocyte cytoplasm during the different part of the oocyte gametogenesis.

1.3.1 Cell Organelles

Inside the cytoplasm, cells have a number of structures with different and specialised functions which are called organelles. The position and state of organelles is of great importance for the cell to achieve its functions. Probably the most known organelle is the cell nucleus of eukaryotic cells that contains the genetic material. Attached to the nucleus is the endoplasmic reticulum which is the organelle responsible for translating RNA coming from the nucleus to functional proteins that will be delivered across the cell after maturation in vesicles. These vesicles are transported across the cell both by dyneins and kinesins — molecular motors — that walk along microtubules originating from the centriole part of the centrosome but also by myosin along actin filaments. All of those processes consume energy in the form of ATP, generated within the mitochondria spread across the cytoplasm. A schematic of the cell with some organelles can be seen on [figure 1.2](#).

The positioning of organelles is crucial for the life of an organism. During the meiotic division of cell, for example, it has been seen that the positioning of the nucleus at the center of the cell in mouse oocytes happens before its migration closer to the cortex to expel the first polar body. Failure to do so result in an incorrect amount of DNA in germinal cell that can lead to infertility.

It is already known that microtubules play a key role in organelle positioning. Microtubules emanating from centrosome position at the two ends of the cell during its division is used to fetch the correct chromosomes. Each chromosome is pulled towards the centrosome which leads to each daughter cell having the same amount of DNA.

Actin plays also an determinant role in organelle positioning process, like in drosophila oocyte maturation where it positions the nurses cell away from the dumping canal [Huelsmann, Ylanne, Brown, 2013]. In a later chapter ([Organelle Positioning](#)) we will develop a few keys points where actin is indispensable in organelle positioning and how this relate to the biomimetic actin networks we reconstitute.

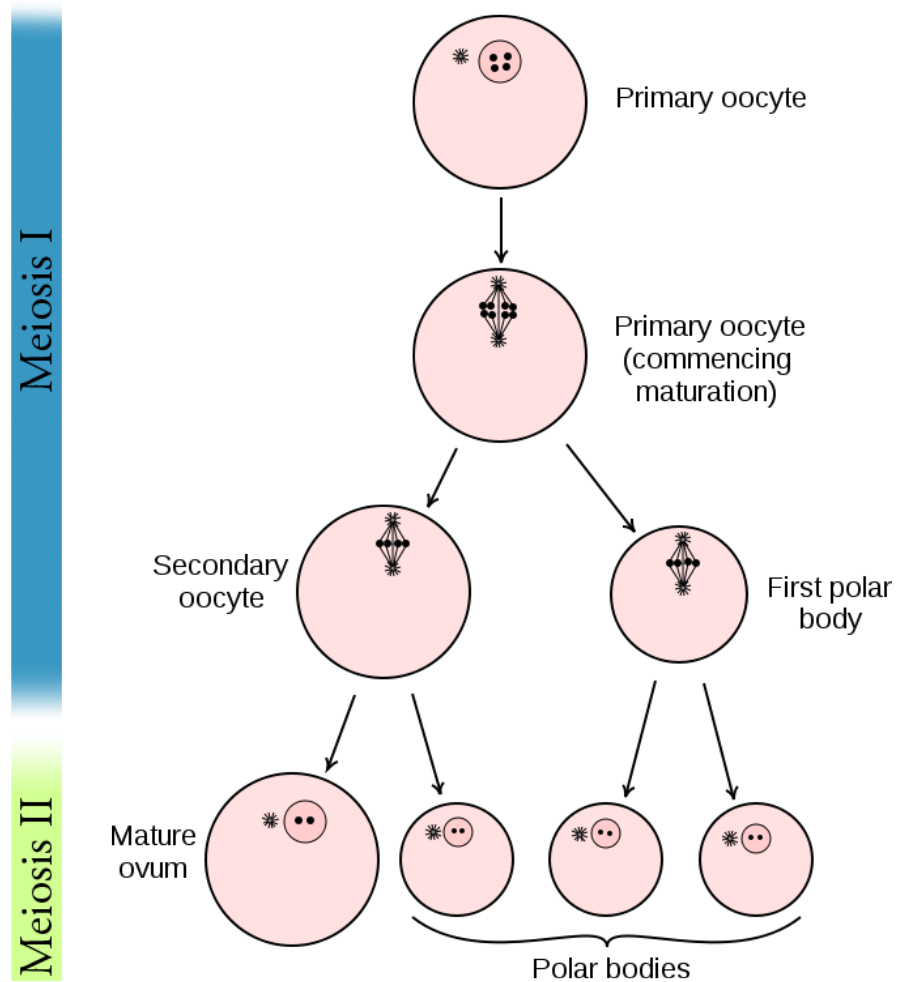


Figure 1.1: Asymmetric division of oocyte into polar bodies. The Primary oocyte asymmetrically divide into a secondary oocyte and a smaller polar body each containing half the DNA of the mother cell. The secondary oocyte will divide asymmetrically a second time to become the mature ovum while expulsion a polar body. This asymmetric division process allow the formation of a large haploid cell. Adapted from Wikipedia – Gray's Anatomy – and [Alberts, Johnson, Lewis, et al. 2008].

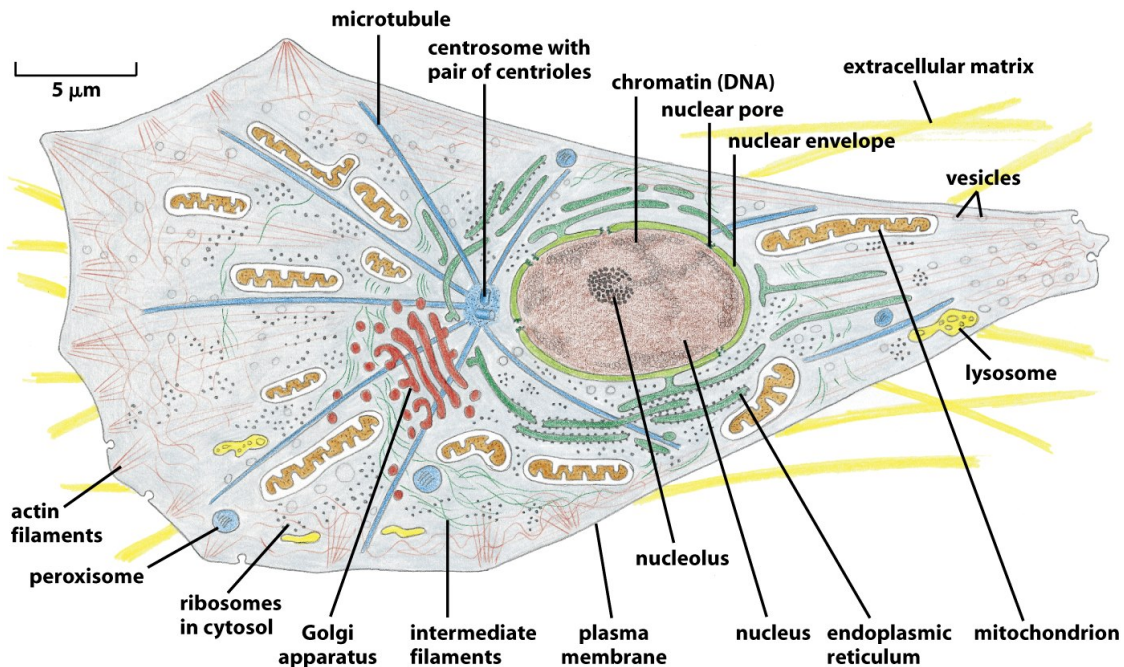


Figure 1-30 Molecular Biology of the Cell 5/e (© Garland Science 2008)

Figure 1.2: Schematic of an eukaryotic cell, adapted from [Alberts, Johnson, Lewis, et al. 2008]. One can see the many component that constitute majority of cells. Cell shape and size can highly vary, from quasi spherical with a typical size of ten micrometers to elongated neurones that can be tens of centimeters long.

1.3.2 The Cytoskeleton

The cytoskeleton, literally skeleton of the cell, is the structure which gives it shape to a cell. As for other multicellular animals that possesses skeleton, its shape is often a hint on how a organism moves. As feet, fins and wings are characteristics that will tell you whether a animal prefer land, sea or air, the cytoskeleton will tell you many things about a cell.

Unlike the (exo)-skeleton of animals which is rigid and static, the cytoskeleton of cell is a highly dynamic structure that keep remodeling itself on a short time scale compared to the speed at which a cell moves. Thanks to this dynamics cytoskeleton can achieve its functions. As vertebrates skeletons are necessary to transmit force from one part of the body to another, the cytoskeleton is responsible to not only transmit the forces the cell is exerting, but also to generate these forces. The cytoskeleton connects a cell to its environment, both mechanically and biochemically.

We will consecrate a longer part of this work to describe the cytoskeleton.

1.4 The Role And Composition Of The Cytoskeleton

We have already introduced the cell cytoskeleton in a previous part, and we will describe its components and functionality more in detail here. The cytoskeleton has three main functions, it connects the cell both physically and biochemically to the external environment, generate and coordinate the forces that give the cell its shape and allows it to move. It is also responsible for organising spatially the cell content [Fletcher,

Mullins, 2010]. The cytoskeleton is also in particular sensitive to spatial and temporal information that can affect cell fate and the assembly of the cytoskeletal structure. This can be seen for example with the bud scar of budding yeast that persists after division.

1.4.1 Composition of cell cytoskeleton

The cytoskeleton is mainly composed of three types of filaments. Microtubules, intermediate filament and actin filament, also known as microfilaments.

Microtubules are the widest structure with a diameter of 20nm (Fig 1.3) and the stiffest of the three kinds of filaments with a *persistence length* in the order of millimeters, much longer than the size of the usual cell. Microtubules are extensively studied [Valiron, Caudron, Job, 2001]. Microtubules are formed by the polymerisation of a heterodimer of tubulin that leads to the formation of polar (oriented) filaments that can be walked on by molecular motors. These molecular motors can be decomposed in two families – kinesins and dyneins – depending on the end toward which the motor preferably walk. Microtubules are mostly known for their action during mitosis where they will form majority of the mitotic spindle that drive the segregation of the chromosomes in two groups, each group ending in one of the daughter cells.

Microtubules have the characteristic of being highly dynamic by alternating between two state of rapid growth and a rapid shrinkage. The transition from microtubule growth to shrinkage is called a *catastrophe*, the transition from shrinkage to growth is called a *rescue*.

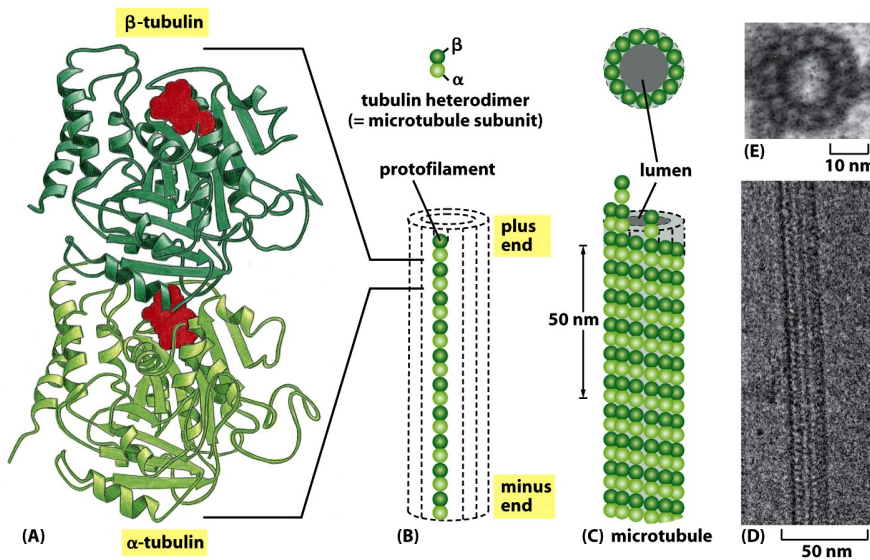


Figure 16-11 Molecular Biology of the Cell 5/e (© Garland Science 2008)

Figure 1.3: Structure of an heterodimer of tubulin and assembly into a microtubule. Electron microscopy of a single microtubule filament. From *Molecular Biology of the Cell*. A) Structure of heterodimer of tubulin B) Heterodimers can assemble forming polar filaments. C) Filaments can assemble into microtubules. D,E) Electron microscopy image of microtubules.

Intermediate filaments are of medium diameter in the order of around 10nm, in between actin and microtubules filaments, hence their name. Unlike microtubules and actin filament, intermediate filaments are composed by several sub-families of proteins and are non-polar.

Intermediate filament have an important role in the mechanical properties of the cell due to the fact that they are particularly resistant to stretching.

Unlike actin and microtubules, they are thought to be passive, with mechanical properties mainly deriving from how multiple filaments are linked together laterally.

Actin, is the third component of the cytoskeleton, the one on which we will focus most of our effort. Actin monomers, also called *G-Actin* for globular actin can polymerise. By Polymerizing actin monomers forms into actin filaments (*F-actin*), the thinnest of the three kind that form the cytoskeleton. Actin is produced in the cell as a globular protein of ~40 kDa that once associated with ATP or ADP polymerises into helicoidal filament with a diameter between 7 and 9nm. The formed actin filament are polar, where both extremity are respectively called the plus (+) or barbed end, and the minus (-) or pointed end. The polarity of the actin filament is of importance as this give rise to a preferred direction for most processes that can happen on the filament.

The actin protein is highly conserved across species, and is known to directly interact with hundreds of proteins [DosRemedios, Chhabra, Kekic, et al. 2003].

Single undecorated filaments will behave as semi-flexible polymers at the scale of the cell with a persistence length in the order of 10 μm [Isambert, Venier, Maggs, et al. 1995]. When they assemble into different structure and network, or associate with other proteins and molecule the resulting mechanical and dynamic properties can be highly changed.

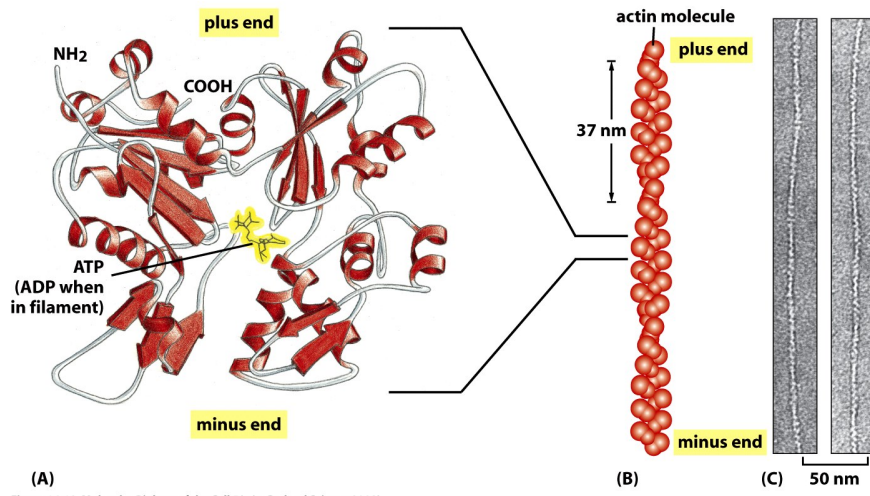


Figure 1.4: A) Structure of a single monomer of actin, and electron microscopy snapshot. — from [Alberts, Johnson, Lewis, et al. 2008].

Dynamics of actin polymerisation

The assembly mechanisms that allow to go from single monomers of actin (also refer to as G-actin for globular actin) to actin filament (also refer as F-actin) need to be well understood to explain the different networks structures created by actin filaments in the presence of other proteins.

The polymerisation of ATP/ADP actin monomer to form an actin filaments need to go through the step of forming an actin proto-filament which is constituted of at least 3 actin monomers. This will most of the time

Actin Gels dynamics,

be the kinetically limiting step. Once proto-filaments are present in solution, single monomers can be freely added or removed on both ends of the filament. The process of forming these proto-filament is called the nucleation and is the rate limiting factor to form actin filament from actin monomers. To circumvent this limitation experimentally one can use actin filament seeds, or actin nucleators to direct the polymerisation on the cell.

We need to distinguish between the dynamics of polymerisation and depolymerisation on both ends of the filament. Indeed it has been show that the association and dissociation rate are differing between the pointed (-) and barbed (+) end. The barbed end has a higher dynamics than its pointed counterpart which is the reason for its (+) name. The dynamics of polymerisation is higher both in the case of ATP and ADP, though the rate constant of association and dissociation differ for both kind of filaments.

Elongation rate constants



Figure 1.5: Association and dissociation rate of both ATP and ADP actin on pointed and barbed end as measured in [Pollard, Borisy, 2003]. The difference of equilibrium constant between the barbed end (bottom) and pointed end (top) in the presence of ATP allow filament treadmilling.

The equations that drive the polymerisation can be written as follow

$$\frac{dC_{barbed}}{dt} = k_{+,barbed} \cdot [G^- \text{Actin}] - k_{-,barbed}$$

$$\frac{dC_{pointed}}{dt} = k_{+,pointed} \cdot [G^- \text{Actin}] - k_{-,pointed}$$

Where *barbed* and *pointed* designate respectively the barbed and pointed end, and k_+ and k_- are the polymerisation and de-polymerisation rate. The concentration in barbed and pointed end denoted by $C_{barbed/pointed}$. By assuming that the number of pointed ends is equal to the number of barbed ends, one can derive the steady state which give rise to the critical monomer concentration below which an actin filament cannot grow: $[G^- \text{Actin}]_c$.

The rate constants of elongation of actin have been determined and depend of whether the monomer is bound to ADP or ATP [Pollard, 1986]. We should consider the fact that the ATP bound to actin will hydrolyse to ADP-P_i before releasing the inorganic phosphate. The hydrolysis and phosphate release rates also depend on whether the monomer is part of a filament or in solution. The hydrolysis of ATP-bound actin into ADP bound actin in the filament, leads to an imbalance of actin (de)-polymerisation on both ends. The actin filaments preferably grow from the barbed end and shrink preferably from the pointed end.

This will lead to a phenomenon known as treadmilling where a single actin monomer bound to an ATP molecule, will be incorporated at the + end of the filament and progressively migrate toward the - end, eventually hydrolysing it ATP into ADP before detaching from the filament on the pointed end. During this process the filament will grow / shrink until it reaches the stationary state where its length would stay constant but the treadmilling continues.

Treadmilling requires an imbalance in the global rate constant on the barbed and pointed end and an energy source, in the case of actin this is provided by the hydrolysis of ATP into ADP+Pi before releasing the inorganic phosphate, without which treadmilling would not occur.

Practically, this can be approximated by having only ATP monomers at the barbed end of actin filaments while the pointed end is typically constituted only of ADP monomers, thus the critical concentration is lower at the pointed end compared to the barbed end. The growth speed of the filament depends on both ends depends on the monomer concentration in solution. It is between the critical concentration of both ends, there exists a concentration at which the polymerisation on (+) exactly compensate the depolymerisation on (-).

Actin network can be controlled by a host of actin binding proteins

Despite the already complex process of actin polymerisation and the numbers of parameter that we have already introduced, the formation of an actin network is an even more complex process that involves many other components. Especially, actin monomers and filaments can interact with a high number of proteins that will affect the previously introduced dynamics. We will present some categories of such proteins in the following.

Formins

Formins are polymerase proteins that will increase the polymerisation rate of actin filaments by dimerizing and binding to the barbed end. It has the particularity of being processive, meaning that it will stay bound to the barbed end while catalysing the addition of new monomers. The processivity of formins also permits the control of the localization of actin polymerisation where formin proteins are present, like the tip of filopodia [Faix, Rottner, 2006] [Bornschlogl, 2013]. *Formins* posses domains rich in proline, capable of binding to profilin (*FH1*) which allows formin to elongate F-Actin using actin monomers bounds to profilin [Pruyne, Evangelista, Yang, et al. 2002] [Pring, Evangelista, Boone, et al. 2003].

Actin depolymerization and severing

Like polymerisation that can be enhanced by formins, depolymerization can also be speed up. ADF/Cofilin is a protein which is able to increase the rate of actin depolymerization. ADF/Cofilin can do so by increasing

Actin Gels dynamics,

the off rate at the pointed end [Carlier, Laurent, Santolini, et al. 1997], or by actively severing the filament in different points, thus disassembling the formed network [McCullough, Grintsevich, Chen, et al. 2011].

It should be noted that depolymerization can not only be enhanced at the pointed end, indeed forming that accelerates the polymerisation is also able to speed-up the detachment of actin monomers from the barbed end.

Capping Protein

To regulate polymerisation, cells also have the possibility to reduce or stop the polymerisation. To achieve this, some proteins will bind to the growing end of actin filaments and prevent the addition of new monomers. *Capping Protein* (CP) being one particular example that will specifically bind to the barbed end of a growing filament and prevent it from growing. Capping proteins are necessary to prevent polymerisation of actin in undesired areas and are essential for the structure and mechanical properties of actin gel [Kawska, Carvalho, Manzi, et al. 2012]. *Gelsoline* is another example of capping protein, that unlike CP can only attach to the barbed end of an actin filament after severing it. Gelsoline is hence both a severing and a capping protein.

Cross-linkers

We have seen that some proteins were able to attach to actin filaments. When such a protein is able to attach to many filaments at once, it can act as an attachment point between the two filaments, preventing them from moving with respect to each other. Such proteins are referred to as cross-linkers.

The amount of freedom in movement between the two filaments is dependent on the cross-linker used. For example, α -actinin will allow rotation of the two filaments at their anchoring point whereas cross-linker like fascin will prefer a parallel conformation of the filaments and favor the formation of actin bundles.

Cross-linkers are essential for the formation of elastic networks as they allow forces to be carried from one actin filament to the other. The quantity of cross-links in a network will often be a key parameter in the elastic properties of a network. The distance between the link points in the network (both cross-links and entanglement points) will give the typical network mesh-size which is used to calculate the viscoelastic response of networks : [Morse, 1998a].

Stabilizing actin filaments

As actin networks are dynamic constructs that are changing shape and properties with time, it is convenient to be able to stabilize those networks. Tropomyosins are proteins capable of binding on the side of actin filaments to stabilize them.

The use of phalloidin, a toxin extracted from fungus (*Amanita phalloides*), binds between F-actin subunits on the filament, and hence prevents it from de-polymerising. Though, it is known that stabilizing actin filaments with phalloidin will increase their stiffness as measured by the persistence length which can change the mechanical properties of the formed actin network.

Profilin

Profilin is a protein that will bind to the barbed end of single monomers of actin in solution. By doing so it will first prevent the association of monomers into dimers and trimmers, thus preventing the nucleation of actin filament. It thus allows a better control of localisation of actin filament both *in vivo* and *in vitro* in the presence of actin seeds of actin nucleator.

Profilin was for a long time been believed to be only a sequestering protein that inhibit polymerisation [Yarmola, Bubb, 2009], though it has a more complex behavior, and if it prevent polymerisation of actin filaments by the pointed end, it can facilitate polymerisation. One of the cause of increase in polymerisation speed by profilin is the fact it binds preferably to ADP-Actin and increase the exchange rate of ADP into ATP.

Branching Agent

A type of network found of the leading edge of cells lamellipodia is dendritic network. It is characterise by tree-like structure of actin filament in which thanks the Arp2/3 complex branching agent a mother actin filament will form a daughter filament on its side.

We have seen previously that crosslinker are proteins capable on linking two or more actin filament together by binding on their side. Another mechanism involving binding on the side on actin filament is responsible for a closely related network, the branching mechanism.

The Arp2/3 complex is composed of seven subunits, two of which are highly similar to actin, from Arp2 and Arp3 family for Actin Related Proteins, giving the complex its name. Arp2/3 will bind on the side of a pre-existing actin filament, hence initiating the growth of a daughter filament with an angle of 70° to the mother filament. The newly created daughter filament pointed end is terminated by the Arp2/3 complex that will stay attached to the mother filament, thus increasing the number of available barbed end, without changing the number of available pointed end. Cf Nature Review by Erin D. Goley and Matthew D. Welch [Goley, Welch, 2006] for a longer review about the Arp2/3 complex.

In cells, the Arp2/3 complex is needed to be activated by a Nucleation Promoting Factor (NPF). Among them is the WASp protein (Wiskott-Aldrich Syndrome protein) and its neural homologue N-WASP which are from the same family as SCAR/WAVE [Machesky, Mullins, Higgs, et al. 1999]. All these activators of Arp2/3 have in common a WCA motif. The wild type protein need to be activated in order to activate Arp2/3. The activation is done by a change in conformation that expose the active region and provide the first actin monomer necessary for the nucleation of the daughter filaments ([Figure 1.6](#)). To circumvent the activation process of these proteins, we use a reconstructed version of the protein that cut all region before the poly-proline. This confer to pVCA the ability to be permanently active. This region can also be replaced by streptavidin in order to selectively bind pVCA to selected regions. Characterisation and more detailed description of pVCA can be found in [Noguera, 2012].

Unlike Cells that are able to control the localisation of actin nucleation process thanks to activation of WASp and its homologue, the *in vitro* control of localisation of actin polymerisation is directly done by the localisation of pVCA.

The network formed by Arp2/3 is called a dendritic network, and is in particular found at the leading edge of the cell in the lamellipodia. It is such a network that is present in the bead system we will study hereafter.

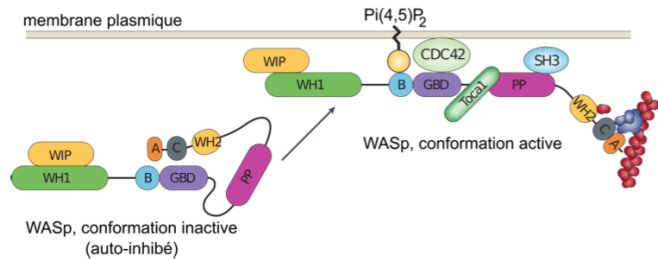


Figure 1.6: Organisation of Wasp domains. A change in conformation make the protein active, which allow the activation of the Arp2/3 complex and the nucleation of a daughter filament. Adapted from [Goley, Welch, 2006]

As for crosslinkers dendritic networks are able to carry force across single actin filament by the intermediary of Arp2/3. Two dendritic network of Arp2/3 can also entangle and allow forces to be carried across them [Kawska, Carvalho, Manzi, et al. 2012].

Molecular Motor

A particular kind of protein that can bind to cytoskeleton filaments are molecular motors. Molecular motors are proteins that will consume energy in the form of ATP, hydrolyse it to change conformation and produce forces.

The motors that move along actin filaments are part of the myosin superfamily, they are both responsible for the transport of cargo along filaments, cell motility, division, and muscle contraction. They acquire their name from their discovery in 1864 by Willy Kühne who extracted the first myosin II extract from muscle cell [Hartman, Spudich, 2012].

The myosin super family is divided into subfamilies number with roman literals. As of today we count more than 30 family of myosin [Berridge, 2012]. Muscle myosin is part of the myosin II family and is often referred to as conventional myosin for historical reason as being the first discovered. Non-muscle myosin are also referred to as unconventional myosin.

Myosin motors seem to be shared among all the living domain, hinting for an early emerging of myosin in the evolution. All the myosin motors move on actin filaments toward the barbed end, with the exception of myosin VI which moves towards the pointed end [Buss, KendrickJones, 2008].

Different subfamily of myosin are used for different function in cells. Even in subfamilies each type of myosin can have specific functions. For example, conventional myosin found in muscle cell are use for large scale cell contraction. In contrast, myosin V is known to transport cargo and is found to be responsible for actin network dynamics and vesicle positioning [Holubcova, Howard, Schuh, 2013].

Myosin II As stated before, the myosin II family both encompass conventional myosin ans well as Non-muscle myosin II (NMII). Both have a similar structure (Fig 1.8).

All myosin II are dimers constituted of two heavy chains and the light chains. The heavy chain are held together by a coil-coiled alpha helix referred to as the tail. On the other side of the protein sequence is a globular head, which is responsible for ATP hydrolysis and is able to convert the energy from the hydrolysis

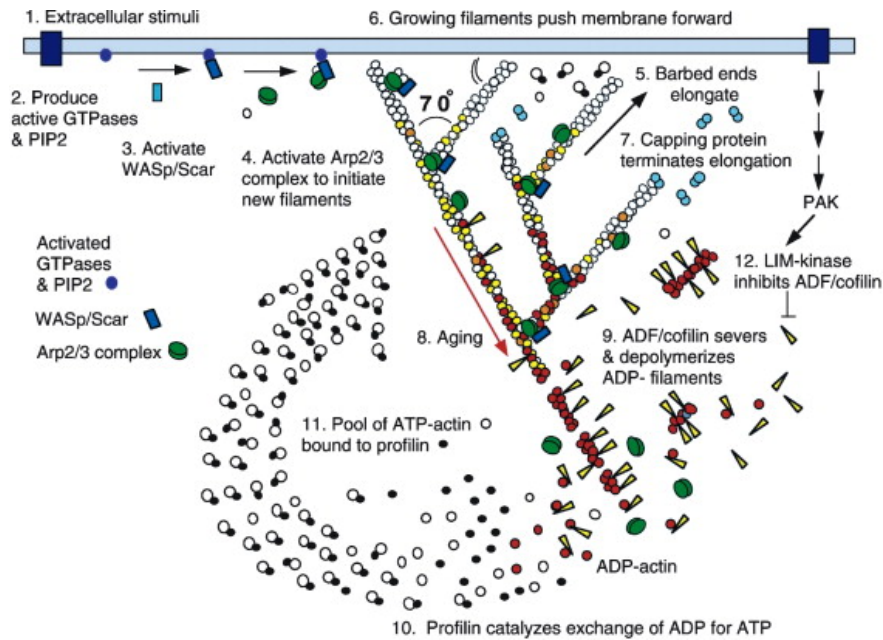


Figure 1.7: Adapted from [Pollard, Blanchard, Mullins, 2000]. Schematic recapitulating the formation of a dendritic network at the leading edge of a cell where several of the function of proteins can be seen. An actin nucleation promoting factor (Active WASp, blue rectangle at the membrane) will activate Arp2/3 (green blob) which will act both as nucleation factor and a branching agent. From an activated Arp2/3 will grow an actin filament pointing toward the membrane. Newly growing barbed ends, rich in ATP-actin (white circle) can eventually be capped by capping proteins (light-blue pairs of circles) which will terminate their growth. Aging monomers in actin filament will slowly hydrolyse their ATP (yellow and red circle), eventually releasing the inorganic phosphate before detaching from the pointed end. Depolymerisation is helped by severing protein (sharp triangle) and Actin Depolymerisation Factor (ADF). ADP-actin monomer will bind to profilin (Black dots) increasing the turnover rate to ATP-actin which will be reused by the leading edge of the cell.

into mechanical force. It is also the part that will bind to the actin filament. In between the tail and head is the neck domain that act as a lever to transmit the force generated by the head to the tail. The length of the neck influence the length of the movement done by the cargo at each step of the myosin as well as the size of the step the myosin can effect. The two light chains are situated in the neck region and are responsible for the myosin activity regulation.

Myosin II dimers can align and assemble by the tail region, forming myosin minifilaments. These minifilaments are bipolar, having numbers of myosin head with the same orientation at each extremities.

In the myosin II family, conventional myosin and NMII differentiate by the size of the minifilaments they form. Muscle myosin will form minifilaments aggregating around 200 dimers, where NMII minifilaments will be composed only of 10 to 20 minifilaments. The other characteristic of unconventional myosin with muscle myosin is the mode of activation. Conventional myosin activation will be regulated by the amount of Ca^{2+} available, whereas its counterpart is activated by the phosphorylation of the Myosin Light Chain (MLC).

Another parameter that discriminate muscle form cell myosin is their duty ratio. The duty ratio is define as the ratio of the time the myosin stays attached to its actin filament over the typical time of a contraction cycle. By noting τ_{on} and τ_{off} the time the myosin head spent attached/detached from the filament, the duty-ratio or duty-cycle can be noted :

$$r = \frac{\tau_{on}}{\tau_{on} + \tau_{off}}$$

We will see in the following that the duty-ratio might have an important effect on the processivity of the myosin.

It should be noted that as minifilaments can attach on actin filaments on both ends, they can also act as a bridge that holds two points close to each other, though having the properties of crosslinkers.

Myosin V Myosin V is an unconventional myosin. Unlike myosin II it does not aggregate into minifilaments. Though, myosin V has a similar structure to myosin II but with a longer neck, this confer to myosin two the ability to realize longer step on actin filament. Indeed, myosin V step is of 36nm, a length close to the repeat length of actin filament this concede to myosin V motors the ability to walk along actin filament without having to rotate around it with the helix they form. At the end the tail domain myosin V posses another globular domain capable of binding to its cargo, and the variability of this region is what mostly define the difference between the different type of myosin V.

Myosin V also has a high duty-ratio, this leads to dimers having almost always one of the two head of the myosin to be bound to actin. It grants to the myosin V the ability to walk in a processive manner toward the barbed end of the actin filaments, both head successively binding 36 nm in front of the other head.

Myosin cycle We saw earlier that the duty ratio of myosin was the ratio of time the head of the myosin spent attached to the actin filament. Indeed, myosin can generate displacement through a cycle of ATP hydrolysis and attachment/detachment described below for a Myosin II motor:

The cycle can be decomposed in 5 steps, last of which will be responsible for the forced exerted on the myosin cargo.

- The myosin start in the ‘rigor’ conformation where it is lightly bound to the actin filament.

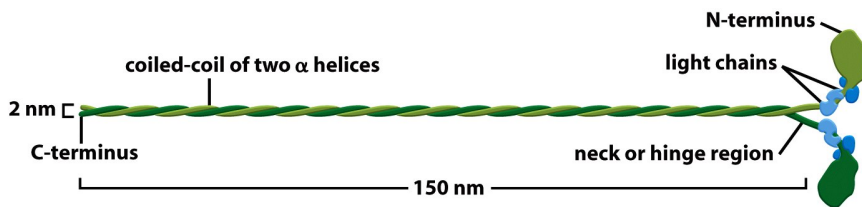


Figure 16-54a Molecular Biology of the Cell 5/e (© Garland Science 2008)

Figure 1.8: Schematic of a dimer of myosin motors with the example of Myosin II. Each of the myosin monomer is colored in a different shade of green. From Right to Left, the myosin head, with the N terminal, is the part of the myosin that binds to the actin filaments. The neck region with the light chain act as a lever arm. Finally the tail, constituted with coiled-coil alpha-helix that aggregate to form minifilaments. Adapted from Molecular Biology of the cell.

- An ATP molecule binds to the myosin head inducing the detachment of the myosin from the actin filament.
- ATP molecule is hydrolysed into ADP+Pi, providing energy which is stored into a conformational change of the myosin which effects a recovery stroke.
- Inorganic phosphate is released as the myosin head attaches to the actin filament.
- The actin-bound myosin change conformation, applying forces on it's cargo. This step is known as the power-stroke and is responsible for most of the applied force or displacement of the myosin. During the power-stroke the ADP bound to the myosin head is released, leading back to first step of the cycle.

This principle is the same for all kinds of myosin. In the case of Myosin II the duty-ratio is only of about 5%, which leave Myosin II detached from the actin filament most of the time. A single dimer cannot then achieve processivity. The tail of myosin II can bundle itself with the tail of other myosin II motors. They form large bipolar thick filaments of tens of dimers. As each myosin dimer attaches and detaches independently from the actin networks the effective attachment of the filament increases with the number of motors in the minifilaments. Indeed the probability of having at least one motor attached increases with the number of motors. The constant attachment of at least one myosin II head in minifilaments insure that the filament does not displace with respect to the actin network when others myosin heads recover from their power stroke and reattach, thus conferring processivity to myosin II minifilaments.

The bipolar nature of myosin II minifilaments also allow them to act as force dipoles, each of the extremity pulling the surrounding actin network or filament toward the center of the minifilaments. This is the mechanism at the origin of muscle contraction and can allow to build-up tension in actin network.

1.4.2 The actin cortex

The actin cortex is a thin layer of between 200 to 500 nm that can be found just underneath the plasma membrane of a cell. The properties of the actin cortex makes it a key component to diverse processes. Its capacity to resist to, and transmit forces is indispensable for locomotion of many cells by allowing the retraction of the rear of the migrating cell and will be described in more detail in the next section. Its structure is also essential for the cellular division as contractility is necessary to generate cortical tension and achieve the separation of the two daughter cells.

Todo

Actin Gels dynamics,

Sketch actin cortex

The actin cortex is constituted of actin filaments that can be parallel or orthogonal to the membrane as one can see using electron microscopy on cells [Morone, Fujiwara, Murase, et al. 2006].

We saw through the bud scar of budding yeast that the full cytoskeleton could retain memory of past events. It is also the case for simple actin networks as shown in [Parekh, Chaudhuri, Theriot, Fletcher, 2005] who describe how actin-network growth can be determined by network history, showing actin cortex could also act as a memory for cell.

1.4.3 Cell Motility

The way cells move highly depend on their environment and the type of cells. We can distinguish several strategies of movement, mainly categorised into amoeboid and mesenchymal movement. The type of motility for certain cells can be characteristic of malignant tissue, and play a significant role in the ability of the cells to invade nearby tissues.

Lamellipodium based Motility

We can have a first look into the mesenchymal mode of locomotion of cells, which is also often referred to as crawling. To understand how a cell is able to crawl, to move itself, we will in particular take the example of the lamellipodium. Lamellipodia is a characteristic structure of cells moving on a 2D substrate. By its nature, motion using lamellipodia is one of the easiest to study using microscopy which might explain why it is one of the best known process of cell displacement. None the less, it does not diminish its importance in tissues behavior as all epithelial cell can be considered as moving on a 2D substrate. Beyond lamellipodia, structures that are responsible for cell motion are filopodia and pseudopodia. They mainly differ from lamellipodia by their shape and the organisation of the actin structure inside. Lamellipodia-based motion can move a cell up to a few micrometers per minute.

Todo

Cite speed ? Ofer2011 ?

The action necessary to move in a mesenchymal way can be decomposed in three steps. First the cell needs to grow a protrusion. Growing this protrusion is typically governed by actin polymerisation just underneath the plasma membrane. The lamellipodium is such a protrusion which is constituted by a 2D dendritic actin network that polymerizes at the leading edge. Second the cell's protrusion needs to attach to the surface. This is done through trans membrane proteins that are bound to the actin cortex on the inside of the cell. The actin cortex will act as a scaffold to transmit the force across the cellular to these anchor points. Last part is traction in which the rest of the cell is pulled toward the attached protrusion. The traction force is mediated through the cytoskeleton and actin cortex while the contraction force themselves can originate from actin network contraction and reorganisation due to myosin motors ([Fig 1.11](#)).

Todo

Find review on lamellipodia

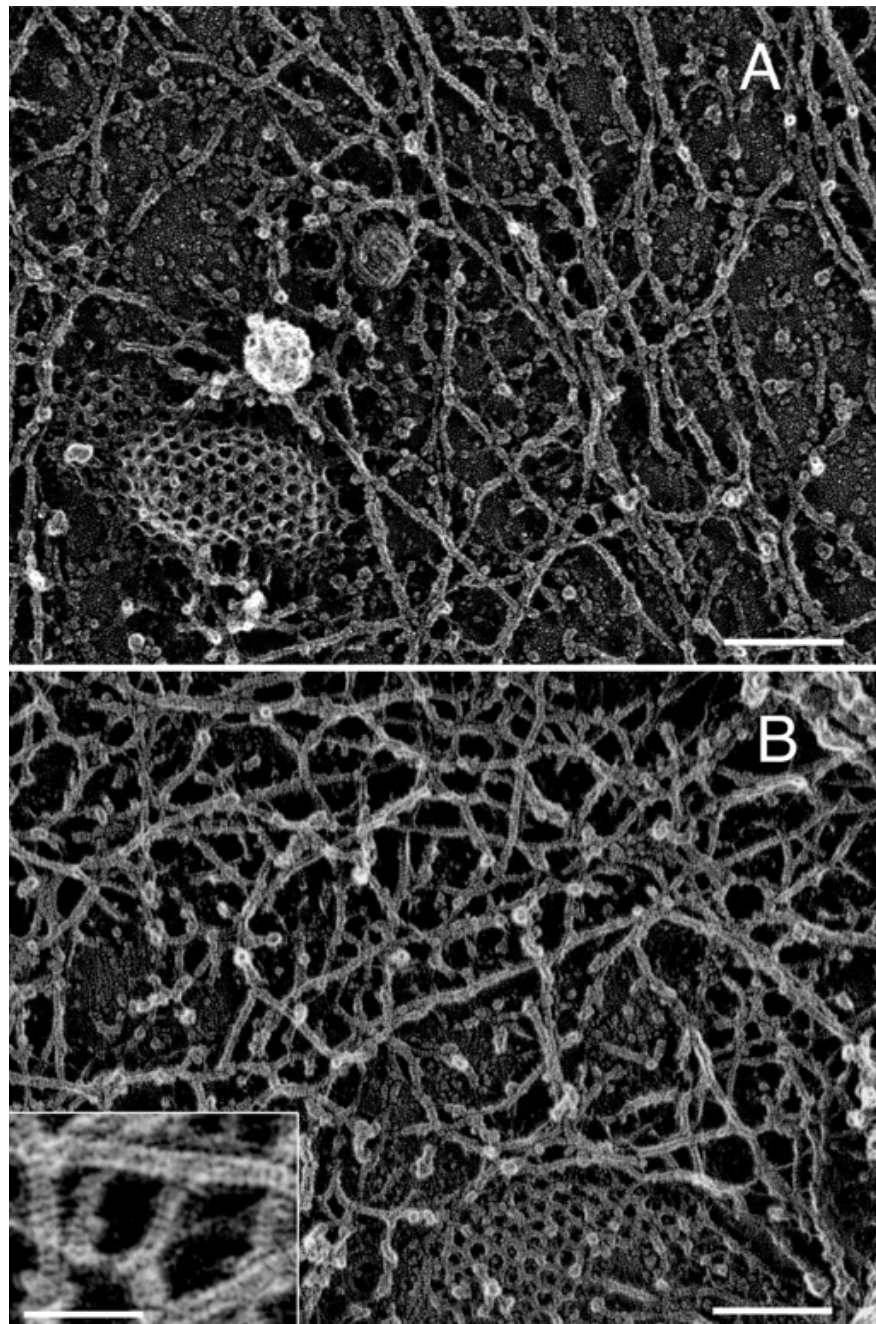


Figure 1.9: Electron microscope view of the actin cortex in rat cell. The inset show a periodicity of ~5nm in filaments characteristic of actin. Scale bars are 100nm, inset 50 nm. Extracted from [Morone, Fujiwara, Murase, et al. 2006].

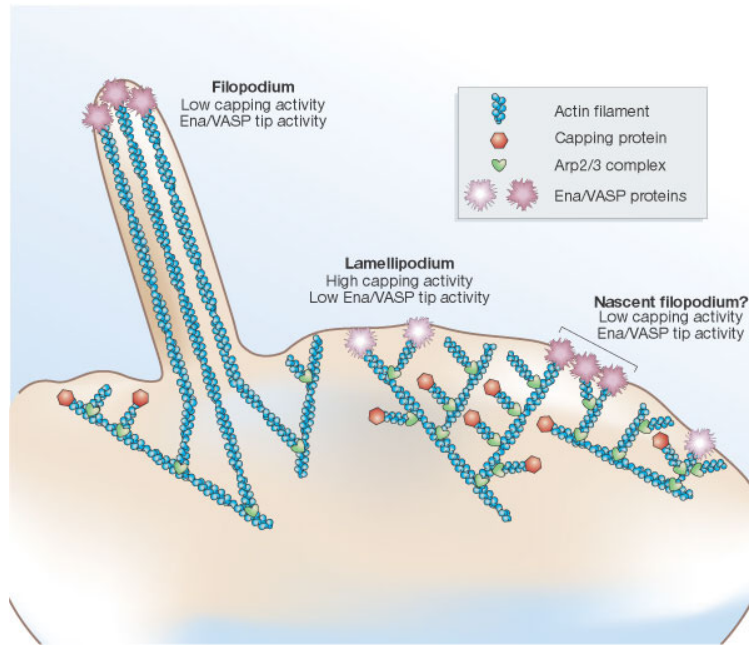


Figure 1.10: Polymerisation at the leading edge of the cell. NPF situated on the membrane of the cell localize the polymerisation. The lamellipodium will be characterized by a dendritic network formed by Arp2/3. Parallel actin structure can form a growing protrusion called filopodium. Adapted from [Schafer, 2004]

Blebbing based Motility

The second mode of motility which is known as amoeboid is more characteristic of 3D displacement of cells. In this mode, the cell will also form protrusions but will not rely on adhesion to move its body. This motility rely on blebs, that are blister-like protrusion that happened on the cell surface. A bleb forms on the surface of cell when the membrane detach from the actin cytoskeleton underneath it, or if the cortex ruptures. The small protrusions are formed quickly grow as they lacks the force supporting layer that the actin cortex provides. While growing, the bleb fills with the cytosol. The actin cortex can rapidly reform on the bleb slowing down its growth. In some cases, the reformation of the actin cortex in the bleb and the rebuilding of the tension inside the bleb by myosins mediated contraction is enough to reverse the bleb. Though, the content of the cell can also drain itself into the bleb as it grows and while the main body of the cell contract and empties, thus moving the cell from its old position to a new one in the direction of the initial growth of the bleb.

At their initial state, blebs are simple membrane protrusions filled with cytosol and empty of organelles. The stop of their growth is due to the spontaneous formation of an actin cortex on the inner side of the bare membrane.

By their relative simplicity to the rest of the cells, blebs are the perfect system to be reconstituted *in vitro* in liposomes.

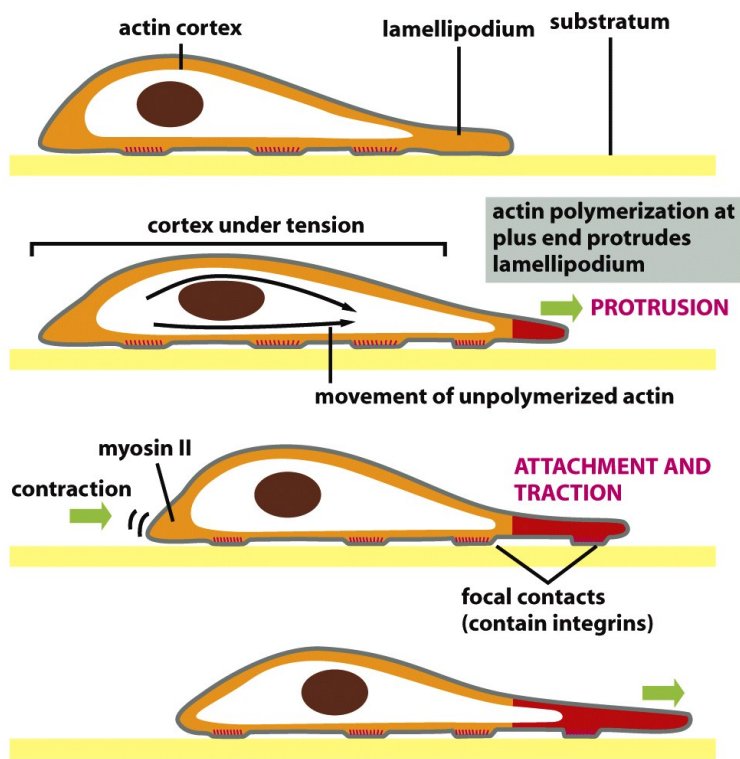
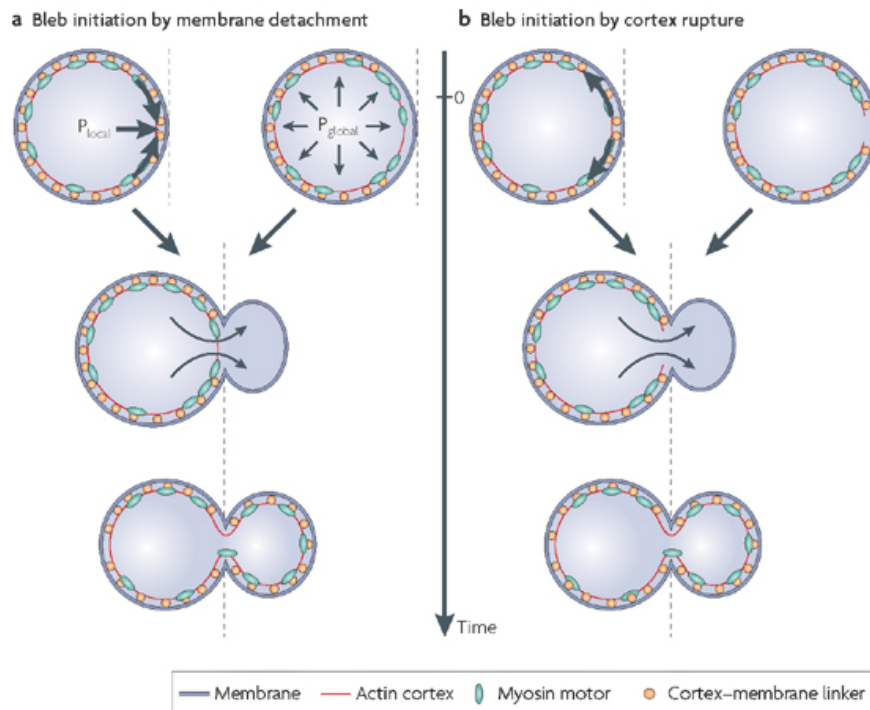


Figure 16-86 Molecular Biology of the Cell 5/e (© Garland Science 2008)

Figure 1.11: Schematic of Lamellipodium base motility. The lamellipodium grows at the leading edge of the cell and attach to a focal point. The actin cortex under tension contract and is capable to pull the rear of the cell.



Nature Reviews | Molecular Cell Biology

Figure 1.12: Formation of bleb can be done either by a) detachment of the membrane from the cytoskeleton, or b) by a rupture of the cytoskeleton. In both cases the inner pressure of the cell lead to the inflation of the membrane at the point of rupture/detachment. The acto-myosin cortex will rapidly refer on the formed bleb slowing its growth. Extracted from [Charras, Paluch, 2008]

1.4.4 Organelle Positioning

We have seen previously that organelle positioning plays an important role in cell function. Several mechanisms involving actin are at the origin of structure positioning in cell. The positioning of organelles by actin can have a wide range of impact from being necessary for the correct cell division, to allowing locust eyes to adapt in the dark by repositioning mitocondrion [Sturmer, Baumann, Walz, 1995].

We already know that the actin cortex is a necessary element in cell motility. It also plays a determinant role in organelle positioning. It has been shown [Chaigne, Campillo, Gov, et al. 2013] that the correct range of elasticity of the actin cortex during oocyte division is needed to get spindle positioning. The correct spacial position of this spindle is necessary to perform a viable division of the cell.

The actin cortex is not the only actin structure in the cell, beyond the thin and dense layer just below the cell is a softer and sparser actin structure that has a crucial role in organelle positioning.

During cell division, there are several stages that require actin structures. As shown previously [Azoury, Lee, Georget, et al. 2011] the expulsion of polar body during oocyte asymmetric division is strongly dependent on the time evolution of a sparse actin network that can be found in the cell. Actin structures are also required at a later stage to permit the correct capture of chromosomes by microtubules and achieve correct haploid division. [Schuh, Ellenberg, 2008] also show that a similar sparse actin network contracted by myosins is necessary for spindle migration.

Especially in oocyte that are typically large, the effect of gravity is not negligible. The presence of a sparse “actin scaffold” is discussed in [Feric, Brangwynne, 2013], where it is found that an actin network is present to balance the gravitational force.

In drosophila, nurses cell need to expel their content into oocytes. It has been observed [Huelsmann, Ylanne, Brown, 2013] that during this phase, the nurse’s cells nucleus is pushed away from the dumping canal by single actin filaments polymerising from the membrane and forming a soft and sparse actin network.

1.5 In vitro reconstituted actin networks

Living cells are complex organisms, for which each function requires a number of interacting proteins and components. To understand the action of each individual component it is needed to isolate or modify their actions independently.

In order to achieve the precise tuning of each component independently two approaches are envisageable. An approach referred to as “Top-Down” where starting from the full system — in our case the cell — we will modify or remove each of the component and study the global change of behavior. This is a complex process that might be difficult to interpret as biological systems have often multiple pathways and feedback loop to regulate each of their processes. With the large number of components that constitute a living cell, it is also relatively difficult to come up with the minimal system necessary to replicate a behavior.

The other approach, also referred to as the bottom-up approach, require to reconstitute the system component by component until it replicate the expected behavior. It is also a complex process, as there are a large of component to chose from that can potentially be added to the reconstituted system, but often lead to a wider range for the testable parameter as well as minimal number of interacting component. This allow for a deeper understanding of the governing principle of the system, and often permits access to a wider range of accessible conditions and individual tweaking of component.

In our lab we are mainly interested in the bottom-up approach and the use of biomimetic system. We try to reconstitute biologically relevant behavior with the minimal system constituted from pure protein components.

In particular in this manuscript we are interested in mimicking the motility process by which the *listeria* pathogen is able to hijack cellular mechanisms, recruit proteins responsible for actin polymerisation at the leading edge of the cell, and use them to polymerize actin on its surface. This is what allows the *listeria* to propel itself fast enough (1.5 to 2 μm /min) [Dabiri, Sanger, Portnoy, Southwick, 1990] to be able to pass through cell membrane from one cell to the other.

The bead motility system is a minimal in-vitro system capable of replicating the *listeria* motility.

1.5.1 Bead motility assay

The *Listeria* pathogen is a 1.5 to 5 micrometer cylindrical bacteria that enter cells, hijacks its actin polymerisation machinery to propel itself and infect neighbour cells. It does so by the recruitment of a single protein on its surface : ActA, that activates the Arp2/3 complex. By the recruited of Arp2/3 a dense branched and entangle actin network growth that will eventually form a comet behind the bacteria propelling the bacteria at the speed of actin comet polymerisation. *Listeria* comets are composed of a wide range of protein, it has though been shown [Loisel, Boujemaa, Pantaloni, Carlier, 1999] that the number of required component can be highly reduced.

The simpler system that can replicate the *listeria* motility is the bead motility assay, it consist of a micrometer-sized bead covered with a nucleation promoting factor that will activate Arp2/3 present in solution. This NPF can be ActA as in the case of *listeria*, but one can use other NPF like N-WASP or pVCA. In the experiments presented in this work we use pVCA. The NPF covered bead is in a G-Actin solution. Capping Protein is added to prevent polymerisation from happening away from the bead surface as well as the components necessary for actin polymerisation (ATP, Salt..., see *Material and methods*)

Due to the presence of Capping Protein in solution and NPF on the surface of the bead, the polymerisation of actin will happen only on the surface on the bead forming a thin and dense actin gel capable of sustaining stress depending on the different protein concentration. Unlike in the case of *listeria* which control on which of its side the nucleation process happens, this is not controlled on bead motility assay. Though, in the right condition [Kawska, Carvalho, Manzi, et al. 2012] the dense actin gel formed on the bead surface can accumulate stress induce by polymerisation of inner layer until symmetry breaking occurs. The gels ruptures on one of the side of the bead, leading to the formation of a comet on the opposite side.

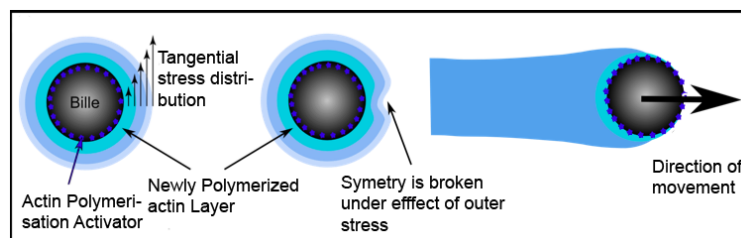


Figure 1.13: Scheme of bead motility assay. The NPF (yellow stars) will localize the actin polymerisation on the surface of the bead thus increasing stress on the outer actin layers. At a sufficient level of stress, the outer layer ruptures, leading to symmetry breaking, formation of a comet, and propulsion of the bead. Adapted from [Plastino, Sykes, 2005]

The further polymerisation of the actin network on the surface of the bead will make the comet grow, propelling the bead forward. This is what makes the bead system a biomimetic system replicating the listeria motion.

It should be noted that during the movement of this system, two phases can be distinguished. In the first phase, the system present a spherical symmetry with an homogeneous actin network around the bead. The gel is growing from the surface and is accumulating stress due to the polymerisation of inner layers.

If the gel is able of accumulate sufficient stress, by polymerisation, the symmetry breaking event happens, and the system enters in a second phase with the formation of a comet.

The condition that lead to symmetry breaking are investigated in [Kawska, Carvalho, Manzi, et al. 2012]. In the absence of Capping Protein, the actin polymerisation seem not to be restricted enough near the surface of the bead, and the formed network is not able to generate or sustain enough stress to achieve symmetry breaking. At high Capping Protein concentration, the growth of the gel is too impaired to also permit symmetry breaking. The concentration of Arp2/3 is also critical as Arp2/3 form branched network, and these branched network are primordial for the ability to sustain stress.

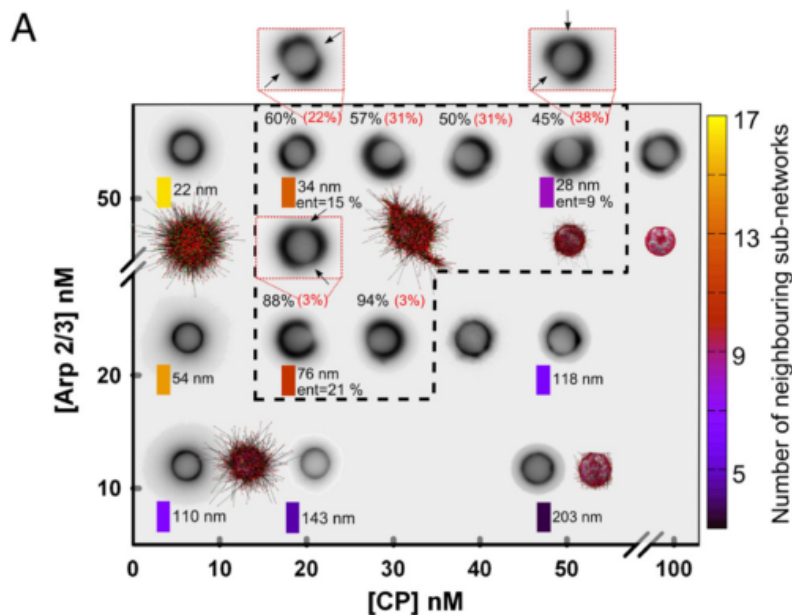


Figure 1.14: Phase diagram showing symmetry breaking in bead motility assay as a function of concentration of Arp2/3 and Capping Protein. Symmetry breaking only occurs inside the area delimited by dashed line. Experiments are displayed as inverted fluorescence image. Adapted from [Kawska, Carvalho, Manzi, et al. 2012]

In the rest of this manuscript we use the bead motility system but only consider it during the first phase, where the symmetry breaking has not yet occurred, or in condition where it should not occur. In particular we will investigate condition at 25 nM Arp2/3 and concentration of Capping Protein varying from 0 to 50 nM. This correspond in Fig 1.14 to both condition where no symmetry breaking can occurs, but also to condition in which symmetry breaks with the highest probability. It should be noted that unlike other study that also characterize actin network growing on bead [Pujol, dRoure, Fermigier, Heuvingh, 2012], our system is still dynamically polymerising and thus changing with time.

1.5.2 Liposomes

Beads are used as model biomimetic system that replicate the polymerisation mechanism happening on the leading edge of the cell. Because of their composition and rigidity, phenomenon observed on beads cannot necessarily reproduce all the interactions and processes that take place on cell membrane. Cells are finite compartments with a limited amount of actin that act on the dynamic of polymerisation. The fact that cell size is in the order of the persistence length of actin filaments also play a role on the structure of actin network. Indeed at these scale as a single filament can never reach the length at which it can be considered fully flexible.

Liposomes are one of the biomimetic system that are capable of capturing some interactions between cell membranes. Liposomes are lipid bilayers that imprison an aqueous compartment and exhibit many characteristics similar to cells. The inside of liposomes can act as a biochemical reactor of limited size with the lipid bilayer actin as a separation to the outside, like the cell membrane. The composition of the lipid layer can be varied in order to reflect the composition of cell membrane. In particular it is possible to attach proteins to the liposome membrane. Finally the size of the liposomes can be varied, leading to actin networks of size and shape similar to those found in cells.

It is possible to mimic the cellular actin cortex using liposomes, and especially its contractility. A crosslinked actin network, can be formed and attached to the outer leaflet of liposomes, and contractility can be triggered by injecting molecular motors. The behavior of the system will depend on the attachment between the reconstituted actin cortex and liposomes membrane. Weak attachment lead to a favorable rupture of the actin cortex during the increase of tension, implying a symmetry breaking as in bead system. In the case of strong attachment the liposomes actin cortex will accumulate tension until it has enough force to crush the supporting lipid layer thus collapsing the liposomes [Carvalho, Tsai, Lees, et al. 2013]. This system also allow the observation of the system through time giving extra insight into the dynamic of actin network.

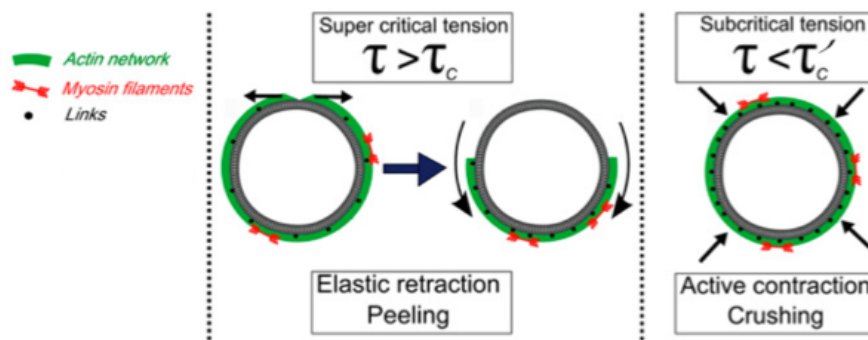


Figure 1.15: Effect of reconstituted rigid actin cortex attachment to a liposome membrane under constraint generated by myosin filaments. On weak attachment the actin network ruptures thus leading to a “peeling” of the actin cortex. With stronger attachment the actin cortex can sustain higher stress, until the underlying liposome ruptures (“Crushing”). Adapted from [Carvalho, Tsai, Lees, et al. 2013]

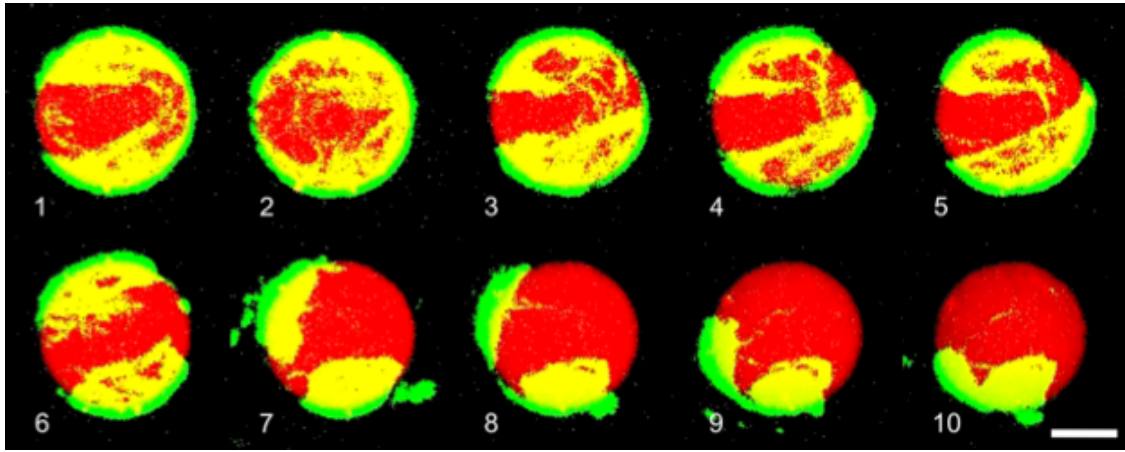


Figure 1.16: 3D reconstruction of an acto-myosin cortex (green actin) peeling on a liposome (red) through time (1.4 second between frames). The actin cortex contraction happened after the injection of Myosin II. Scale bar is 5 μm . Experiment and reconstruction done by Joël Lemière.

1.6 Membrane Physics

The cells plasma membrane is a biological membrane that separate the cell from its outside environment. It consist of a lipid bilayer in which are present numbers of protein. A lipid bilayer is formed of two layers of lipid and has a thickness of a few nm thickness. The first attempt to theoretically describe these membranes have been done by W. Helfrich [Helfrich, 1973] in 1973 in a model based on the elasticity and fluidity of lipid bilayers as well as the self assembly properties of lipids.

In the case of close lipid bilayer, the potential energy stored by the deformation of a lipid bilayer by unit area can be written as

$$H = H_{ext} + H_{curv}$$

In which H_{ext} is due to the extension/ compression of the membrane, and H_{curv} is due to the local curvature of the membrane.

The density of energy cost of extension H_{ext} cab be written as a function of the elastic area compressibility modulus K_a and the relative variation surface of the membrane A :

$$H_{ext} = \frac{1}{2} K_a \left(\frac{\Delta A}{A} \right)^2$$

K_a express how much energy is required to expand the surface of the lipid bilayer and is due to the exposition of more hydrophobic surface to water when expanding it. K_a is expressed in J.m^{-2} , or N/m and is close to 2 time the surface tension between the lipids and water.

For closed lipid bilayer, the total curvature energy can be expressed as the sum of curvature energy H_{curv} :

$$H_{curv} = \frac{1}{2} \kappa (c_1 + c_2 - c_0)^2$$

In which κ is the bending modulus of the membrane, c_1, c_2 are the principal curvature of the membrane. c_0 is the spontaneous curvature of the membrane, the curvature the membrane would adopt when free of external constraint.

An important parameter which is introduced in membrane is the membrane tension σ which is the stress associated with an increase in membrane surface. The tension σ is linked to the energy required to expand the membrane H_{ext} by :

$$\sigma = \frac{\partial H.A}{\partial \Delta A}$$

ie

$$H_{ext} = \sigma \left(\frac{\Delta A}{A} \right)$$

In which

$$\sigma = K_a \left(\frac{\Delta A}{A} \right)$$

Membrane tension is a key parameter as it can be measured in cells, and is one of the parameters responsible for cell sorting [Maitre0212]. In particular between cells, the tension of the couple (membrane+actin cortex) can be determined by using the contact angle between cell which is the angle between interfaces as defined in Figure 1.17.

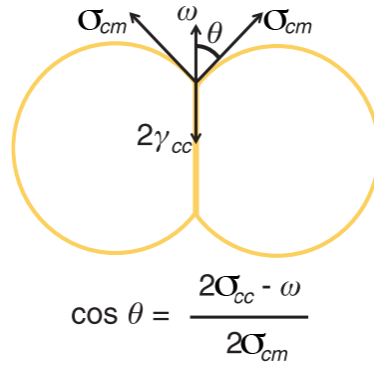


Figure 1.17: Surface tension govern doublet shape, adapted from [Maitre, Berthoumieux, Krens, et al. 2012]. The equilibrium of forces on the contact line govern the angle of contact 2θ . ω corresponds to the adhesion tension between the two cells, σ_{cm} corresponds to the tension between the cell and the medium, σ_{cc} corresponds to the cortex tension between the two cells.

In a later part, we use a reconstituted biomimetic made of liposome. The injection of Myosin motors changes the tension of the acto myosin cortex attached to a membrane. By determining the geometrical parameters of this system, and in particular the evolution of the contact angle with time, we are able to measure the variation of tension of the acto myosin cortex due to molecular motors.

1.7 Actin networks as viscoelastic material

We have seen previously that while polymerising, G-actin assembles into F-actin filaments. The stiffness of filament can be measured by a characteristic number called the persistence length (l_p). More precisely, the persistence length characterise the average loss of correlation between the tangent along the considered

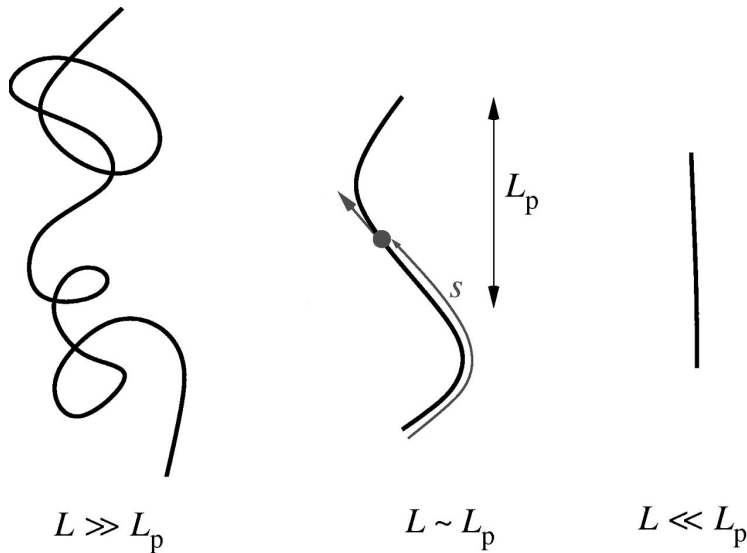


Figure 1.18: Schematic of polymers with length respectively big compared to persistence length (A), in the order of the persistence length (B) and small compared to persistence length (C), s as defined on (B) is the *curvilinear abscissae*, that is to say the distance between two point of the polymer measured by “following” the polymer. Adapted from [Liverpool, 2006]

polymer. With s the curvilinear abscissae along the polymer, and $\Theta_{(x,y)}$ the angle between the two tangent at two different abscissae:

$$\langle \Theta_{(s,s+l)} \rangle = \exp\left(\frac{-l}{l_p}\right)$$

For actin filaments, the persistence length is in the order of 10 μm [Isambert, Venier, Maggs, et al. 1995]. This means that for scales much smaller, the actin filament can be considered as rigid. This is the case in the cell cortex where the meshwork has a typical size smaller than 250 nm. In the other extreme, at length scale much bigger than l_p , filaments can be considered as flexible. While in typical cells, the cell size is rarely much bigger than the persistence length of actin, *Xenopus* eggs can be as big as 1 mm, so hundreds fold the actin persistence length. Still for the majority of cells, the typical size we are interested in is about the persistence length of an actin filament, making it neither purely rigid nor completely flexible.

For the above reasons, actin solutions are often compared to semi-flexible polymers, and models that predict the behavior of actin networks often take foundation on polymers physics [Morse, 1998b] [Morse, 1998a]. Still, if these models rely on local microscopic parameter, experimental methods only have access to bulk properties of the studied material, and it is from these properties, and through the models that we can deduce possible values for the microscopic models [MacKintosh, Kas, Janmey, 1995].

1.7.1 Elastics Modulus

The elastics moduli are probably the easiest to understand. They are a characteristic of how a material will deform non permanently under an applied force. The stiffer something is the higher its elastics moduli will be. There are two specific elastic moduli of interest in this manuscript, *Young's Modulus* and *shear modulus*. The first one describes how a material will react to compression or extension, while the second describes how a material resists shearing. For isotropic and homogeneous material, the Young's modulus (E) and the

shear models (G) are related by the Poisson ratio (ν):

$$G = \frac{E}{2(1 + \nu)}$$

Both G and E units are homogeneous to N/m^2 or Pa . It is interesting to have an idea of the order of magnitude of a few usual materials. Aluminum will have an elastic modulus $G_{Al} \simeq 70 \text{ GPa}$ while rubber will be more in the order of $G_{Rubber} \simeq 0.1 \text{ GPa}$. The elastic modulus of muscle cell is in the order of $G_{muscle} \sim 10 \text{ kPa}$ and brain tissues around $G_{brain} \sim 0.1 \text{ to } 1 \text{ kPa}$ [Engler, Sen, Sweeney, Discher, 2006].

A more formal definition of the Young's modulus, is the ratio between the stress σ along the direction of the deformation and the relative deformation ϵ .

$$\begin{aligned} E &= \frac{\sigma}{\epsilon} \\ &= \frac{F/S}{\Delta L/L_0} \end{aligned}$$

In which F is the applied force, S is the cross section of the material, ΔL is the elongation and L_0 is the initial length of the considered material. (Figure 1.19 A):

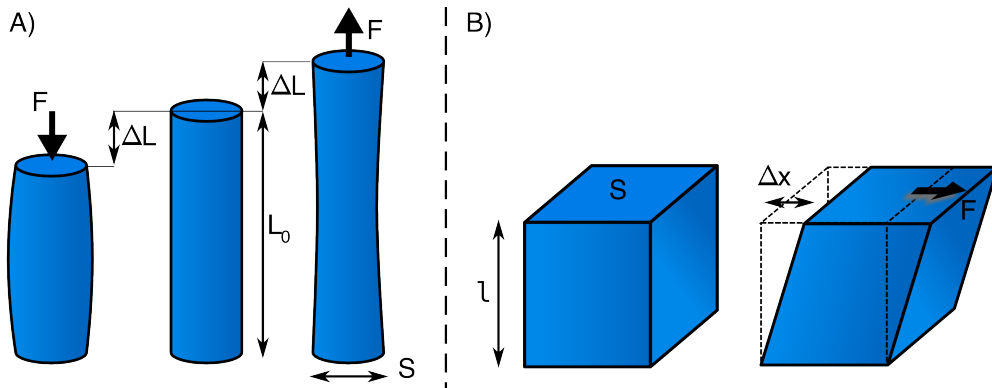


Figure 1.19: Schematic of Young Modulus definition. F , force applied to sample, S surface of cross section when uncompressed, L_0 , length when no load applied. For both compression and extension, in the regime of small deformation, the relative change of length is proportional to the applied force. Here, the material can be seen to expand/contract in the direction orthogonal to the direction of application of the force, in the case of an incompressible material ($\nu \neq 0.5$) this can be seen as the conservation of volume of the material.

The shear modulus is defined for a deformation parallel to the surface on which it is applied :

$$\begin{aligned} G &= \frac{\tau_{xy}}{\gamma_{xy}} \\ &= \frac{F/S}{\Delta x/l} \end{aligned}$$

In which τ_{xy} is the shear stress, γ_{xy} is the shear strain, F is the applied force on the cross section of the material S . l is the thickness of the material and Δx is the transverse displacement (Fig 1.19 B).

Other characteristic numbers can also be defined. In the case of isotropic elastic material, only two of those parameter are required to completely define the properties of the material.

1.7.2 Poisson Ratio

We have seen that the shear modulus is linked to the Young modulus using the Poisson ratio. The Poisson ratio is another characteristic of a material that define how much a material will compress/expand in the directions orthogonal to its elongation.

Poisson ratio is the negative ratio of transverse to axial strain :

$$\nu = -\frac{d\epsilon_{trans}}{d\epsilon_{axial}}$$

In which ϵ_{axial} is the relative deformation along one the axis of compression/elongation and ϵ_{trans} correspond to the relative deformation along an axis orthogonal to the axis of deformation.

Having volume conservation of material during compression or elongation require a Poisson ratio of 0.5. Such value have been found in bulk measurements of actin network at 21.5 μM of actin [Gardel, Valentine, Crocker, et al. 2003]. Material with a Poisson ratio of 0.5 are said to be incompressible. A Poisson ratio lower 0.5 correspond to material expanding less than incompressible materials, some cell and tissues are known to have Poisson ratio lower than 0.5 [Mahaffy, Park, Gerde, et al. 2004]. Another critical value is 0, at which the material only expand or contract in the direction of the main stress.

Material with a Poisson ratio superior to 0.5 would show a bigger deformation in the orthogonal direction than incompressible material, leading to a global increase of volume if compressed.

1.7.3 Viscosity

Like elasticity, viscosity is something tangible we are used to work with in everyday life. The more viscous a material is the more difficult it is to move something in it at high speed. And indeed, viscosity is the pendant of the elastic modulus but considering forces induced by deformation rate instead of displacement.

$$\begin{aligned} \frac{F}{S} &= \tau_{xy} \\ &= \eta \frac{\partial v}{\partial z} \end{aligned}$$

In which τ_{xy} is the shear stress, F is the force exerted on the surface S . η is the viscosity, and is expressed in Pa.s , v is the deformation rate along the direction z .

At room temperature water has a viscosity of around 1 mPa.s, and honey of 10 Pa.s. The consideration of viscosity in problems will often depend on the timescale and deformation rate. At short timescale tissues often behaves elastically, whereas at long timescale the effect of viscosity will be seen [Thoumine, Ott, 1997]. In actin network, the effect of viscosity at short time scale can be as high as elasticity [Gardel, Valentine, Crocker, et al. 2003].

1.7.4 Viscoelastic

Typically, no material is purely elastic or purely viscous. While glaciers seem purely solid at the time scale of a few days, observation on longer time scale ranging from month to years show that ice is not only a solid but can also flow. Of course ice in its solid form is not the only material which is both solid and viscous. In order to describe such behavior one needs the theory of viscoelastic materials. A number of models have

been and are still developed to describe viscoelastic behavior. The Kelvin-Voigt and Maxwell models are two of the simpler ones. A thought experiment to understand each of these model is to put a spring and a dash pot in parallel or series. Such model systems will have a viscoelastic behavior.

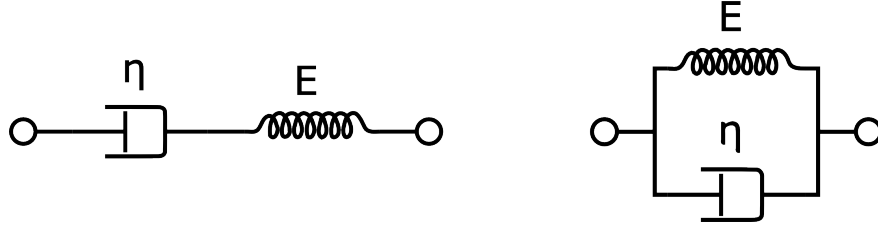


Figure 1.20: Maxwell model schematic on the left and Kelvin-Voigt model on the right. Both are a simple approach to express the properties of a viscoelastic solid. The response to a creep compliance will differ in both case. The Maxwell model will mostly behave like a fluid with viscosity η after a long time, where the Kelvin-Voigt model will mostly reflect the elastic component at constant stress exerted. (Schematic in Public Domain, adapted from Wikimedia).

The idea for more complex models is similar, where any material can be seen like an (infinite) combination of springs (for elasticity), and dash-pots, (for viscosity).

Viscoelastic theory try to explain the mechanical properties of a system by using a single parameter which is the viscoelasticity of a material. This can be done by describing E as a relaxation modulus depending on time. In the case of linear system we can express the strain on the material at a given time as a function of its history :

$$\sigma(t) = \int_0^t E(t - \tau) \frac{du}{d\tau} d\tau \quad (1.1)$$

In which $\sigma(t)$ is the time depending stress, and $u(t)$ is the know strain.

Using Rheology, it is common to measure the properties of a material using a sinusoidal strain of known amplitude u_0 and frequency $f = \omega/2\pi$: $u(t) = u_0 \cos(\omega t)$, which also imply a sinusoidal strain rate. Using the complex notation $\dot{u} = u_0 i \omega e^{i\omega t}$. In equation (1.1), and operating the change of variable $t - \tau \rightarrow t'$ leads to :

$$\sigma(t) = u_0 \int_0^\infty E(t') i \omega e^{i\omega(t-t')} dt'$$

By making the time dependent part in factor, the rest can be rewritten as two integral with respectively a Real and imaginary prefactor :

$$\sigma(t) = u_0 e^{i\omega t} \times \left(\omega \int_0^\infty E(t') \sin(\omega t) dt' + i\omega \int_0^\infty E(t') \cos(\omega t) dt' \right) \quad (1.2)$$

The two integrals in brackets only depends on the pulsation ω and the properties of the considered material. They are both in factor of the complex strain $u(t) = u_0 e^{i\omega t}$ We thus define the storage modlus of the material as the real part of ((1.2) in bracket) E' :

$$E'(\omega) = \omega \int_0^\infty E(t') \sin(\omega t) dt'$$

And the loss modulus as the imaginary part of ((1.2) in bracket)

$$E''(\omega) = \omega \int_0^{\infty} E(t') \cos(\omega t) dt'$$

And define the complex frequency dependant young modulus as :

$$E^*(\omega) = E'(\omega) + i.E''(\omega)$$

Thus we can write (1.2) as :

$$\sigma(t) = E^*(\omega).u(t)$$

In this representation of $E^*(\omega)$, the real part will correspond to the elastic response of the material, which correspond to in-phase response under oscillatory strain. The imaginary part correspond to the viscous response of the system, out of phase under sinusoidal strain. The complete knowledge of $E^*(\omega)$ at all frequency completely characterize the material.

Models for actin network have been extensively studied as viscoelastic material both theoretically [Morse, 1998a], [Kruse, Joanny, Julicher, et al. 2005], and experimentally [Mizuno, Tardin, Schmidt, Mackintosh, 2007]. Actin network have also been shown to exhibit linear characteristic behavior, but also and non linear ones in a certain range in concentration [Yao, Becker, Broedersz, et al. 2011], [Gardel, Valentine, Crocker, et al. 2003].

The actin network we will study hereafter are in the condition where linear behavior is expected, thus we will use the viscoelastic theory to interpret the relation stress/strain observed in order to determine the mechanical properties of the formed actin gels.

1.8 Optical tweezer

Optical tweezers, or optical traps are a technique that allows to trap object near the focal plane of a microscope at the focal point of a high power laser. It is a versatile technique that allows to trap both fabricated objects and part of living cell. Optical traps allow to apply force up to a few tenth of pico newtons.

To understand that light can trap an object, it is instructive to keep in mind that despite having no mass, photons carry momentum, and as for any massive object, changing the trajectory requires a force. According to Newton third law, when applying a force with a photon on a object, the object will in turn exert the opposite force on the photon, thus changing the trajectory of the photon. Thus if a photon changes trajectory in a material, the material apply a force on the photon (Fig 1.21), meaning that the photon also apply a force on the material. In particular, the higher the refractive index of a material is, the more light beams are deviated, and hence the more photon apply forces on material.

In particular, it can be shown that this leads object with higher refractive index than surrounding medium to be attracted by toward higher light intensity (Fig 1.21). In parallel laser beams, with a Gaussian intensity profile, this will lead to the object being attracted toward the center of the beam.

In addition to the lateral trapping, laser focus lead to another intensity gradient along the direction of propagation of the beam, the intensity being at its maximum at the laser waist.

A laser coupled into a microscope objective then act as a three dimensional potential that traps particle similar to a tweezer. Usually the trapping in parallel to the direction of the laser is week compared to the trapping in the perpendicular directions.

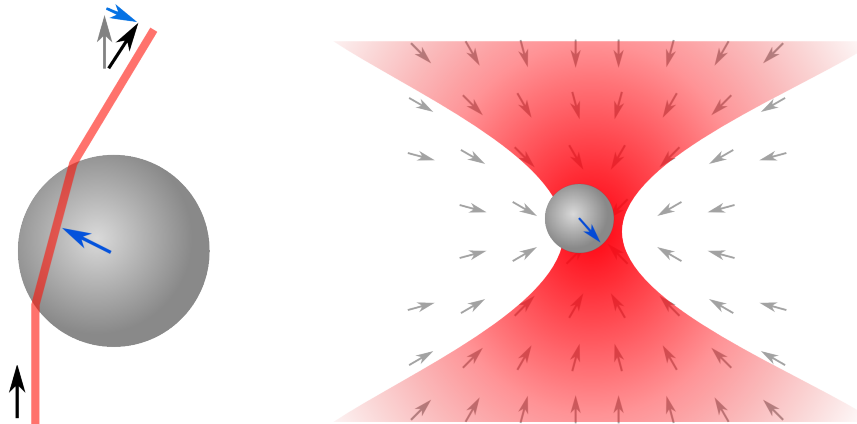


Figure 1.21: Deflected light by a transparent bead change the momentum of light, so the light is exerting a force on the bead. The bead will be attracted towards the highest intensity. For a focused laser beam, the bead will be attracted near the focus of the laser.

One of the quality of optical trap is that in principle, multiple traps can be obtained. A simple method to generate two traps is to split the incoming light into two orthogonally polarized independent beams. Instead of sharing the laser power between the different traps by using polarisation, one can use what is known as multiplexing by time sharing. By switching the laser rapidly between different positions at a much faster rate than the diffusion of trapped particle out of the trap, one is able to virtually achieve multiple traps on the same sample.

In our case, the rapid switching is achieved using Acousto Optic Deflector (aka AODs). AOD consists of a crystal in which a high frequency sound-wave propagate. This sound-wave generates local changes in the refractive index of the material which act as a diffraction grating. In the right conditions, a laser passing through the crystal will be deflected by this grating.

In practice, rapidly controlling the frequency and amplitude of the sound wave in the crystal, allows direct adjustment of laser deflection and hence the trap position. Using AODs also has the advantage of controlling not only of number and position of multiple traps, but also the individual power allocated to each trap and hence the stiffness of relevant trap.

1.8.1 Determination of force and displacement on bead

In addition to allowing the objects to be held in place, the use of a QDP (Quadrant Photo Diode) with optical trap have the advantage of allowing the high frequency quantitative measurement of the displacement and force exerted on an object. Indeed, when the trapped particle is not in the trap center, the laser apply a force on the object. Reciprocally the object apply the opposite force on the light beam, thus deflecting the light beam. Using optics and lenses correctly placed on the Fourier plane of the sample, it is hence possible to translate this change of orientation of the light beam into a displacement of a light spot onto a photo detector with high sensitivity to applied forces.

Through careful calibration of the trap, that give the force/displacement relationship, [Jahnel, Behrndt, Janasch, et al. 2011], [Vermeulen, vMameren, Stienen, et al. 2006], one can then also recover the displacement of the sample inside the optical trap.

Using optical tweezers to not only hold a particle in position, but also get quantitative measurement of its

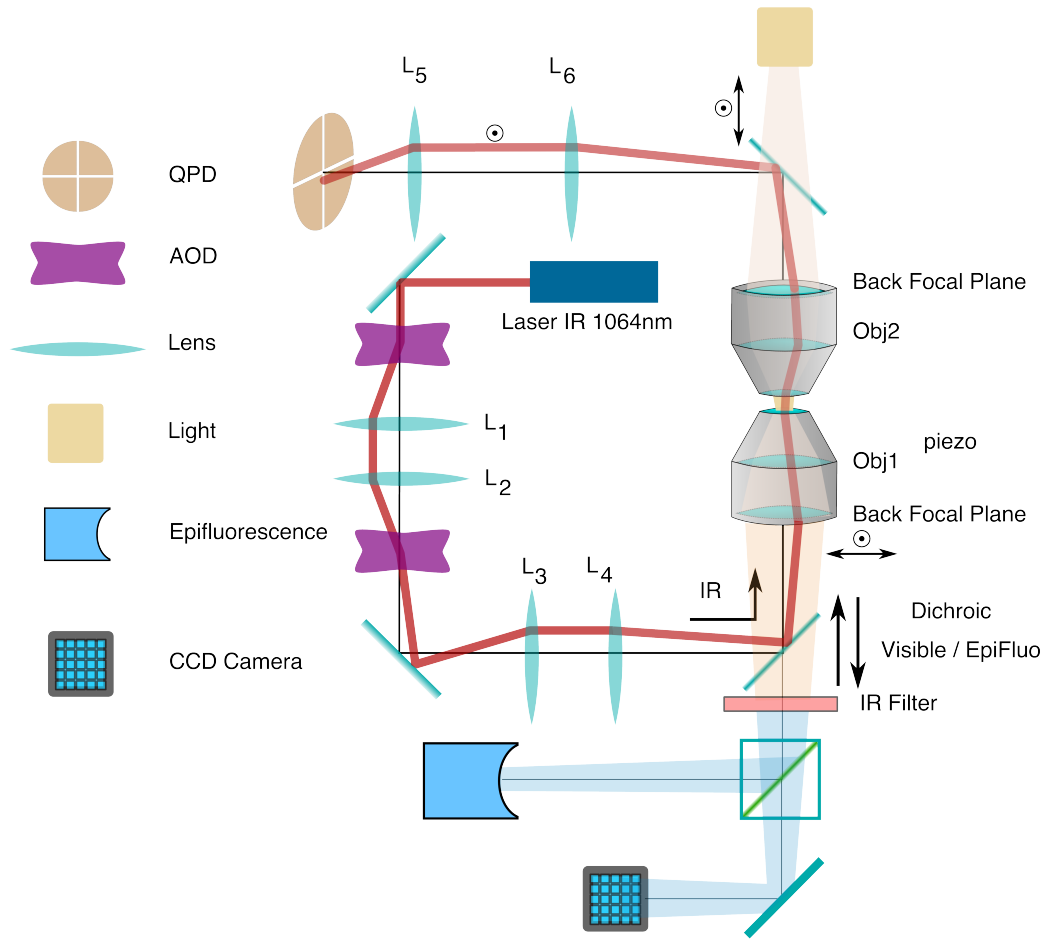


Figure 1.22: A schematic of setup used. The following elements can be distinguished. An 1064nm laser is used for trapping. It first passes through two AODs that move the position of the trap in the X and Y direction. The first couple of lenses (L_1, L_2) between AODs assure that AODs are in conjugated planes. The second pair of lens (L_3, L_4) imaged the AODs plane in back-focal plane of the first objective. Thus a change of angle of the light beam induce by the AOD result in a change of position of the trap. The trapping light is collected by a second objective, and illuminating a Quadrant photodiode (QPD) conjugated with the back focal plane of the collecting objective. By construction QPD and AODs should be conjugated, so deviation of the light beam induced by one of the AODs is not supposed to induce any change of position of the laser spot on the QPD. Additional dichroic mirrors allow to use bright field and epifluorescence simultaneously

displacement and force exerted require calibrated probe. The use of polystyrene beads is one of the artificial probe that can be used to achieve such a goal.

The use of polystyrene bead has multiple advantages, the first being that one can obtain mono-dispersed bead leading to reproducible and predictable trap stiffness. Secondly theory can predict the shape of the potential felt by such a bead in a Gaussian beam [Nieminen, Knoner, Heckenberg, RubinszteinDunlop, 2007].

The third advantage being that beads can be functionalized, allowing specific interaction to be controlled, both in vitro and in vivo. Of course, the calibration is essential for the correct measurement of mechanical property of different system, and the choice of the bead diameter have impact both on biological side and in the physics of the measurement.

CHAPTER
TWO

MATERIALS AND METHODS

2.1 Buffers

2.1.1 G Buffer

G-Buffer is used to conserve actin in monomeric form. Actin is diluted in G-Buffer and kept on ice for at least 12 hours before further use. G-buffer is stored at -20°C. Unfrozen and conserved on ice for weekly use. G-buffer is never refrozen. pH is adjusted between 7 and 8.

Composition of G-Buffer:

- 0.2 mM $CaCl_2$
- 0.5 mM DTT (Dithiothreitol, or (2S,3S)-1,4-bis(sulfanyl)butane-2,3-diol)
- 2.0 mM Tris (tris(hydroxymethyl)aminomethane or 2-Amino-2-hydroxymethyl-propan)
- 0.2 μ M ATP (Adenosine triphosphate)

2.1.2 Polymerisation Buffer

Polymerisation buffer or X-Buffer is used for polymerisation of actin gels on beads as well as bead dilution and cleaning. It is aliquoted and conserved at -20°C. During experiments it is stored on ice for weekly use. X-Buffer is never refrozen.

Composition of X-Buffer :

- 10 mM Hepes (2-[4-(2-hydroxyethyl)piperazin-1-yl]ethanesulfonic acid)
- 0.1 M KCl
- 1 mM $MgCl_2$
- 1 mM ATP (Adenosine triphosphate)
- 0.1 mM $CaCl_2$

2.1.3 X Buffer with BSA

Same as X-Buffer with the addition of 1% BSA (10 mg/ml). BSA is used to prevent non specific adsorption. X-BSA buffer is used in place of X-Buffer for the conservation of the probe beads.

2.1.4 ATP Mix Buffer

ATP-Mix buffer or simply *Mix* containing the ATP necessary for actin polymerisation, It is aliquoted and stored at -20°C. Kept on ice for Weekly use. pH is adjusted between 7.5 and 8.0.

- 12.0 mM ATP,
- 20,0 mM DDT
- 0.88 mM Dabco
- 24.0 mM $MgCl_2$

2.2 Protein preparation

2.2.1 pWA

pWA is use as a nucleation promoting factor. It is expressed from Human pVCA (verprolin homology central and acidic domain) and expressed into Rosetta 2(DE3) pLysS (Novagen) Cell. Purified pWA is conserved at -80°C, never refrozen, and conserved on ice for daily use.

2.2.2 Actin

Actin and biotinylated actin are purchased from Cytoskeleton (Denver, CO, USA), and stored at -80°C. Fluorescent Alexa-488 actin is obtained from Molecular Probes and stored at -80°C, and prepared according to manufacturer recommendation.

Actin is stored in aliquots of 5 μ L at a concentration of ~238 μ M, and fluorescent actin in aliquots of 3 μ m with a concentration of ~106 μ M.

G-actin with 20% fluorescently label actin monomers is prepared the day before the experiments by mixing 1 aliquots of actin with 1 aliquot of fluorescently labeled actin and diluting with G-Buffer until desired concentration.

2.2.3 profiline

Human profilin is expressed by competent cells and purified in our laboratory as described in *Carvalho2013a*. Profilin is conserved at 4°C for a few month and keep on ice for daily use.

2.2.4 Arp2/3

Bovine Arp2/3 complex from Bovine is purchased from Cytoskeleton prepared as recommended by the manufacturer, aliquoted at 1 μ M and conserved at -80°C. Aliquots are never refrozen and stored on ice for weekly used.

2.2.5 Capping protein

Mouse capping protein (CP; a1/b2) is purified as previously described in [Soeno, Abe, Kimura, et al. 1998] was a gift from Laurent Blanchoin .

2.2.6 Myosin II

Myosin II is purified from rabbit skeletal muscle, and fluorescent myosin II is prepared as previously described in [SoareseSilva, Depken, Stuhrmann, et al. 2011]. Functionality of Myosin II is confirmed by motility assays. Gliding speed shows an average of 4.5 + 1.5 μ m/s (N = 27)

The working buffer for Myosin contains

- 25 mM imidazole
- 50 mM KCl
- 70 mM sucrose
- 1mM Tris
- 2 mM MgCl₂
- 1 mM ATP
- 0.1 mM DTT
- 0.02 mg/ml β -casein,

then adjusted to a pH of 7.4. In the working buffer and myosin II forms minifilaments of approximately 0.7 μ m length which correspond to about 100 motors.

2.3 Lipids, reagent and proteins

Chemical are purchased from Sigma Aldrich (St-Louis, Mo, USA). EPC (l- α -phosphatidylcholine) and *1,2-distearoyl-sn-glycero-3-phosphoethanolamine-N-[biotinyl polyethylene glycol 2000]* (biotinylated lipids), *1,2-dioleoyl-sn-glycero-3-phosphocholine* are purchased from Avanti polar lipids (Alabaster, USA). Monomeric actin containing 10% or 20% of labeled Alexa-488 actin and 0.25 % of biotinylated actin is diluted in G-Buffer

2.4 doublets preparation

Cell-sized liposomes are formed by electro formation [Angelova, Dimitrov, 1986]. 20 μL mix of EPC lipids and PEG-biotin lipids (present at 0.1 %, mol) with a concentration of 2.5 mg/ml in chloroform/methanol 5:3 are deposited on glass plates coated with ITO. Glass is then dried with nitrogen; placed under vacuum for 2 hours.

A chamber is formed using the ITO plates with their conductive sides facing inside, then filled with sucrose buffer (200mM sucrose, 2mM Tris adjusted at pH 7.4). Chamber is sealed with hematocrit paste (Vitrex medical, Denmark).

An alternate current voltage of 1V and 10 Hz is applied between the ITO-coated surfaces for 75minutes to form liposomes.

Formed liposomes are incubated 15 minutes with 160 nM streptavidin in order to coat them with streptavidin. Liposomes coated with streptavidin tends to aggregates. Solution containing doublets is then diluted 30 times. Waiting 15 minutes increase the ratio doublets/single liposome by still avoiding aggregates of more liposome.

A bulk solution of 40 μM actin monomers — 10% fluo and 0.25% biotinylated — is diluted 40 times in working buffer (25 mM imidazole, 50 mM KCl, 70 mM sucrose, 1mM Tris, 2 mM MgCl₂, 1 mM ATP, 0.1 mM DTT, 0.02 mg/ml β -casein, adjusted at a pH 7.4) and polymerized for one hour. The adjunction of 1 μm of phalloidin after 1 hour prevent further depolymerisation

Actin filaments are diluted to 0.1 μM (10x), mixed with streptavidin-coated doublets of liposomes, and incubated for 15 min. The mix is diluted 5 times to reduce fluorescent background form actin monomers in solution

2.5 Bead Preparation

Carboxylated polystyrene beads (Polysciences, Philadelphia, PA) of $4.34 \pm 0.239 \mu\text{m}$ (Standard deviation) diameter were used as actin-bead and probe-beads.

Beads are stored at 4°C.

Before coating by BSA (probe bead) or pWA (actin-bead), bead solution is cleaned by centrifugation at 5000 rpm, 2min. Supernatant is removed, and pellet is resuspended in X-Buffer. Procedure is repeated twice.

2.5.1 Actin-Bead Preparation

Cleaned polystyrene beads are incubated for 20 min at 20°C under agitation with 2 μM pVCA. Centrifuged at 5000rpm 2min, supernatant is removed and pellet diluted by 4 in X-buffer on ice for the day.

2.5.2 Probe Bead Preparation

Cleaned polystyrene beads are incubated under agitation with 10 mg/ml BSA at room temperature for 30 minutes. Passivated beads are then centrifuged, separated from supernatant, the pellet is resuspended in X-BSA buffer and stored at 4°C for weekly use.

2.6 Force indentation experiments

2.6.1 Preparation of sample

Equal amount of each actin and probe beads are placed in the polymerization mix consisting of :

- 2 μ L BSA at 10%
- 3 μ L of ATP-Mix Buffer
- 1.5 μ L Profilin (114 μ M)
- 1 μ L beads (50% actin-bead 50% probe bead)
- 0.5 μ L Arp2/3 (22,3 μ M)
- between 0 and 2 μ L CP (0.5 μ M)
- Completed to 15 μ L using X-Buffer.

5 μ L of G-Actin (20% fluorescent) is then added to the previous mix. This moment is $t=0$ for the experiment and recorded. The experimental chamber is build by 2 coverslips that are separated by VaLaP. VaLaP is a mix of vaseline Lanoline and Parafine. The chamber is prepared by gently depositing 20 μ L of the final beadds mix at the center of the lower coverslips and 4 drops of VaLaP are deposited at the position where the corner of the upper (18x18mm) coverslip will rest. The VaLaP act as a spacer and prevents the sample to be squashed. The upper coverslip is then placed on top of the sample and the chamber is sealed using VaLaP.

2.6.2 QPD positioning and calibration of microscope

The prepared sample is placed on the microscope and a drop of water is deposited on top of the upper coverslip to assure immersion of the light collecting objective. The collecting objective and the quadrant photodiode are place on top of the sample ([Fig 2.1](#)).

The trapping laser is then aligned with the photodiode while verifying that no object is trapped during the process. The conjugation of the back focal planes of the objective with the AODs and the QPD is optimized by adjusting the distance of both objective with the sample.

A trapping laser is positioned near the center of the microscope field of view using LabView software. The QPD is adjusted in X and Y direction to $\Delta X = \Delta Y = 0V$. This is done with no object is trapped in the laser focus.

2.6.3 Initial bead trapping

Two maximum strength trap (~50mW/trap) are created near the center of the microscope field of view, separated by 15 to 20 μ m. The traps are then moved in the Z-direction near the middle plane of the chamber by displacing the 3D piezo controlled stage. Temporarily removing the Infra Red filter ([Fig 2.1](#)) from the microscope allows to see the reflection of the trapping lasers on the upper and lower coverslip and to determine the localisation of the middle plane of the observation chamber.

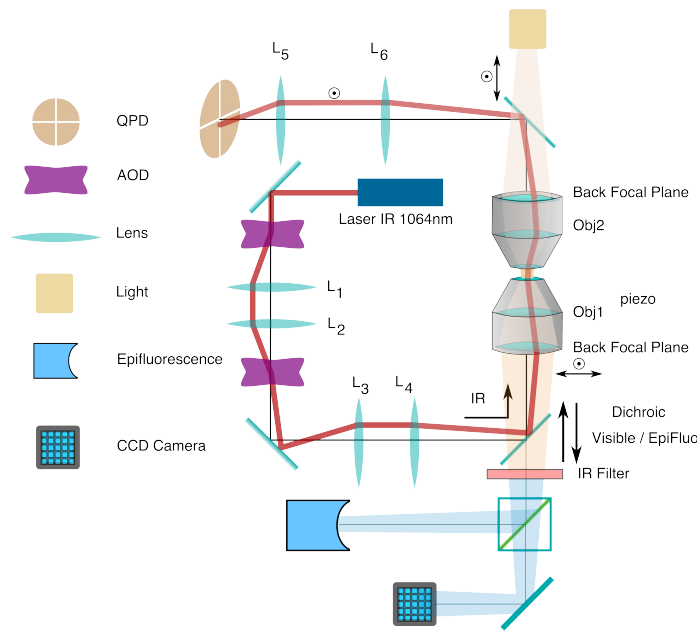


Figure 2.1: Schematic of experimental setup. The QPD situated after the collector allow to determine the force exerted on the trapped sample. It need to be correctly position before each experiment.

The operator then captures one probe-bead and one actin-bead in each of the traps. Both types of beads can be recognized using fluorescent microscopy, as actin-beads are promptly cover with a fluorescent actin which can clearly be distinguished from the probe bead that remain dark. In the case where 2 identical beads are trapped one of the two traps can selectively be disabled or decreased in stiffness, letting the bead escape from the trap, and the procedure can be repeated.

The operator will then move the two traps roughly one micrometer in each direction to check that the two beads are effectively trapped in the tweezer and that no external forces act on the beads.

For practical reasons, the traps are aligned along one of the principles axis of the AOD before starting the indentation experiments.

2.6.4 Indentations

The operator set the parameter of the experiment in the software:

- Average bead radius,
- Approach/Retraction Speed.
- Resting Time
- Laser Power

For each pair of actin/probe bead, the initial minimum approach distance of the traps is set to 5 to 8 μm before a single indentation cycle is done. If the maximum measured force between the two beads is not higher than

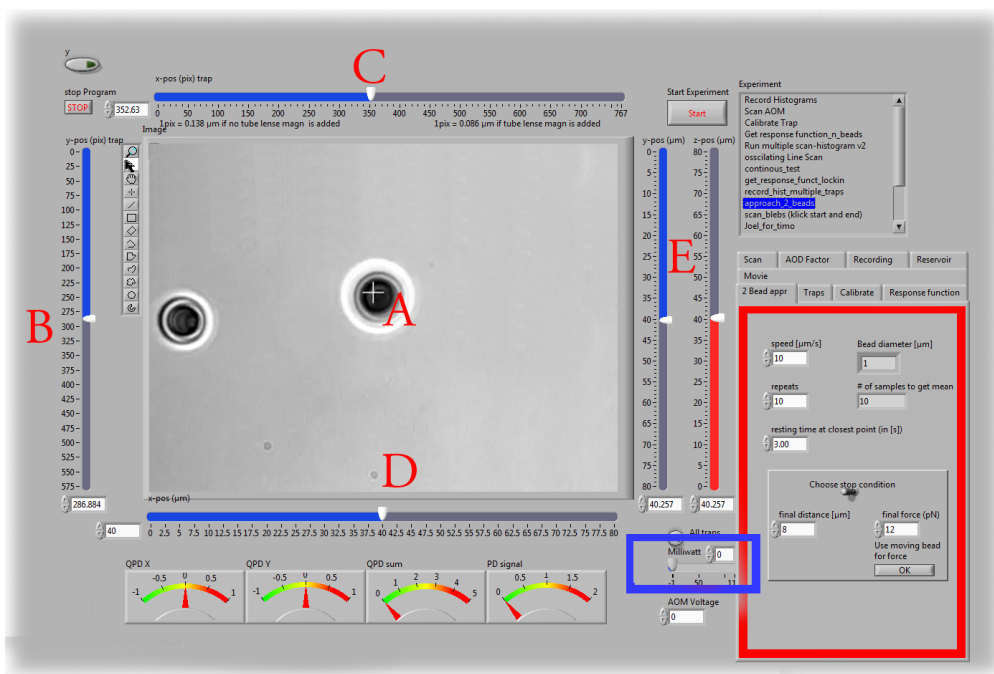


Figure 2.2: Software responsible for controlling the optical tweezer. Sample containing 2 polystyrene bead and a trap (A, white cross) holding one bead. Cursors (B,C) are available to displace the optical trap(s). Cursors can control the position of the stage is X (D), Y (E, blue) and Z (E,red). Blue Rectangle highlight the slider that allow to control trap power. Red Rectangle highlight the area when some of the parameter of the experiment can be set (approach speed, resting time at closest point). 3 indicators at the bottom of the screen indicate the voltage on the QPD.

8 to 10 pN, the minimum approach distance is reduced by 0.25 to 1 μm and the procedure repeated. Once the maximum achieved forced is in the 10-15pN range the right distance is found and up to 10 automatic force-indentation experiments are performed. Before each indentation the software automatically does a “scan” of each bead to ensure correct calibration. An indentation cycle has the following step:

- Probe trap is approaching the actin-bead at constant speed until the minimal approach distance has been reached.
- Rest for 3seconds resting time
- Probe trap return to its initial position at constant speed
- Cycle is repeated as many times as set.

During this cycle the deflection of the laser induced by the probe-bead and actin-bead are recored by the QPD.

After an indentation cycle is finished the experimenter can try to perform the indentation on the actin-bead from another direction, or release the actin-bead on proceed to a new one.

In the case where the indented actin network shows sign of inhomogeneity or symmetry breaking, the experiments are stripped not taken into account for further analysis.

The date and time of each indentation cycle is recorded to extract the time of polymerisation for each sample.

2.7 Time Shared Optical Trap

The optical trap is build on an inverted microscope (Olympus, IX71) equiped with a fluorescence (200W mercury lamp, Osram, Munich, Germany). The sample is observed through a Olympus 60X water immersion objective with numerical aperture NA=1.2.,from Olympus, that also serves at entry point for the laser of the optical tweezer. The light source is an infrared fiber laser ($\lambda = 1064\text{nm}$, YLP-1-1064, IPG, Germany). X, Y positioning and stiffness of the trapping force are controlled by 2 Acousto Optic Deflectors (AODs, AA-Optoelectronics, France) that are placed in the conjugated plane of the back focal plane of the objective. Multiple traps can be achieved by switching the laser between multiple positions within a switching time in the order of 5 μs , and resting on each position 20 μs or more.

Light refracted by the trapped sample is collected by a 40X (N.A:0.9, Olympus) water immersion objective and imaged on a quadrant photodiode (QPD) conjugated with the back focal plane of the light collection objective. Signals from the QPD (ΔX , ΔY and Σ) are sampled at 500kHz, by a Digital To Analogic Aquisition card (NI PCIe-6363, National Instruments, Austin, Texas), controlled using a custom Labview software (National Instruments) coupled with Matlab (Mathworks, Natick, MA). Raw signals are preprocessed by binning all voltage measured during the time the laser rest at one position. Finally to mean and standard deviation is stored for further processing.

The trap stiffness is inferred from bead radius, laser power, number of present traps and control experiment data. In control experiment the trap stiffness is calibrated using the power spectral density of trap beads, and was determined to be as high as 80 pN/ μm at full laser power (119mW) for a single trap.

Coarse positioning of the sample is done through a pair of micrometer precision screws capable of translating the microscope stage in X and Y. Finer positioning in X,Y and Z direction are done with the help of 3D piezzo with an accessible range of 80 μm in each direction and a sub-micrometer accuracy.

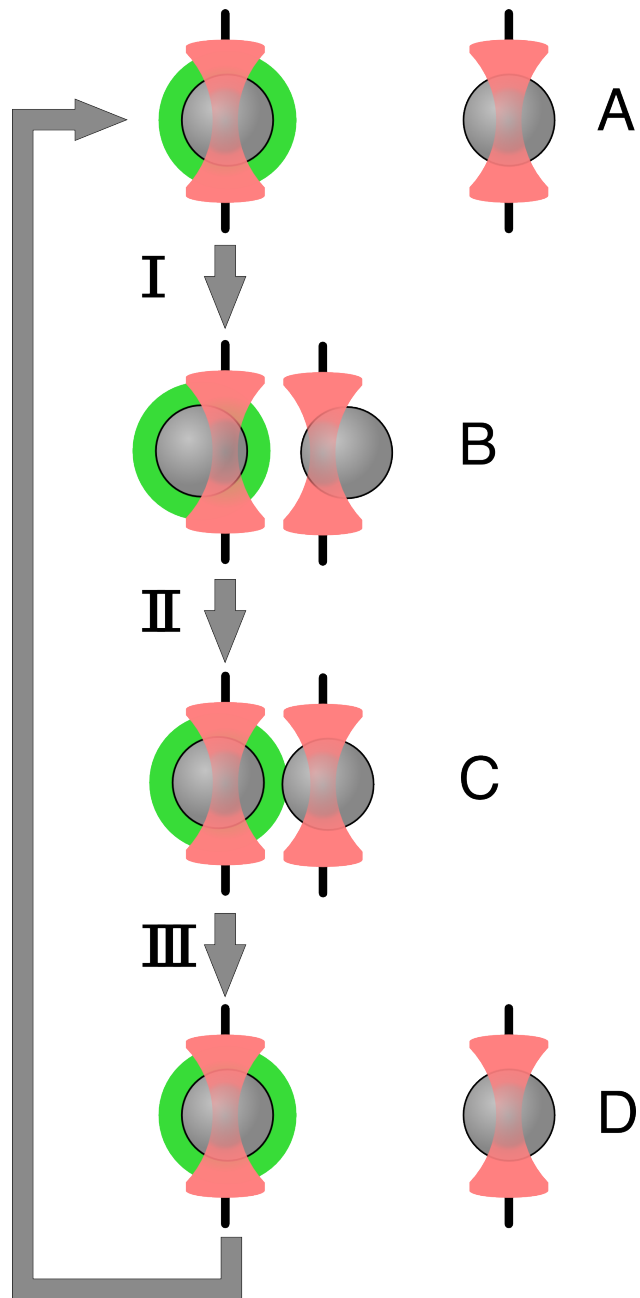


Figure 2.3: Schematic of indentation experiment. On the left is the actin-bead, covered with actin, in the static trap, on the right the probe-bead in the mobile trap. At the brining of experiment (A) the probe bead is situated far from the actin-bead. During the approach phase (I) the moving trap approach toward the static trap at 10 $\mu\text{m/sec}$ until it reached the minimal approach distance (B). The moving trap stay at the minimal approach distance for 3sec (II), which constitute the relaxation phase.C) The actin gel are relaxed, the distance between bead is smaller than on B. III) the moving trap retract at 10 $\mu\text{m/sec}$ back to its initial position.

2.8 Oocyte

2.8.1 Oocyte obtention

Oocyte culture, collection and micro injection where done at College de France by Maria Almonacid.

Oocytes were collected from 11 to 15 week old mice (WT), fmn2-/- as previously described in [Holubcova, Howard, Schuh, 2013] and maintained in Prophase I in M2+BSA supplemented with 1 μ M Milrinone. Oocyte are then injected with cRNA using a micro-injector Eppendorf FemtoJet. Imaging was carried at 37°C.

**CHAPTER
THREE**

MECHANICAL PROPERTIES OF A FAR REACHING ACTIN CLOUD

3.1 Introduction

We have seen that the actin cytoskeleton play a major role in cellular mechanics. It is necessary for force generation, and a key component of cell motility. It has also been extensively studied both in cells and biomimetic systems.

Actin can form a variety of networks in cells , ranging from dense branched networks at the leading edge of the lamellipodia to bundled parallel structures forming the filopodia. Reconstruction of actin networks have been achieved in biomimetic systems using purified components [Plastino, Sykes, 2005], [Loisel, Boujemaa, Pantaloni, Carlier, 1999], [BernheimGroswasser, Wiesner, Golsteyn, et al. 2002], [Pontani, vdGucht, Salbreux, et al. 2009], and many properties of these network have been measured.

It has been determined that the actin cortex is a mechanical support for the plasma membrane and that it extends over a few hundreds of nanometers. Many cellular processes hint for actin structures connected to this cortex to be key elements in organelle and chromosome positioning.

In this part of the manuscript we investigate how a sparse actin structure can emanate from the actin cortex, and we explore its properties. Using the *bead-motility* biomimetic system to reconstitute the actin cortex and its dendritic structure, we show that a sparse network of actin filaments emanating from the cortex has a mechanical effect sufficient to move displace object in the size of cells organelles up to tens of micrometers from the actin cortex.

The branched structure of the actin cortex underneath the plasma membrane of cells hints for a structure governed by Arp2/3. How Arp2/3 and CP can be used to form a biomimetic actin cortex has been widely studied. In [Kawska, Carvalho, Manzi, et al. 2012], both *in vitro* measurements on reconstituted actin cortices on beads as well as simulations investigate the effect of cross-linking and Capping Protein on the formed actin gel. It can be seen both experimentally and in simulation that a network of filaments escape from what is defined as the actin cortex. The effect of these long filaments is not taken into account in the *in silico* system where analysis is restricted to filament shorter than 10 μm . Only the effect of dense entangled actin networks generated from primers randomly placed on the bead surface participate in the increase of tension and contribute to symmetry breaking.

The limit of the dense network visible in epifluorescence is defined in [Kawska, Carvalho, Manzi, et al. 2012] by the position of the half-maximum fluorescent intensity. The properties of these networks are measured by [Pujol, dRoure, Fermigier, Heuvingh, 2012] using magnetic beads and actin stabilized with phalloidin. Though they do not investigate the sparse and softer actin network that originate from the visible part.

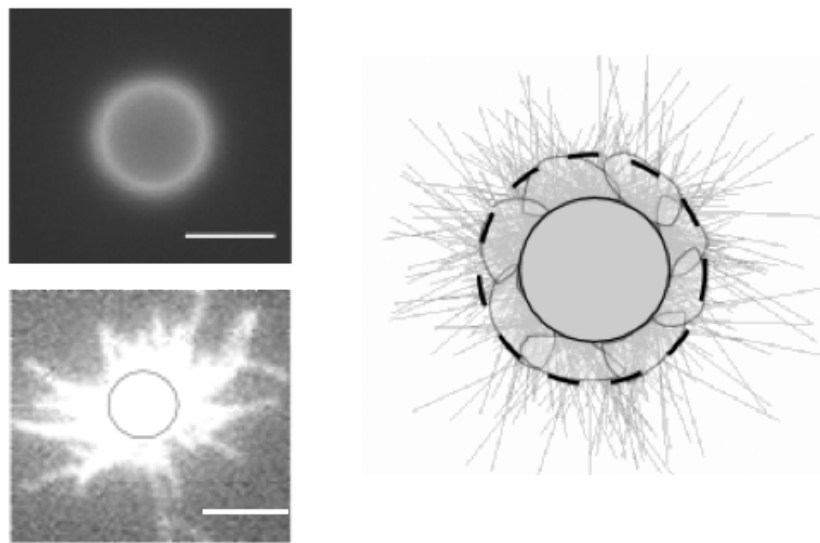


Figure 3.1: Upper Left : Fluorescence image of an actin bead with a growing actin cortex. Escaping filament forming the actin cloud can only hardly be seen. Scale bar is $2 \mu\text{m}$. Lower Left: Total Internal Reflexion (TIRF) image of actin polymerising on an actin bead. Escaping filament and directly visible. The gray circle represents the size of the bead. Right : Representation of the actin growth simulation with delimitation between the entangled branched actin network and escaping filaments. Adapted from [Kawska, Carvalho, Manzi, et al. 2012].

Using *time-shared optical tweezer* we are able to probe the mechanics of this soft actin structure at time scale shorter than the characteristic time of actin polymerisation and forces in the pN range. We show that beyond the dense dendritic network mimicking the actin cortex which has been measured to have an *elastic modulus* in the order of kPa [Pujol, dRoure, Fermigier, Heuvingh, 2012] the soft actin cloud is much softer with a stiffness in the Pa regime. This might explain why such a structure has not previously been seen by less sensitive techniques than optical tweezer. The size of this actin cloud and its ability to sustain forces suggest that in cells the actin cortex is not sharply delimited and that structures escaping from it have a role in organelle positioning.

The questions we address in this part of the manuscript are : How does the far reaching part of the gel ? What are mechanical properties ? How does it change through time ? Is the gel elastic or viscous ?

3.2 Actin-Bead System

To reproduce the actin cortex and study the mechanics of actin structures emanating from it *we prepare polystyrene beads* of $4.3 \mu\text{m}$ diameter coated with a nucleation promoting factor. These beads are placed in the *ATP mix buffer* in presence of 25nm of Arp2/3 complex, $4 \mu\text{m}$ of monomeric actin (20% fluorescently labeled) $12 \mu\text{M}$ profilin and a variable amount of Capping Protein. Cf *Material and Methods*. These beads are referred to as actin-bead.

These conditions are chosen in order to grow a dense network on the surface of actin-bead as in [Kawska, Carvalho, Manzi, et al. 2012]. We place ourselves at 25nM ATP and a varying amount of Capping Protein concentrating in order to cover conditions where the dense gel that forms on the actin-bead is able to accumulate

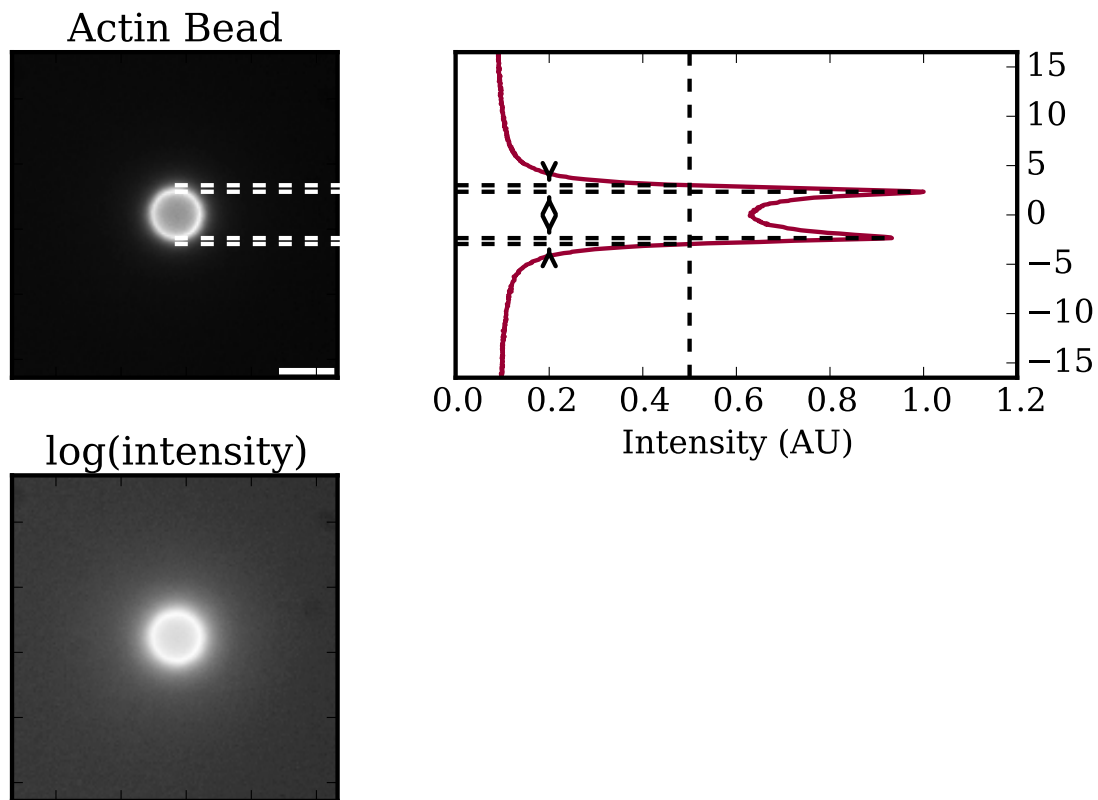


Figure 3.2: Upper Left : Epifluorescence image of polystyrene bead with a growing actin gel in presence of 25 nM of Arp2/3 and 25 nM of Capping Protein. Scale bar is 5 μ m. Upper Right : Normalized intensity profile of fluorescence image with thickness of the gel shown with dashed line as defined in [Kawska, Carvalho, Manzi, et al. 2012] : Distance between maximum intensity and half-maximum intensity. Lower Left: Epifluorescence image of log(intensity).

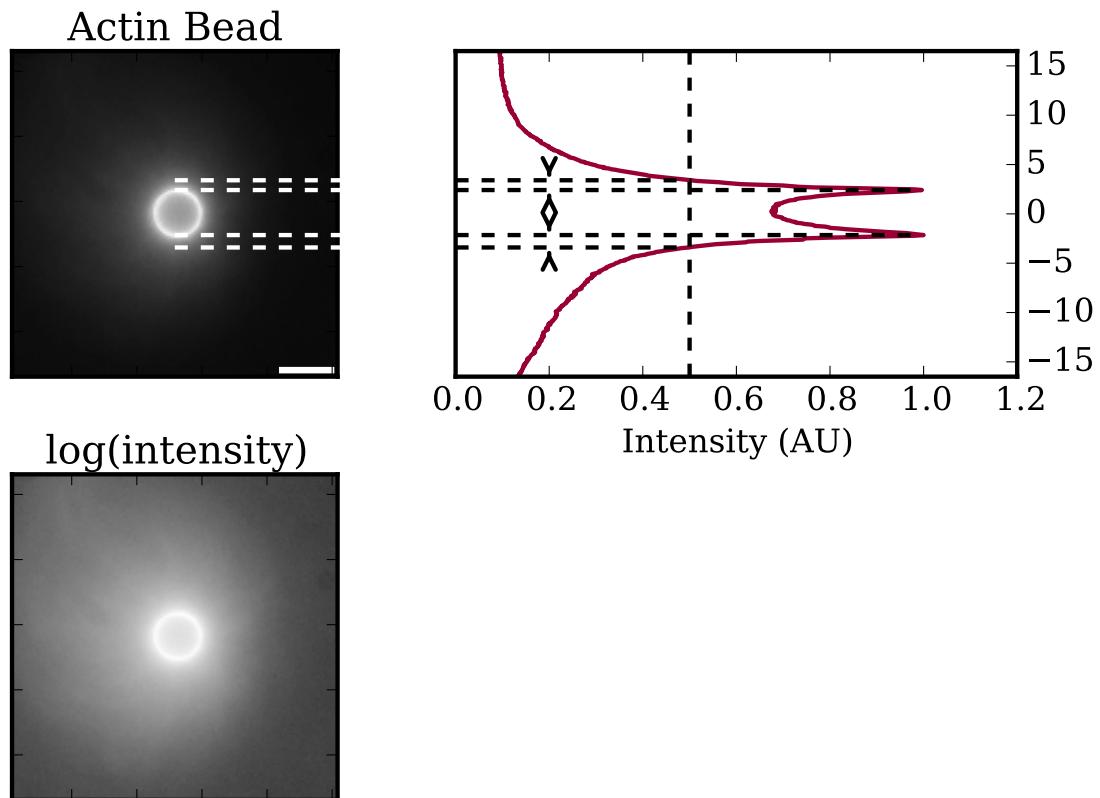


Figure 3.3: Upper Left : Epifluorescence image of polystyrene bead with a growing actin gel in presence of 25 nM of Arp2/3 and absence of Capping Protein. Scale bar is 5 μm . Upper Right : Normalized intensity profile of fluorescence image with thickness of the gel shown with dashed line as defined in [Kawska, Carvalho, Manzi, et al. 2012] : Distance between maximum intensity and half-maximum intensity. Lower Left: Epifluorescence image of log(intensity). In the absence of Capping Protein the growth of filament is not prevented away from the bead surface

sufficient stress to lead to symmetry breaking (CP between 15 and 35 nM). We also investigate conditions where the amount of Capping Protein is to low (< 15nM) or to high (>35 nM) to permit symmetry breaking.

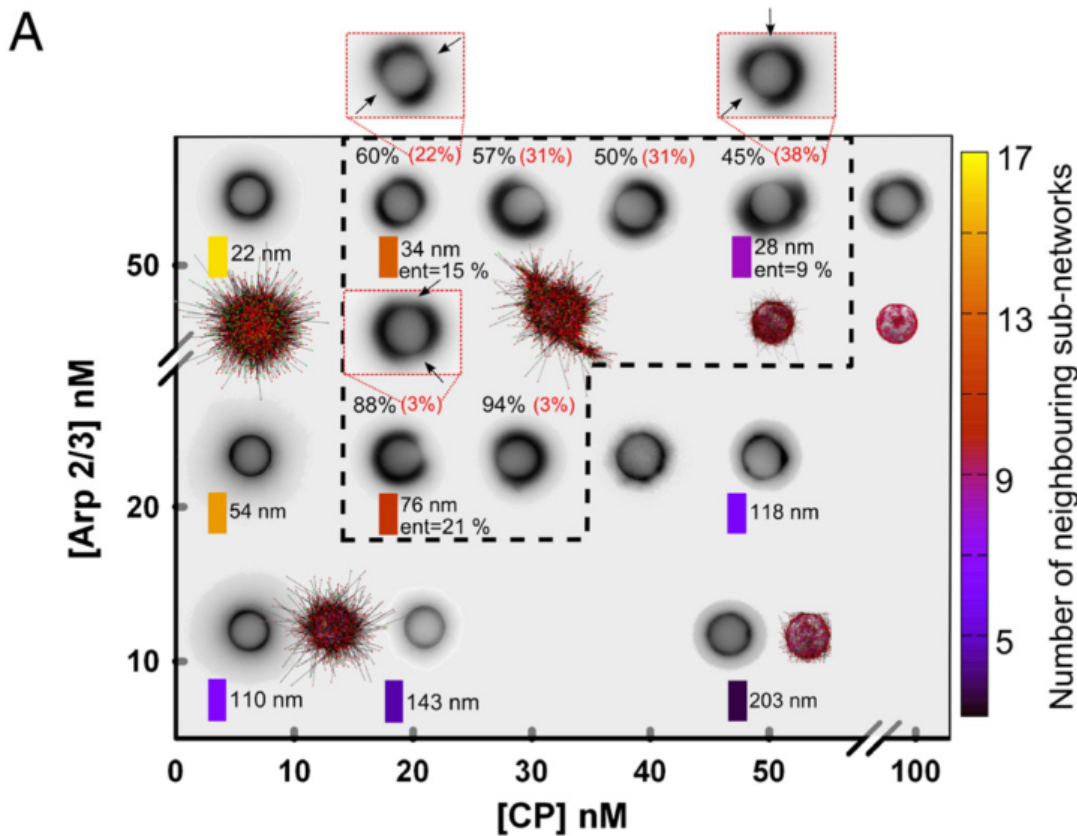


Figure 3.4: Phase diagram showing the concentrating of Arp2/3 and Capping Protein necessary for symmetry breaking (inside dotted line) on 4,5 μm beads both *in vitro* and *in silico*. Inverted fluorescent images and simulation are represented. Adapted from [Kawska, Carvalho, Manzi, et al. 2012]

We select a bead diameter of 4.3 μm in order to get a characteristic symmetry breaking time of 20 to 40 minutes. A smaller bead radius imply a faster increase of stress and a shorter symmetry breaking time. The choice of 4.3 μm allow enough time to proceed with the experiments before symmetry breaking occurs.

All measurements were made on an actively growing actin network which was not stabilized and before symmetry breaking occur for Capping concentration in the range 15 to 35 nM [Kawska, Carvalho, Manzi, et al. 2012].

3.3 Probe Bead System

Beside the actin-bead, the experiment requires a polystyrene bead passivated with BSA. These beads are referred to as probe-beads. The size of the probe-bead was chosen to be the same as the actin-bead, which ensure optical trapping of both beads in the same observation plane. In the case of beads with different

diameters, the axial forces on the beads are different. This axial displacement of the two beads during the indentation process leads to a component along the z-axis which eventually pushes one bead out of the focus.

3.4 Experimental description

To probe the actin network we trap an actin-bead with a growing actin-network and a probe-bead using time-shared *optical trap*, and measure force on the actin-bead using a QPD placed in the back focal plane of the condenser (*material and methods*).

To avoid systematic error of force measurement on moving traps, all the force recording are made on the static bead, which is in our case on the actin bead.

The indentation is a three step process ([Fig 3.5](#)):

- Approach phase at constant velocity $10\mu\text{m/sec}$ unless specified otherwise
- Relaxation phase of 3 second during which both traps remain static
- Retraction phase in which the probe trap move towards its initial position at $10\mu\text{m/sec}$.

3.4.1 Approach Phase

During the approach phase, the probe-trap approaches the actin-trap at constant speed ($10 \mu\text{m/s}$), as shown in [Fig 3.5](#) for times $t < t_1$. During this approach the actin bead will repel the probe bead due to the actin network growing on it. The force felt by the actin bead will progressively increase during the probe bead approach, eventually reaching the maximum as the probe-trap reaches its closest position to the actin trap. Note that during this process the force between the bead displace the beads from the respective trap center. The displacement of the beads in the trap remain small compared to the distance between the two beads. Hence in the following we consider that the probe-bead speed is equivalent to the trap approach speed of $10\mu\text{m/sec}$.

3.4.2 Relaxation Phase

After the approach , the trap remain static for a 3 seconds relaxation phase . The relaxation phase start at t_1 and finish at t_3 as shown on figure [3.5](#). The duration of the relaxation phase is sufficient to allow the partial relaxation of the actin cloud but remain sufficiently short compared to the actin polymerisation speed hence the polymerisation is not expected to change the properties of the network during indentation cycle as well as during repetitive indentation (*Figure #reproc*)

While the actin network relaxes, the forces between the two beads will slowly decrease thus leading to the bead getting closer to their trap center and closer to each other. The decrease in distance during the relaxation phase is small compared to the distance between beads. The decrease of force as well as the minimal change in distance between the two bead can be seen on [Fig 3.5](#) in the middle part.

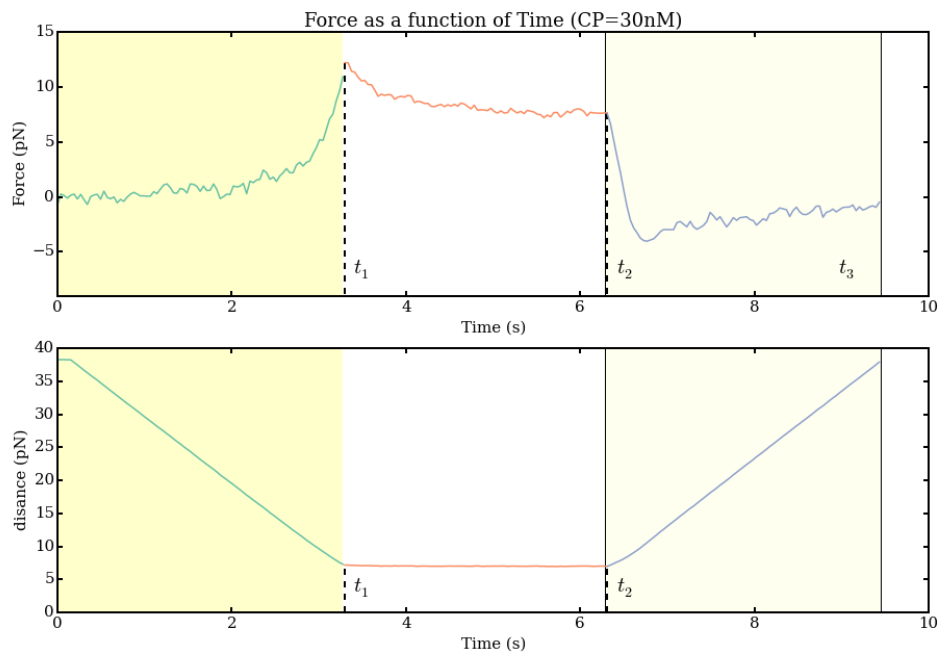


Figure 3.5: Upper graph : Force as a function of time on the actin-beads. Lower graph : distance between beads (distance between traps + displacement of beads from the trap center) as a function of time. First part of each graph (green curve, yellow back) represent the approach phase. Middle part (orange on white) is the relaxation phase, and right part (blue on pale yellow) is the retraction. Shown data is a subsample of around 1 of every 1000 points acquired. We can see on the second graph that the bead displacement on their respective trap is small compared to the dissplacement of the trap and justify the approximation of a probe bead speed equal to the probe trap speed.

3.4.3 Retraction part

After the three seconds of the retraction phase, the probe trap returns to it's initial position at $10 \mu\text{m/s}$ ($t > t_2$). During this phase, the force exerted between the two beads decrease, becomes negative, reaches a minimum, and eventually returns to zero as the probe bead recover its initial position (shown on [Figure 3.5](#) right part). Negative forces represent forces that tends to push the two beads towards each other.

3.4.4 Reconstitution of Force-distance-curve

From the position of he trap with time and the signal measured by the QPD the position of bead in the trap as well as the force exerted on each bead can be calculated. We can then recover the distance between bead centers as a function of time. The force-distance curve representing the force exerted by the probe bead on the actin bead as a function of the distance can be computed and is show in [Fig 3.6](#) where we can still distinguish the three phase of the indentation cycle, also marked by the color of the data.

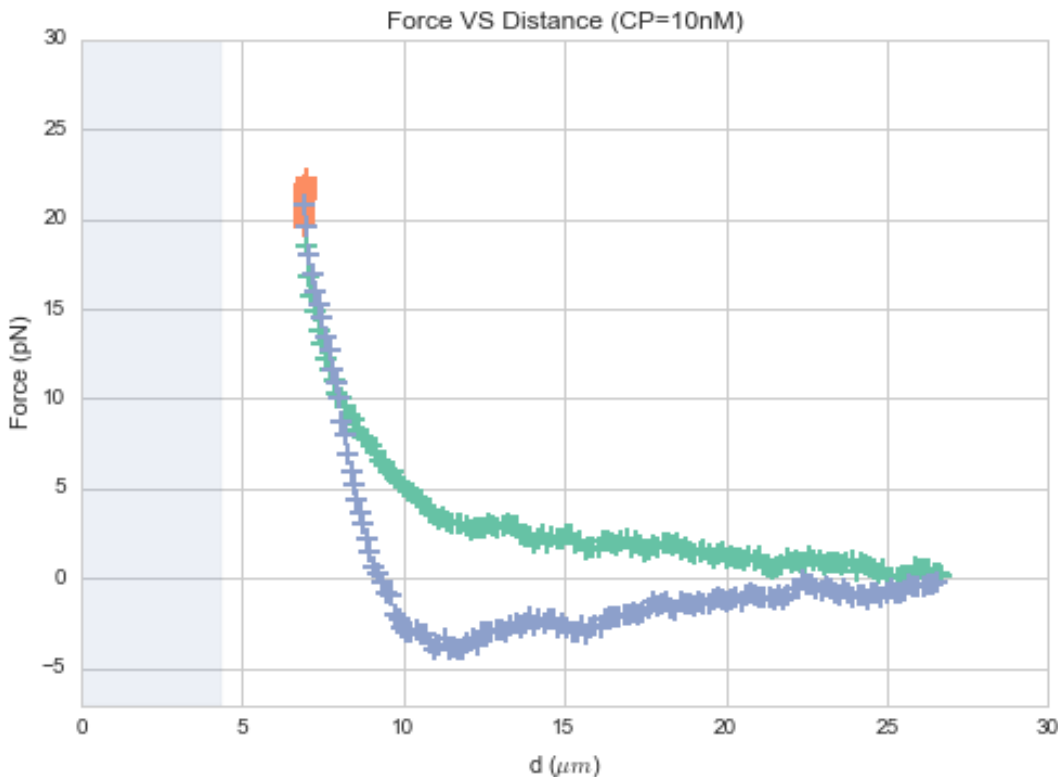


Figure 3.6: Force exerted on the actin bead as a function of the distance between the two beads centers. Color and data are the same as in [Fig 3.5](#). The probe bead starts from the far right, and gets closer while the force increases (green upper part of the curve), reaches a maximum, and enters the relaxation phase (orange part) where the force between the probe and actin bead decrease, while the distance also slightly decrease. During the retraction part (blue) the force rapidly decrease and reaches negative values while the bead returns to its initial position. Shown data is a subsample of 1 every 1000 points of acquired data. Shaded region represent areas where the two polystyrene beads would interpenetrate.

3.4.5 Repetitive indent

To check for reproducibility and non-plastic deformation of the network after indentation, the indentation cycle can be repeated several times at a few seconds interval. As the network is constantly growing during the measurement, this repeat also allows to check for possible change of network properties due to actin polymerisation. The force distance plot is shown in Figure 3.8.

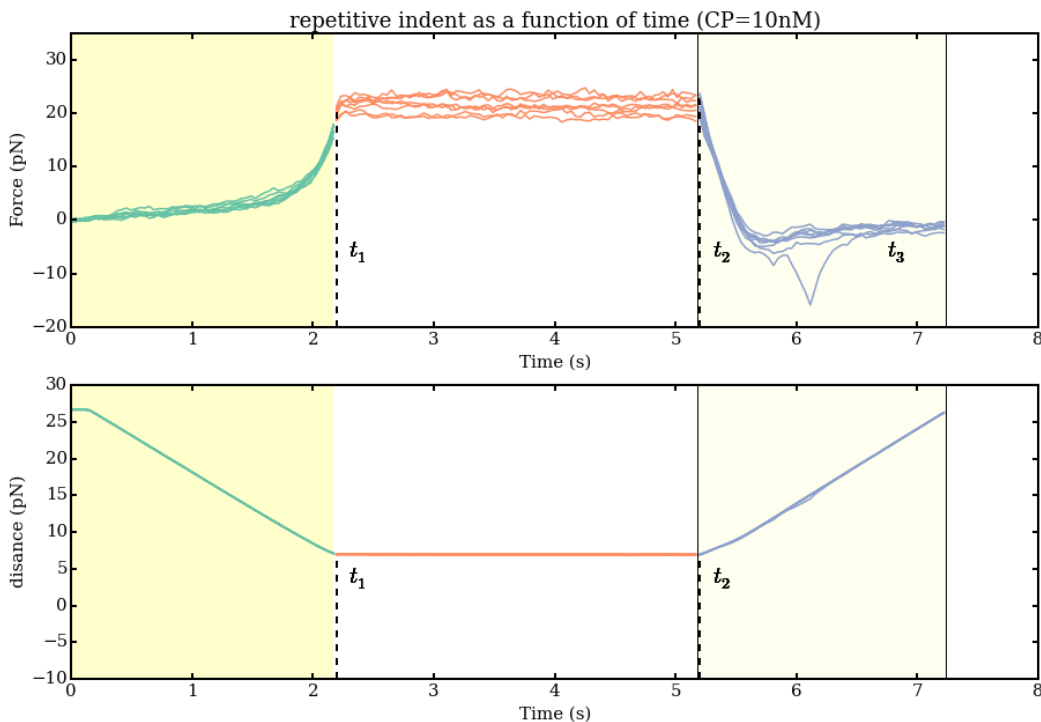


Figure 3.7: Upper graph : Force exerted on actin bead as a function of time for ten repetitive indents. In one of the cycle a sticking event can be seen in the retraction phase 6 seconds after the beginning of the cycle. Lower graph: Distance as a function of time for ten repetitive indents. The ten curves can difficultly be distinguished from one another. This shows the reproducibility of indentation curves.

3.4.6 Effect of approach speed

[Gardel, Valentine, Crocker, et al. 2003] suggest that for frequency higher than 0.1 Hz, force due to the viscous behavior of actin network can be in the same order as the elastic component. To test if such effect is important we measured the effect of the approach speed on the force measurements. Fig 3.9 presents the indentation speed affect the measurement by varying the approach speed from 10 to 30 $\mu\text{m/s}$ on the same actin bead.

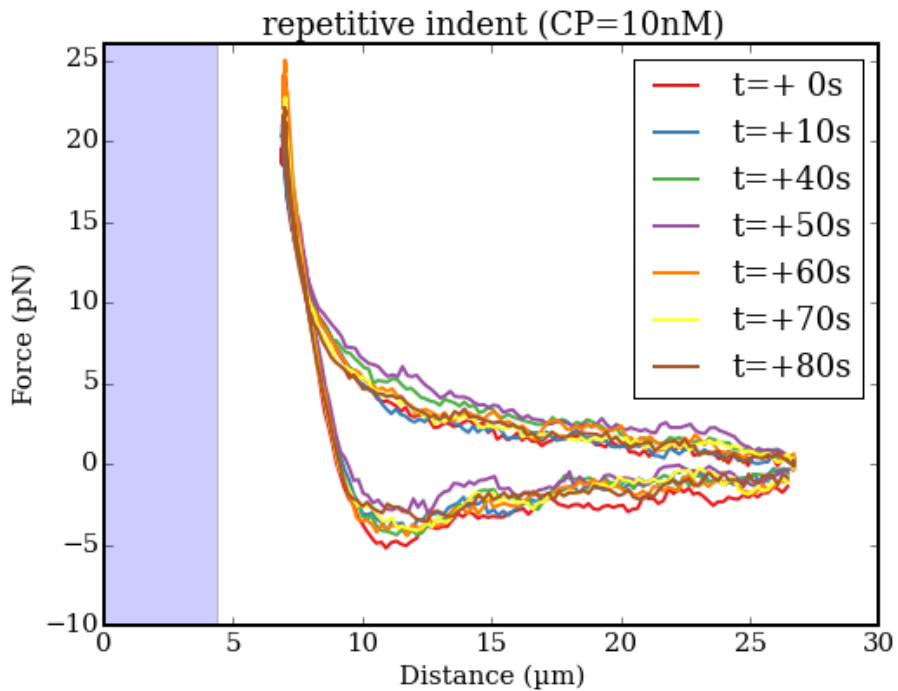


Figure 3.8: Figure showing the reproducibility of indentation process on a bead with 25nM Arp2/3 and 10nM CP Subset of data from Fig 3.7 shown with different color to represent the evolution of the indentation curve over time. Time is relative to first indentation. Shaded area represent zone where the two beads would interpenetrate.

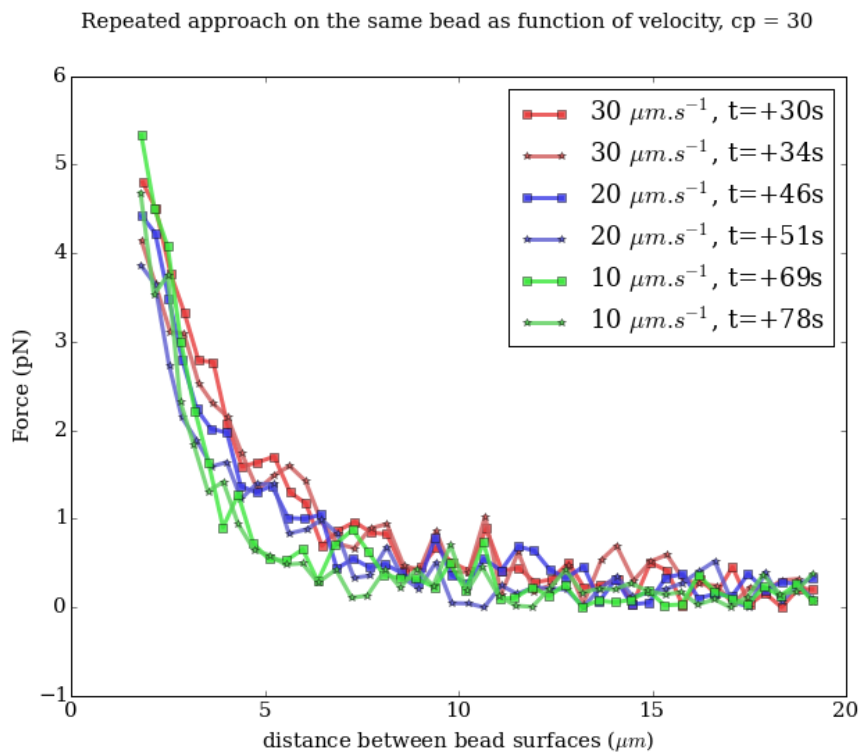


Figure 3.9: Approach phase of repetitive indents at multiple speed on the same actin-bead. The approach phase in the different conditions are similar, hinting for a negligible effect of the viscosity in the actin cloud at the speed considered.

3.5 Experimental observations

Using the bead system, we are able to reconstruct actin cortices *in vitro* and to investigate the mechanical properties inaccessible to other microscopy techniques like TIRF. Beyond the visible actin cortex we can detect the presence of an actin structure that have mechanical effects standing at distances of $> 10\mu m$, hence far beyond the thickness of the actin cortex ($\sim 1\mu m$) Figure 3.10 present a video that shows qualitatively that the actin cloud growing on actin beads is able to repel free floating probe beads before they reach the visible reconstituted cortex.

To quantify the distance at which the probe beads are first affected by the actin-cloud we measure the experimental noise by looking at the fluctuations of the trapped probe bead.

During the indentation we defined d_0 as the distance at which the average force felt by the probe bead is higher than the experimental noise. Typically the standard deviation is 2pN.

The repartition of d_0 with the concentration of Capping Protein is plotted in Figure 3.11.

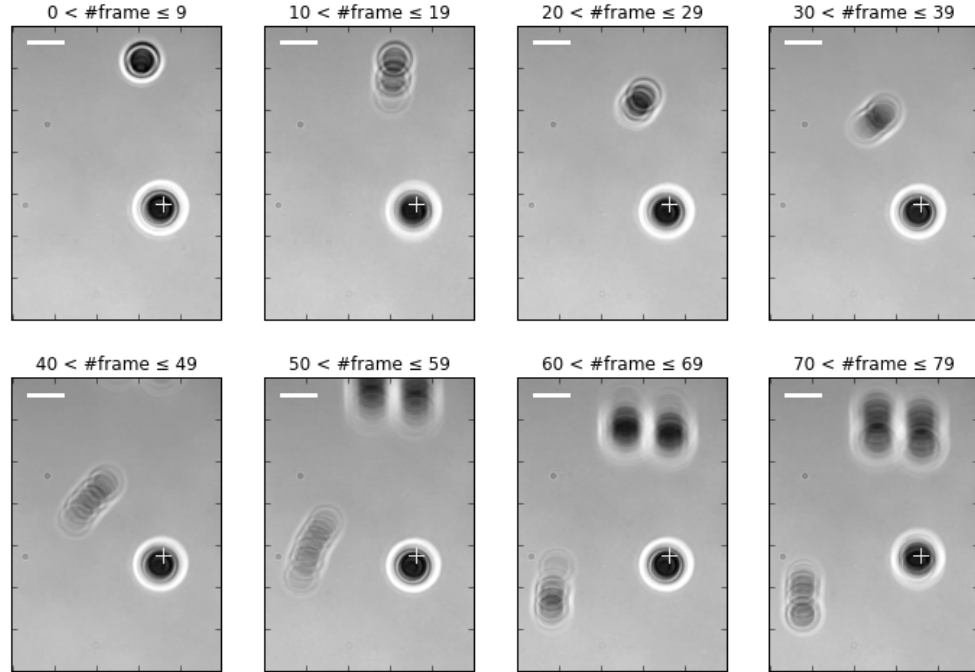


Figure 3.10: Chronophotography representing the displacement a trapped actin bead in a solution with probe bead. During this experiment, the actin bead is kept static in the optical trap (marked b the cross) while the stage is moved. Scale bar is 5 micrometers. Total movie duration is 21 seconds.

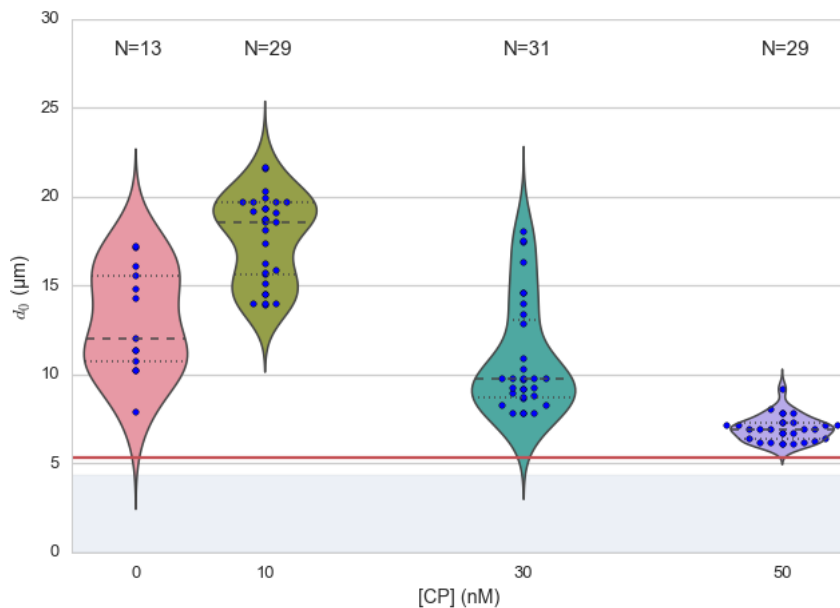


Figure 3.11: Repartition of the bead-center distance at which the actin cloud exert a force higher than the noise (d_0) on the probe bead, as a function of capping protein. Shaded region represent the position of the bead surface ($4.34 \mu\text{m}$) and the red line represent the bead surface+ $1\mu\text{m}$ (upper bound for the in vitro reformed actin cortex measured in [Kawska, Carvalho, Manzi, et al. 2012]). We see in this graph that for symmetry breaking conditions (CP 10 nM and 30 nM) the distance at which the actin cloud apply force on the probe bead is large compare to the thickness of the actin cortex. The distance at which the probe bead is able to detect the presence of the actin cloud decrease with increase in concentration of Capping Protein that restricts actin filament growth. The condition in the absence of Capping Protein are a particular case as no dense actin network forms on the surface of the actin bead.

3.5.1 Approach phase modeling

To extract mechanical properties using the three phases of the experiment we decided to model each part (approach, relaxation and retraction) independently. In particular, we fit force-distance curve of the approach phase using a power law with 3 fit parameters α, β, δ :

$$F(d) = \beta \times (d - \delta)^\alpha$$

In which F represent the force exerted on the probe bead, and d is the distance between bead centers. The powerlaw exponent α is expected to be negative as the force decreases with the distance d , and characterizes how fast the force increase as the two beads approaches. The prefactor β acts as a scaling factor of the force. The offset parameter δ shifts the curve on the distance axis. The model has the particularity that the force on the probe bead tends to $+\infty$ when the distance d get to δ . The force is undefined for values of $d < \delta$. Hence, the offset distance δ practically describe the distance at which the optical trap is not able to indent the network anymore.

In the case of a hard sphere the value of α would tend toward $-\infty$ leading to a infinite force increase at the contact between the two hard-spheres of same diameter and a value of δ equal to the diameter of the hard sphere. In this case $F(d > \delta) = 0$ and $F(d < \delta) = \infty$

The optical tweezer we use can apply forces up to 20pN, and the bead we use have a diameter of 4.34 μm , then have a cross section surface of surface of roughly $4.7\mu\text{m}^2$. Before escaping the trap, the probe bead can move up to 1 μm from its trap center. The material will indent have a typical size in the order of tens of μm , this leads to a maximum Young's modulus of :

$$\begin{aligned} E_{max} &\sim \frac{F_{max} L_{0,max}}{A_0 \cdot \Delta L} \\ &\sim \frac{50 \cdot 10^{-12} \times 10 \cdot 10^{-6}}{(2.15 \cdot 10^{-6})^2 \times 1 \cdot 10^{-6}} \\ &\sim 100 \text{ Pa} \end{aligned}$$

Any material with a stiffness much higher than 100 Pa can be considered as infinitely rigid.

The elasticity of dense actin gels around polystyrene beads has been measured in [Pujol, dRoure, Fermigier, Heuvingh, 2012] and found to be in the order of kPa. Therefore teh optical tweezer are not able to probe the mechanics of the dense gel on the surface of the bead. The value of δ is expected to be $4.34 \mu\text{m}$ as it include partially the dense actin gel.

The model can be fitted independently on each experimental approach phase. An example of such a fit is shown in figure [Fig 3.12](#) and quality of fit can can be measure by the coefficient of determination R^2 which has a media value of 0.97 across all fits.

The approach phase data can be corrected for the distance offset δ and plot in a log-log scale allowing for a better appreciation of the fit result. The corrected distance is noted with c indices $d_c = d - \delta$. In the model the force tends to infinity at $d_c = 0$.

In our experiments, the polystyrene beads have a average diameter of 4.34 μm , thus we expect δ to be higher than the bead diameter. Data with δ values lower than 4.34 μm (21 out of 127) are considered as unphysical and removed from further analysis.

As expected we find negative values for α . Surprisingly the value of alpha does not vary significantly when comparing experiments with different amount of Capping Protein and stay close to -1, with a mean value of -1.10, and a standard deviation of 0.38. The distribution of power law exponent can be seen on [Fig 3.14](#)

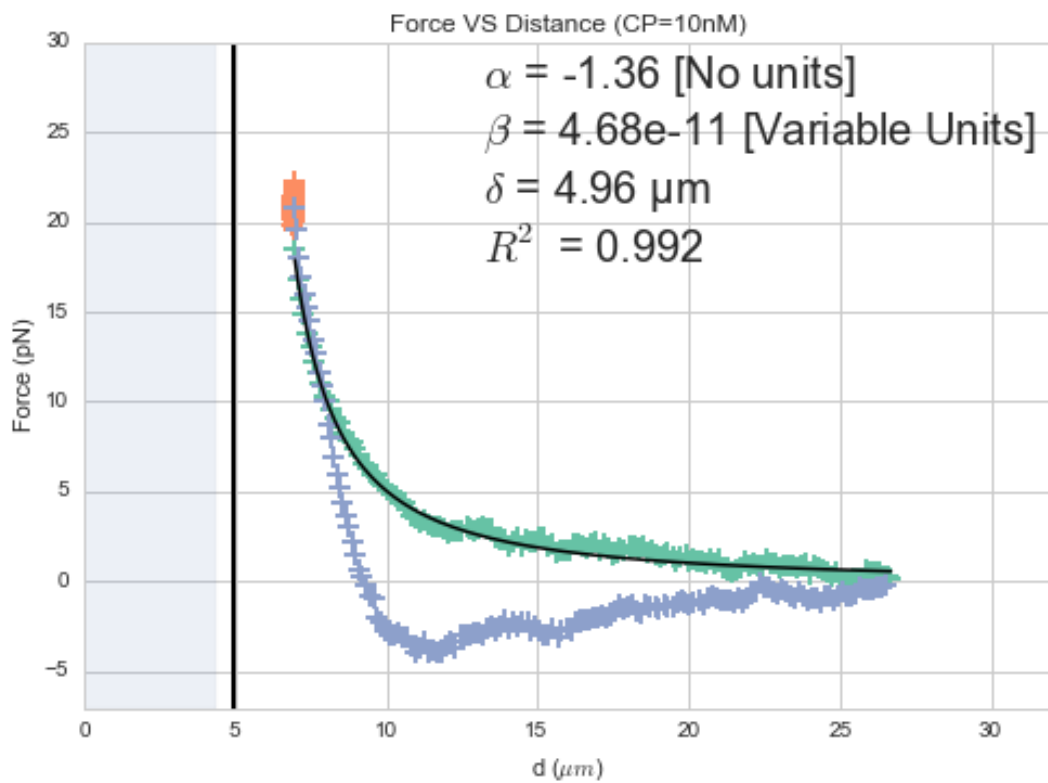


Figure 3.12: Power law model fitted on approach phase data for one experiment in the presence of $[\text{CP}]=10\text{nM}$, with the particular values found for the fit parameters. The vertical line represent the point at which the model diverges and the force goes to infinity, that is to say δ . The shaded region corresponds to the distance at which the two bead would interpenetrates. Relaxation (orange) and retraction (blue) data are not fitted.

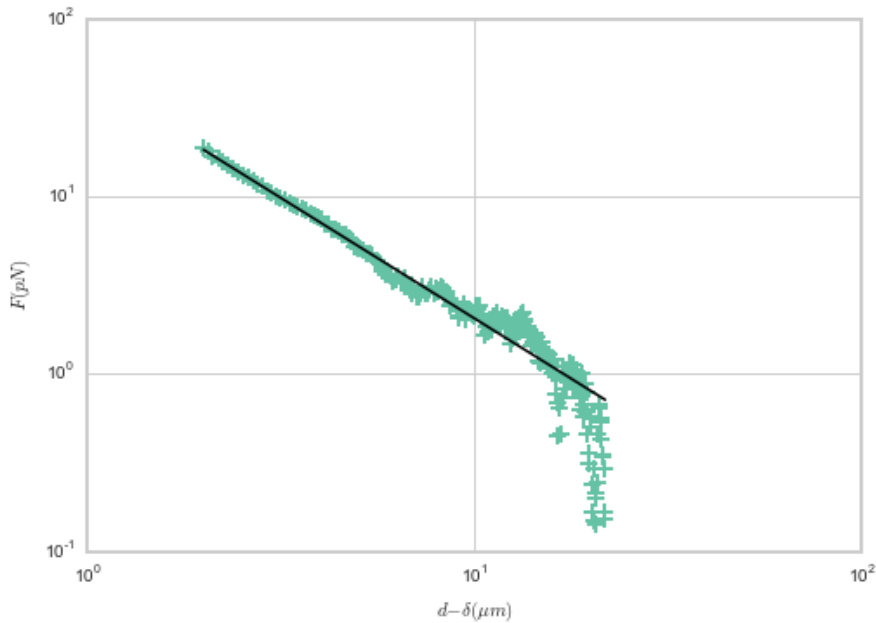


Figure 3.13: Force on actin bead during approach phase as a function of bead distance minus distance offset δ plotted on a log-log scale. Black line represents the power law model with correction of the offset distance. Same data as Fig 3.6 but showing only approach phase.

Due to the scale invariance of the inverse power law found above, all the approach phases data can be rescaled into a single master-curve. This is done by dividing the force by the maximum force F_{max} reached during the approach and rescaling the distance by the minimum approach distance from which δ is subtracted.

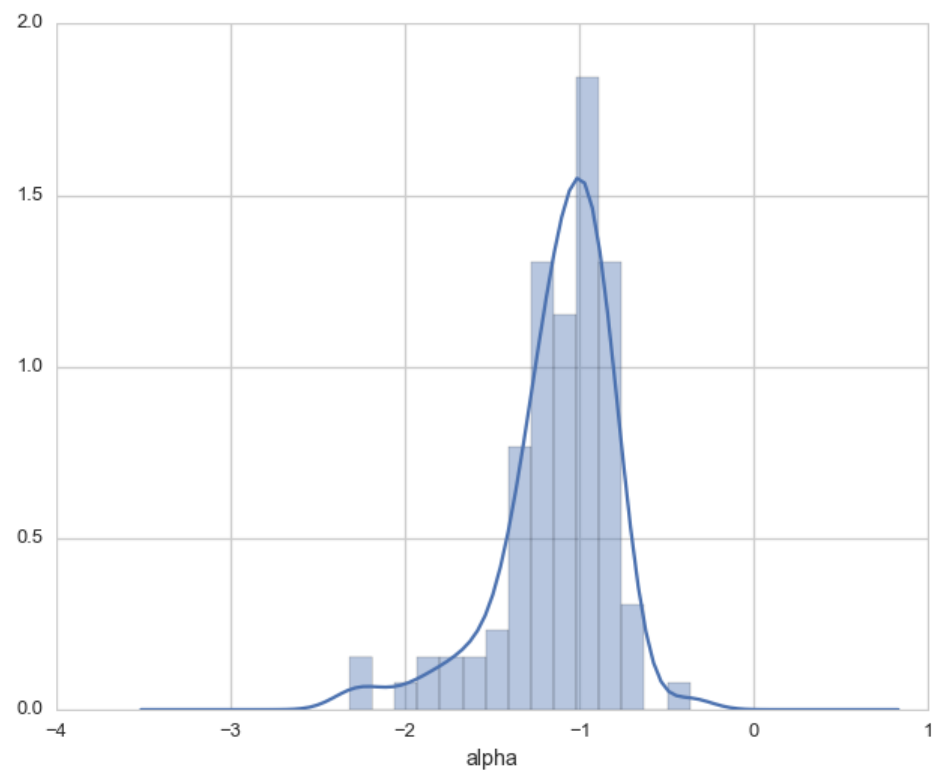
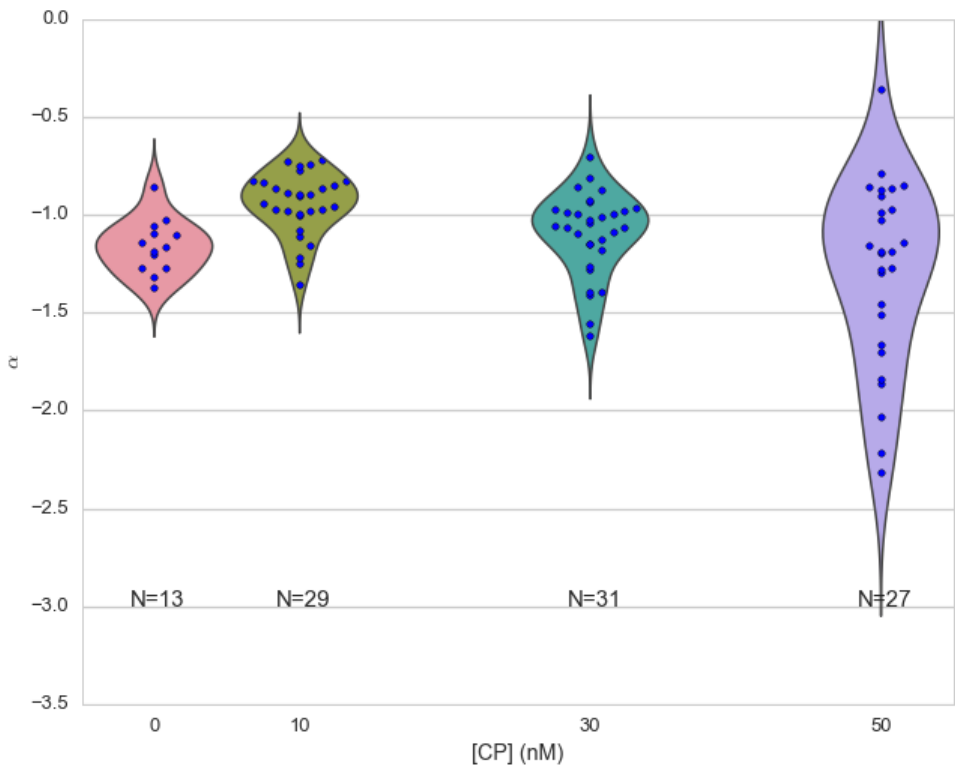
The rescaled data confirm an average power law exponent of ~ -1 , the breakdown of the average exponent beyond $d_c/d_{c,min} = 10$ can be explained by the statistical effect of having less data for long distance.

3.5.2 Variation of parameters with Capping Protein

At the chosen concentration of Arp2/3 the bead system can show symmetry breaking in the correct range of concentration of Capping Protein of 10 to 30 μM . In absence of Capping Protein the dense dendritic network does not form on the surface [Kawska, Carvalho, Manzi, et al. 2012]. At low Capping Protein concentrations ($< 10 \mu\text{M}$) it seem not able to generate enough stress to rupture, and at too high concentration ($> 35 \text{nM}$) the visible gel is thin and do not break symmetry either. We then investigated the variation of each of the fit parameters for concentrating of Capping Protein ranging from 0 to 50 nM.

We have already seen previously that the powerlaw exponent factor α didn't vary with the amount of Capping Protein in solution (Fig 3.14). The two other parameters investigated are the prefactor β . For the same value of α and δ , the higher β is the stronger the interaction between the two beads for the same distance d_c . We can see on Figure 3.16 that the average value for the prefactor decreases with increase of Capping Protein concentration.

The last parameter of our model is δ , distance at which the force diverges. It can be seen in Figure 3.17



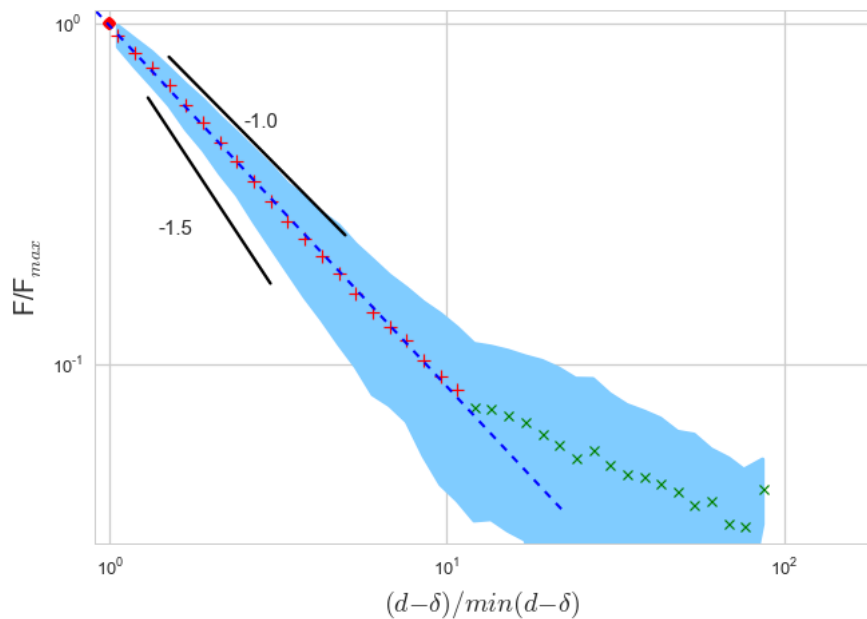


Figure 3.15: Representation of rescale approach data on a log-log scale. Red and green crosses correspond to average values. Blue area corresponds to average +/- standard deviation for each average bin. Red dot in the upper right corner corresponds to the point (1,1) with respect to which all data has been rescaled. Blue dashed line show a powerlaw fit of the average data for $d_c/d_{c,min} < 10$ (red cross), fitted slope is -1.06 . As an eye guide, slope of -1 and -1.5 have been represented.

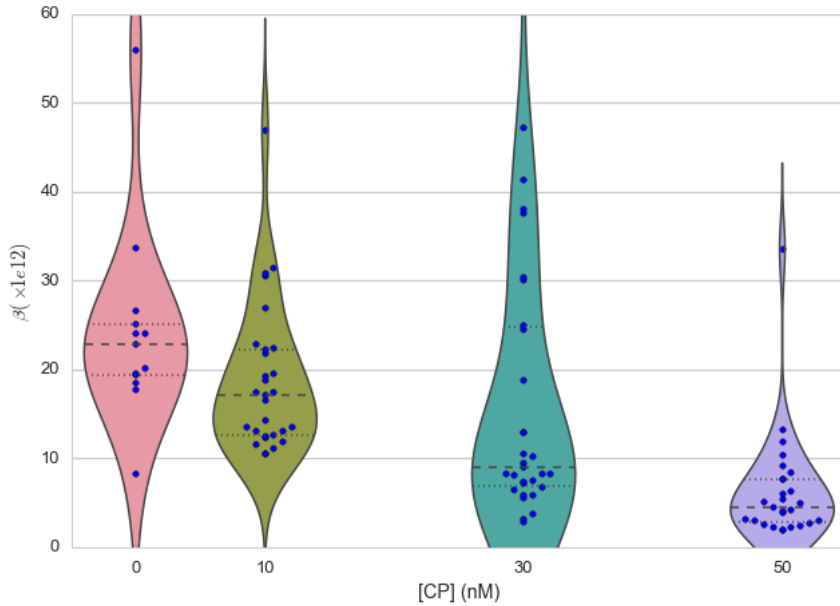


Figure 3.16: Violin plot showing the repartition of prefactor with the quantity of Capping Protein. Decrease of prefactor with increasing amount of Capping Protein indicates a lower force between the probe bead and the actin bead for the same corrected distance between bead centers

that with the exception of zero capping protein, the distance at which the model diverges gets closer to the diameter of the polystyrene bead as the concentration of Capping Proteins in the medium increases. It is interesting to see that the distance offset δ is very close from the bead diameter in the absence of capping protein, when no biomimetic actin cortices forms.

3.5.3 Determination of Young's Modulus

To determine the mechanical properties of the gel between the actin and the probe bead, we model it as a purely elastic material. The viscous effects are neglected in the approach part as the approach at different speed show no clear effect on the approach curves (Figure 3.9). We consider the compression of the material between the two beads. The surface of the compressed material is approximated by the projected surfaces of the bead along the direction of compression (πR^2). The thickness of the compressed material is taken as being the distance between bead centers corrected by the distance offset δ as any material below delta can be considered as infinitively rigid for the optical tweezer.

The stress exerted onto the material projected onto the bead surface or radius R can be written :

$$\sigma = \frac{F}{\pi R^2}$$

For small deformation the local strain of the material u can be written as a function of the corrected bead position d_c and the considered location along the axis between the two bead center x :

$$u(x) = \frac{d_c - x}{d_c}$$

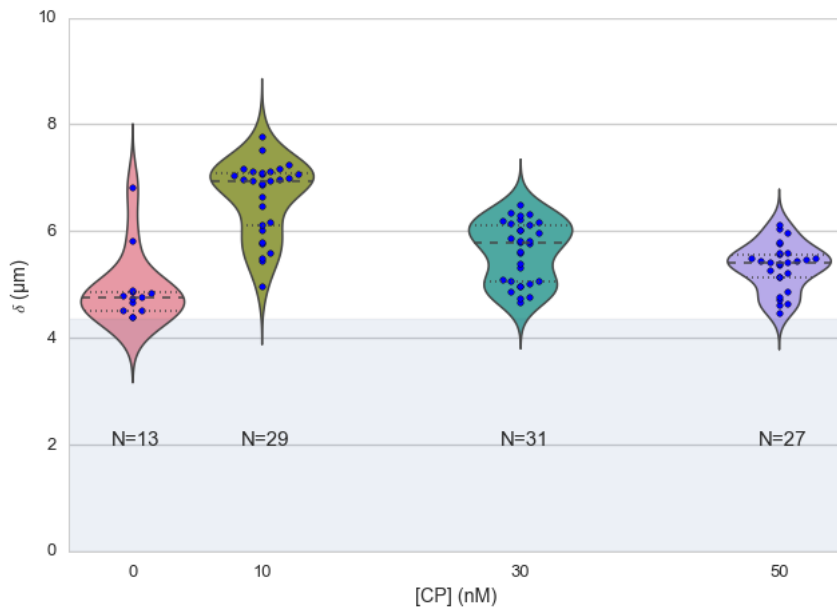


Figure 3.17: Violin plot showing the variation of the offset distance δ with the capping protein concentration. The shaded area represents the non-physical region which would correspond to a diverging force beyond the contact of the two polystyrene beads. Experimental data with δ value in this regions have been excluded from further analysis.

We can express the local differential strain around the position d_c of the bead : $\partial u = -\partial x/\partial d_c$ in which the minus sign reflect the choice of the coordinate system: a decrease in x with a positive Young's modulus E should lead to an increase of the exerted force. The locally felt Young's modulus at the distance d_c is then

$$E(d_c) = \left. \frac{\partial \sigma}{\partial u} \right|_{d_c}$$

By injecting the expression of u and σ this lead to :

$$\begin{aligned} E(d_c) &= -\frac{d_c}{\pi R^2} \times \left(\frac{dF}{dx} \right) \Big|_{x=d_c} \\ &= E_0 d_c^\alpha \end{aligned}$$

In which the value of E_0 can be expressed as function of the power law exponent α and the prefactor β :

$$E_0 = -\frac{\alpha \beta}{\pi R^2}$$

Experimentally, the probed Young's modulus corresponds to the average mechanical properties of the actin cloud between the surface of the actin bead and the surface of the probe bead and do not reflect the variation of the mechanical properties of the uncompressed actin cloud with position. Physically E_0 correspond to the Young's modulus as a corrected distance of $d_c = 1\mu m$ (See Fig 3.18) The geometry of the system and the fluorescence signal suggest a decrease of the density of the actin cloud with the distance from the actin-bead center. All values reported later represent estimation of elasticity of an effective Young's modulus. The

value of this effective Young's modulus are 3 orders of magnitude smaller than know elasticity of dendritic gel formed on bead that are in the order of kPa [Marcy, Prost, Carlier, Sykes, 2004].

This difference in elasticity might explain why the mechanical actions of this actin cloud as not been seen before in other measurement like micro-pipette aspiration, micro needle deformation or Atomic Force Microscopy indentation that have sensitivity in the order of nN while the forces exerted by this actin cloud are in the order of pN.

Nonetheless, [Gardel, Valentine, Crocker, et al. 2003] show that such low moduli can be obtain using sparse entangle actin network, and confirm the idea that the actin-cloud seen with the optical-tweezer indent experiments has a fundamentally different structure than the dense dendritic network on the actin bead surface.

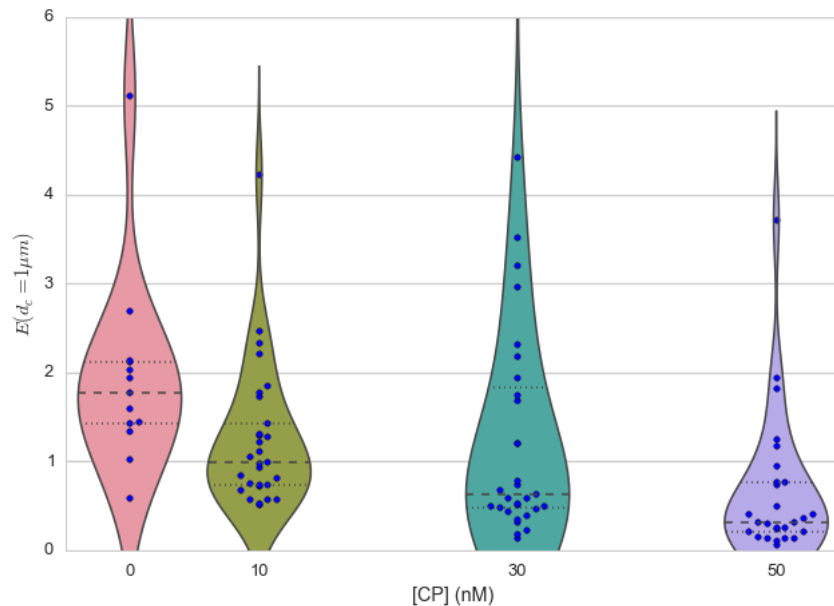


Figure 3.18: Young's Modulus prefactor as a function of capping protein show a decrease of average Young's modulus with an increase of Capping Protein concentration.

3.5.4 Mechanical properties

To investigate the mechanical properties of the network that should arise from a $\alpha = -1$ power law, we model the deformation of the actin cloud by the theory of semi-flexible entangled polymer networks ([Isambert, Maggs, 1996], [MacKintosh, Kas, Janmey, 1995], [Morse, 1998a]).

The Young's modulus of semiflexible filaments in a 3D environment can be expressed as a function of filament contour length density ρ and the entanglement length L_e as [Morse, 1998b]:

$$E = \frac{2.(1 + \nu).7.k_B T \rho}{5L_e}$$

In which ν is the Poisson ratio that allows the conversion from shear to elastic modulus. Previous study have investigated the non-linear stiffening of such actin network for large deformation [Semmrich, Larsen, Bausch, 2008] and found that in our condition, the linear description of theses networks holds to describe the actin-cloud.

Similar to [Morse, 1998a] we express the entanglement length as a function of persistence length and filaments density: $L_e \approx L_p^{1/5} \rho^{-2/5}$. We can reduce the expression of the Young's modulus to a function of the following parameters :

- The Poisson Ratio ν ,
- The persistence lenght of actin filaments L_p
- The mesh size of the network $\xi_0^2 = \rho_0$
- The “size” of the cloud, for which we use the distance at which the force is first significant d_c

We need also the consideration that for a general compressible material, the only variable that changes during compression is the density ρ which could be made to depend on the corrected distance $\rho \rightarrow \rho(d_c)$

Thus leading to :

$$E(d_c) = \frac{(1 + \nu).14.k_B T}{5L_p^{1/5}} \times \rho(d_c)^{7/5} \quad (3.1)$$

The scaling exponent of E in equation (3.1) with d_c should match the exponent of the experimentally found power law α . Thus the density can be expressed in the following form :

$$\rho(d_c) = \rho_0(d_c/d_0)^{5/7 \times \alpha} \quad (3.2)$$

By the definition of ρ in [Morse, 1998a] which is the filament contour length per unit volume, we can determine the mesh-size ξ_0 of the undeformed network:

$$\xi_0 = 1/\sqrt{\rho_0}$$

By comparing this to the phenomenological fit we can express the elastic modulus as a function of the distance and the mesh size, as a function of the fit parameters and characteristic scales of the system.

$$\begin{aligned} E(d_c) &= \frac{(1 + \nu).14.k_B T}{5L_p^{1/5}\xi_0^{14/5} d_0^\alpha} \times d_c^\alpha. \\ &= E'_0 \times d_c^\alpha \end{aligned} \quad (3.3)$$

In which E'_0 can be identified as E_0 in (3.1) to extract the closed form solution for the meshsize ξ_0 :

$$\xi_0 = \left(-\frac{(2 - \frac{5}{7}\alpha).k_B T \pi R^2}{5\alpha\beta L_p^{\frac{1}{5}} d_0^\alpha} \right)^{\frac{5}{14}}$$

The found mesh size is in the order of 0.3 to 0.4 μm which is consistent with previous findings :Morse1998b. The variation of the meshsize can be seen on Fig 3.19 and does not seem to have a correlation with the concentration of capping protein.

We explore the correlation between the mesh size and δ by plotting the mesh size again the distance offset δ (Fig 3.20). Figure 3.21 shows the relation between the mesh size and the offset distance δ independently for each concentration of Capping Protein.

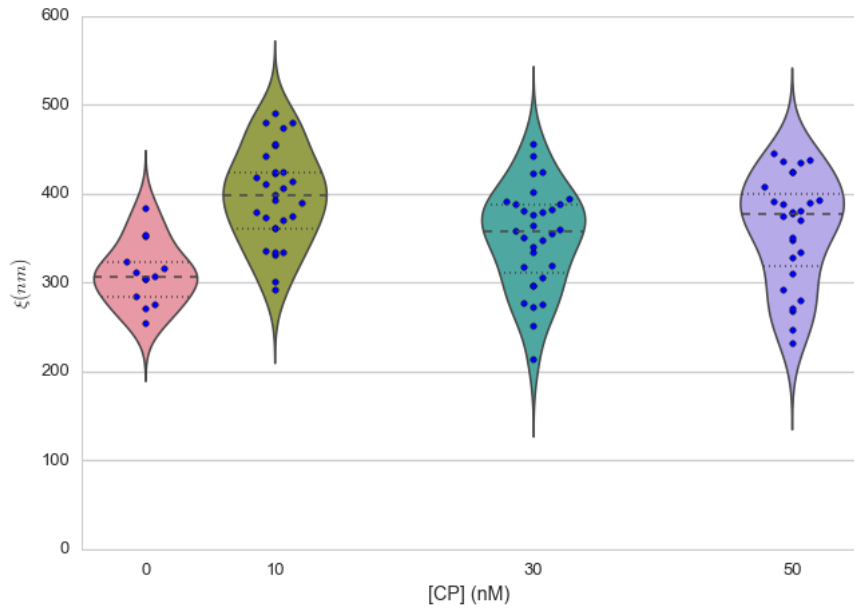


Figure 3.19: meshsize vs capping.

From (3.1) and (3.3) by identifying the prefactor it is also possible to extract the Poisson ratio (ν) of the compressed material :

$$\nu = \frac{1}{2} \times \left(\frac{5}{7} \cdot \alpha + 1 \right) \quad (3.4)$$

The Poisson ratio depends only on the powerlaw exponent and thus varies little with the amount of Capping Protein concentration. We found value of the Poisson ratio that are between 0.07 and 0.16 corresponding compressible foam-like materials that do not expand highly in the direction orthogonal to the compression axis. Previous study of bulk actin network find a Poisson ration of 0.5 (incompressible material) for actin concentration of 21.5 μM . We suspect that the low actin concentration used in our experiments (4 μm) is the reason for the low Poisson Poisson Ratio. Also the local structure of filaments emanating from the bead may explain the large compressibility of our actin cloud.

3.5.5 Interpretation

The results of our data analysis lead to the interpretation that a dense actin gel of elasticity close to $\sim 1\text{kPa}$ is polymerized on the surface of the actin bead. This stiff gel cannot be indented by the optical tweezer. Beyond this dense gel a soft actin cloud with an effective elastic modulus of 1 Pa and below is present and extends on distances that are several times bigger than the thickness of the reconstituted actin cortex (Fig 3.22). The structure of this actin cloud is expected to be quite different from the dendritic gel and be mostly constituted of loosely entangle actin filaments.

In this model, the offset distance δ correspond to the limit of the dense dendritic actin network mimicking the actin cortex that grows on actin bead and which elastic modulus makes it impenetrable by the optical tweezer we use. The value of δ we found are coherent with the measured thickness $e \simeq \delta - 2.R_{bead}$ of

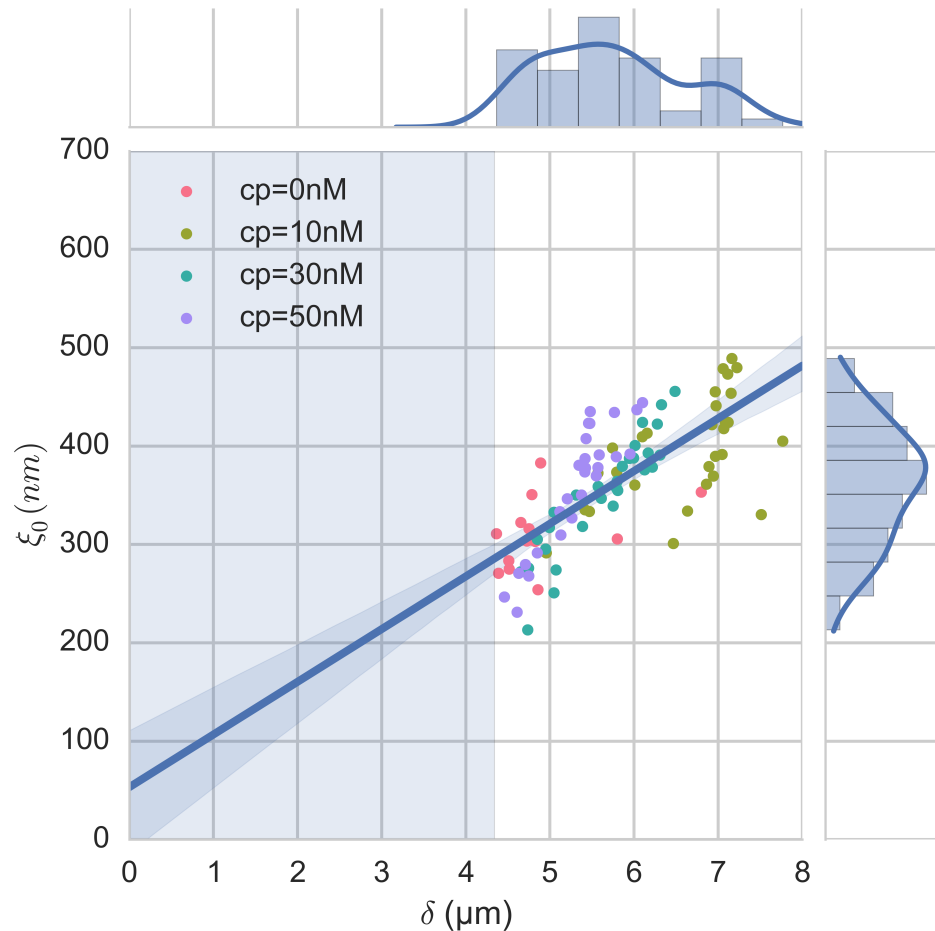


Figure 3.20: Correlation of the meshsize ξ_0 with the distance offset δ , with marginal distribution as histogram on the side and on the top. Shaded regions represent confidence interval at 95%.

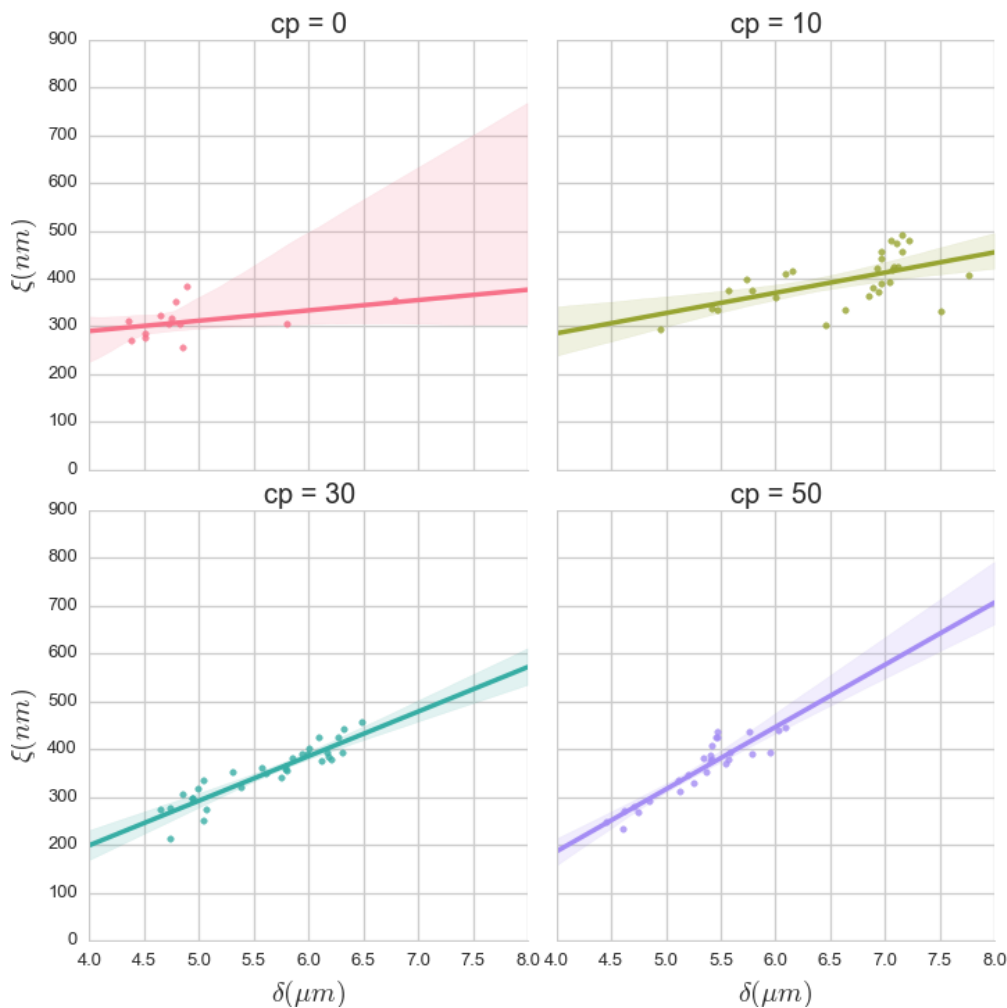


Figure 3.21: Same figure as Fig 3.20 for each concentration of capping protein, with linear regression and confidence intervals at 95%

the biomimetic actin cortex as measured by epifluorescence in [Kawska, Carvalho, Manzi, et al. 2012] and found to be in the range of 1 to 2 μm . The decrease of δ with Capping Protein is also coherent with the decrease of gel thickness.

The filaments composing the actin cloud emanate directly from the actin cortex in which the nucleation of actin polymerisation started at the surface of the bead. Eventually, a few filaments can escape from the network and are capped by the Capping Protein only when the growing extremity is already several micrometers from the bead surface.

The thickness of the actin cortex e as measured in [Kawska, Carvalho, Manzi, et al. 2012] increases with time during the polymerisation of actin. We can predict that the offset distance δ should increase with time, except in the absence of Capping Protein where no actin cortices form. This can be verified on [figure 3.23](#) that show the evolution of δ as a function of polymerisation time.

3.6 Relaxation phase

The approach phase of the indentation cycle has been modeled with a purely elastic mode. However, the force distance plot shows a significant dissipation marked by an hysteresis [Fig 3.6](#). The repetitive indent cycle giving the same force-distance curves ([Fig 3.8](#)) allow to exclude plastic deformation. We can hence reject the hypothesis of ruptures of the actin meshwork or breakage near the entanglement points.

The theory of entangled filaments networks that allowed us to understand the link between the phenomenological model and the mechanical properties of the network also propose a relation to explain the relaxation of the network.

In this model [Morse, 1998a], the visco elastic modulus E is a function of time and can be written as $E(t) = E \times \chi(t)$ with

$$\chi(t) = \sum_{n,odd} \frac{8}{n^2\pi^2} \exp\left(-\frac{n^2\pi^2 t}{\tau_{rep}}\right) \quad (3.5)$$

In which $\tau_{rep} = \frac{l_f^2}{D_{rep}}$ is a single fit parameter that depends on diffusion constant for filament reptation D_{rep} and the filaments length l_f . In this form, χ is a sum of exponential decays with well defined characteristic timescales and amplitudes that decreases as $1/n^2$. To fit this model to the data of the relaxation phase, we can limit ourselves to the first 40 terms of the sum as any of the subsequents terms represent timescales we cannot reach with out experimental resolution.

It should be noted that the value of $\chi(t = 0)$ is 1 and should be treated particularly in order to insure continuity of the force applied on the actin-bead in the model.

Using this sum of exponential decays is coherent with the common findings of power-laws found in the frequency-dependant shear modulus of both *in vivo* and *in vitro* actin networks as well as the relaxation behavior found in cells.

In order to determine τ_{rep} , the Young's modulus determined in the approach phase is used and the model is fitted against the relaxation data. A result of such a fit can be seen on [Fig 3.24](#). The value of τ_{rep} are highly variable and the fit can be difficult when the relaxation is slow or in the order of the measured noise. Variation of τ_{rep} with the concentration in Capping Protein can be seen on [figure 3.25](#), and one example of fit on the [figure 3.24](#)

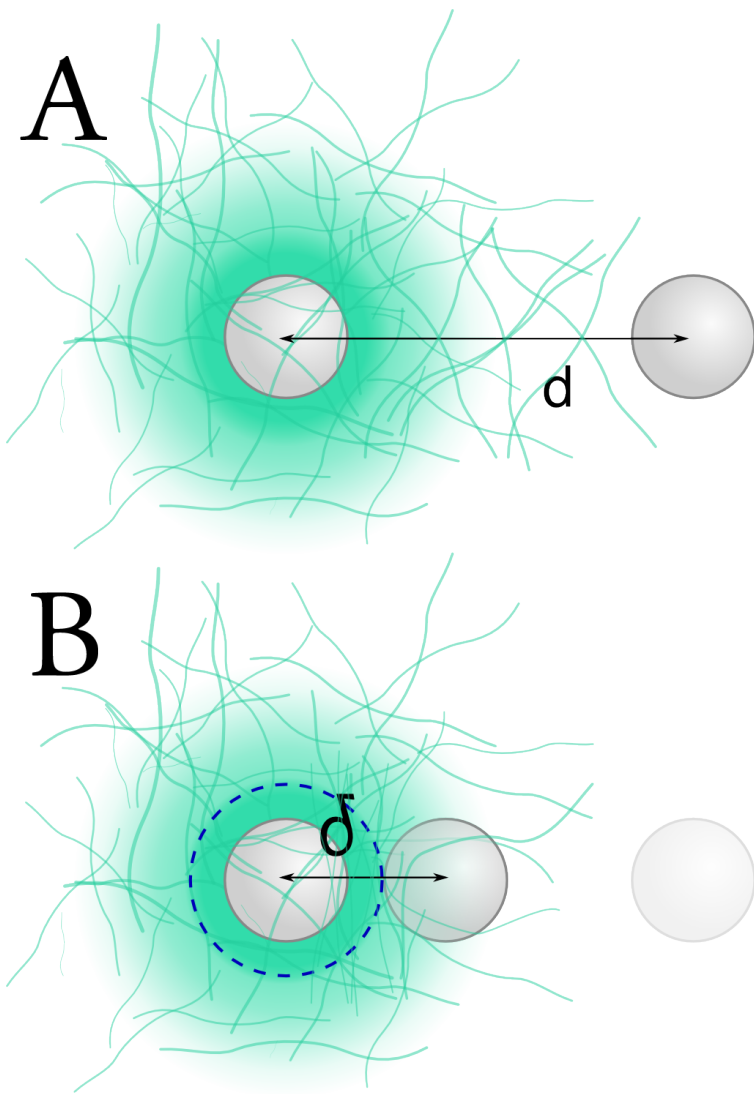


Figure 3.22: A) Schematic of an actin cloud. Left: The actin bead triggers actin polymerisation. Right Probe Bead. On the surface of the actin bead a dense and dendritic network forms a biomimetic actin cortex with an elastic modulus close to the kPa (Dark Green). From this actin cortex emanate a softer actin structure : The actin cloud . The actin cloud is loosely entangled network formed by the filaments escaping from the bead actin cortex and extends on several micrometers. The actin cloud has an average elastic modulus which is several order of magnitude softer than the actin cortex. B) From the point of view of the probe bead in optical tweezer, the system (actin-bead+actin cortex) behave as a hard-sphere of radius $\delta - R$

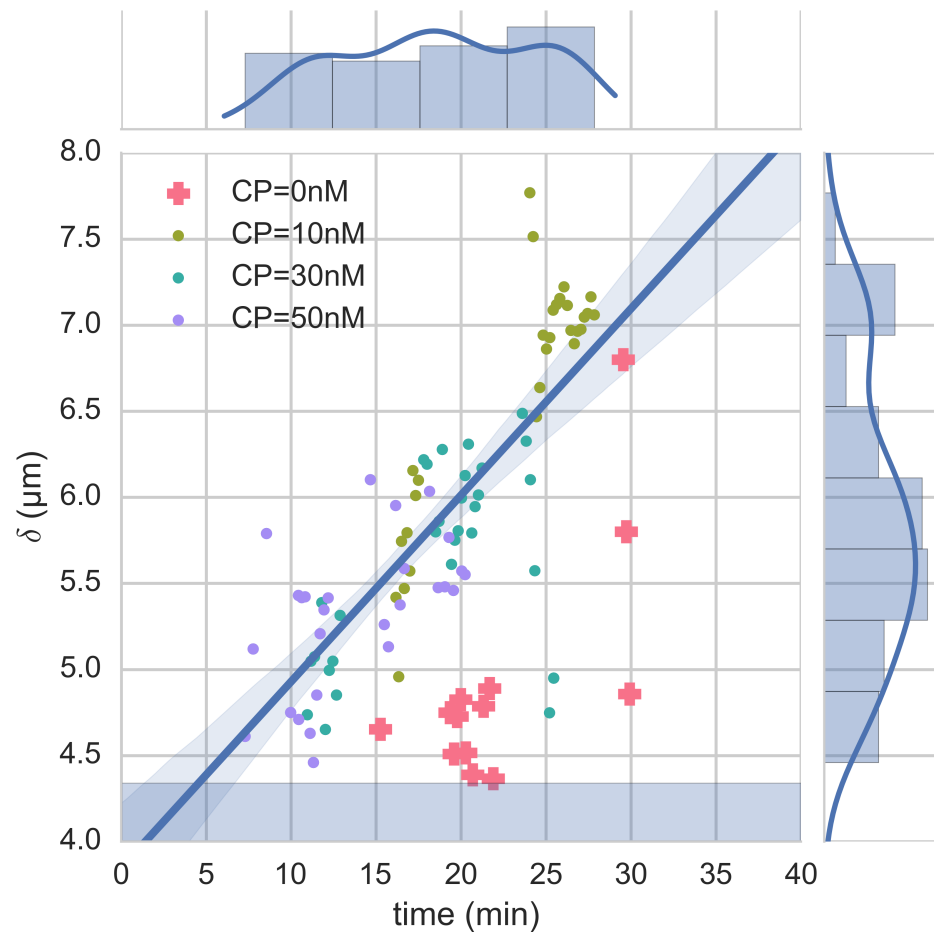


Figure 3.23: Distance offset δ as a function of time (min) since mix of actin, ATP and beads. Linear fit with confidence interval at 95% (light shaded area) and bead surface (dark shaded area). Sample in the absence of Capping Protein are not taken into account in the regression (Pink +). The increase of δ with time is coherent with the measured increase of the gel thickness e as measured in [Kawska, Carvalho, Manzi, et al. 2012]

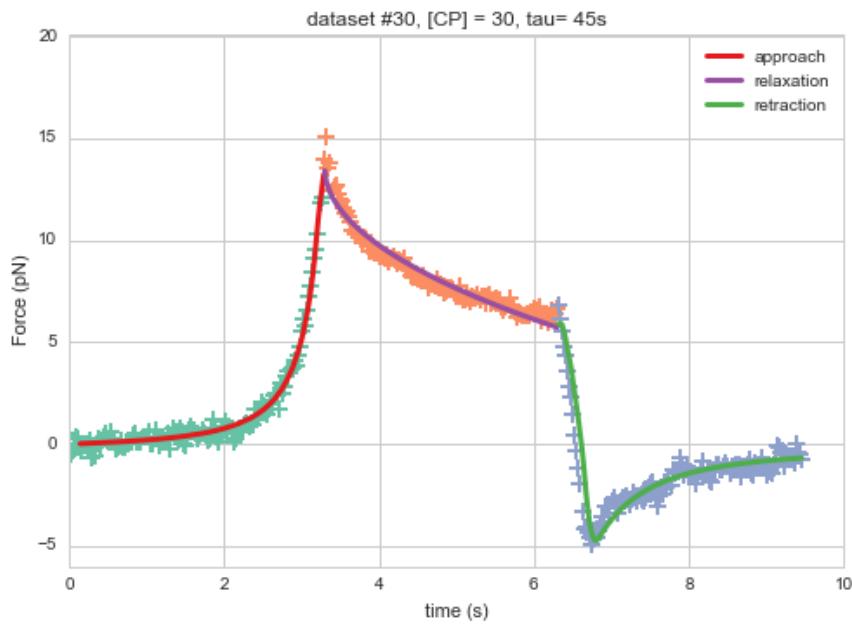


Figure 3.24: Force as a function of time as well as fit for the 3 phases, approach, relaxation and retraction.

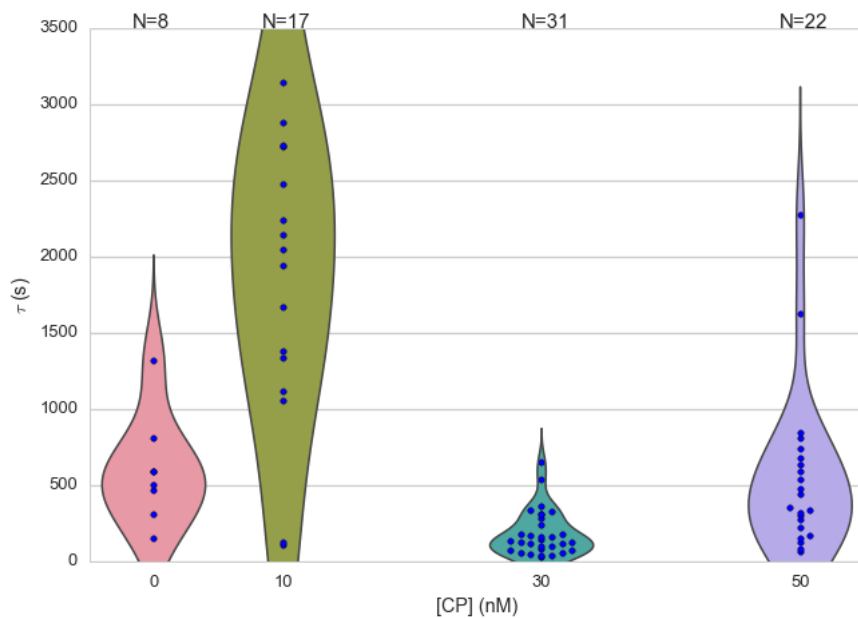


Figure 3.25: Violin plot showing the repartition of τ_{rep} as a function of capping protein. Outlier (τ_{rep} negative or greater than tens of minutes removed)

We can see here that the polymer model introduced in [Morse, 1998a] allow to completely fit the succession of approach and relaxation phases. To check if the fit parameters give realistic value, we can estimate the diffusion constant for filament reptation D_{rep} .

$$D_{rep} = \frac{k_b T}{\gamma l_f}$$

In which $\gamma \approx 2\pi\eta_s/\ln(\xi_0/d_f)$ is the friction coefficient per unit length. γ depends on the solvent viscosity η_s , the mesh-size ξ_0 and the filament diameter d_f (7nm for actin). We use $\eta_s = 10^{-3} Pa \times s$ for water and a mesh size in the order of 400nm as determined from the approach phase (Fig 3.25). Using τ_{rep} given by the fit, this lead to filaments length ranging from 3 to 8 μm , which is consistent with TIRF experiments and simulation as done in [Kawska, Carvalho, Manzi, et al. 2012].

3.6.1 Retraction Phase

During the retraction phase the force decreases, becomes negative after a retraction of 3 to 4 μm , and show a slow return to 0 at large distance. Sticking event can be seen when the force becomes abruptly negative before relaxing as fast. Figure 3.26 show such a sticking even happening during an indentation cycle.

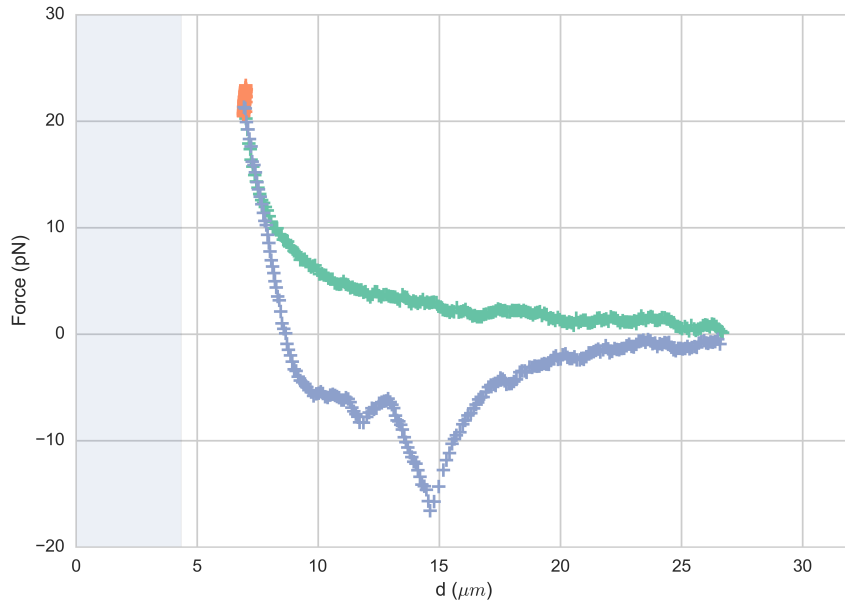


Figure 3.26: A sticking event at $d=15\mu m$ where the force can be seen decreasing rapidly up to -18 pN before quickly returning to its normal value. A second smaller sticking even is present at $d=12\mu m$. Sticking even appear roughly 20% of the experiments.

We assume that the sticking events are characteristic to non-specific interaction between the probe bead and the actin cloud. In the case when no sticking even is present, we assume partial closing of the actin cloud beyond the probe bead during the relaxation phase and model the retraction curve as a transition between the damped-approach curve and a penetration of the probe bead through the closing actin cloud.

Durring the approach phase the force exerted on the actin-bead is $F(d) = \beta(d - \delta)^\alpha$. During the relaxation phase the force decrease from $F(t_1)$ to $F(t_2)$ with the relation :

$$\frac{F(t_2)}{F(t_1)} = \chi(t_2 - t_1)$$

We can write that the force exerted on the actin-bead during the retraction can be written as a sum of the force felt during the approach, damped during the relaxation (F_{da}), plus a force due to the closing of the actin network behind the bead $F_{closing}$.

$$F_{ret}(d) = F_{da}(d) + F_{closing}(d)$$

$$F_{ret}(d) = \chi(t_2 - t_1) \cdot \beta(d - \delta)^\alpha + F_{closing}(d)$$

$F_{closing}$ is computed using the fit parameter α , β , δ and τ_{rep} (Fig 3.27).

On a double logarithmic scale and at long distance $F_{closing}$ also seem to follow a power law (F_{plaw}), when no sticking events are present.

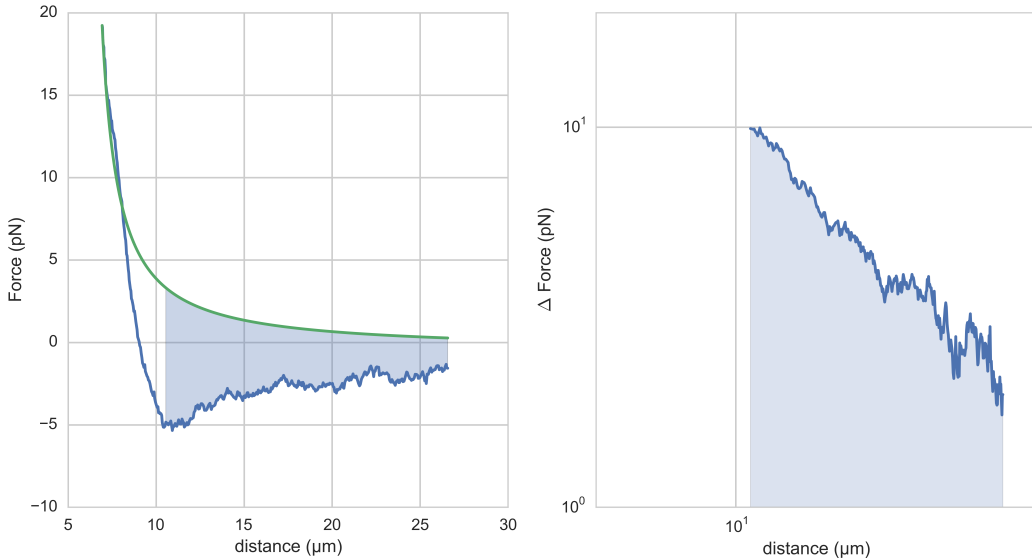


Figure 3.27: Left : Retraction phase with approach phase fit damped by $\chi(t_2 - t_1)$ in green. Blue area under the curve is plotted on a log-log scale on the right, follow a powerlaw.

$F_{ret}(d)$ seem though to follow the force felt durring the approached damped by $\chi(t)$ (F_{da}) for $d \simeq D_{bead}$ and $F_{da} + F_{plaw}$ for $d > 10\mu m$. The typical size of the bead being D_{bead} we expect the transition from one regime to the other to be done on a length scale of D_{bead} . Thus we use a smoothing function which is a convolution between the projected bead area and a linear ramp function which can be seen on figure 3.28

The complete retraction force can be seen on figure 3.24 and is equal to

$$F_{ret}(d) = F_{da}(d) \times (1 - S(d)) + F_{plad}(d) \times S(d)$$

Where $S(d)$ is the interpolation function for a bead of $4.34\mu m$ diameter. We can see that the model fit correctly the retraction and especially the position and value of the minimum of the retraction function without fitting parameter when we use the diameter of the probe bead as a typical scale for the transition when changing direction.

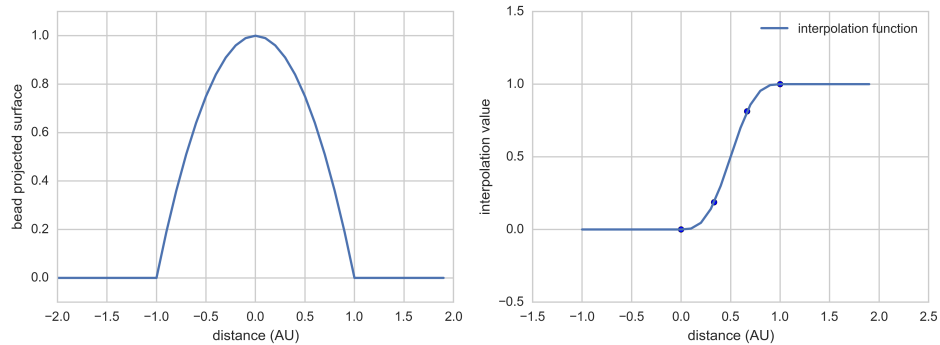


Figure 3.28: Interpolation function used to smooth the transition from F_{da} to $F_{da} + F_{plaw}$

3.7 Discussion

The actin cytoskeleton plays an important role in many cellular functions. The actin cortex, just beneath the cell membrane is not only a crucial structure for cell motility and the mechanical properties, it is also an essential component in cell division and the positioning of the spindle. Other actin structures, that spawn from the nucleus to the cell membrane are responsible for cells organelles positioning like in plants where the nucleus is to ward the anticlinal wall of the cell [Iwabuchi, Takagi, 2010], or during nurses cell maturation where the nucleus pushed away from the dumping canal:cite:Huelsmann2013. The mechanical link from the outside of the cells to the nucleus using actin bundles has already been show previously [Jaalouk, Lammerding, 2009]. We show here that these actin structure should not be the only one taken into account to explain organelles positioning.

Our experiments shows the existence of a sparse and stiff actin cloud emanating from a biomimetically reconstituted actin cortex. This actin cloud is capable of staining forces of tens of pico newtons, enough to hold organelles in place. Using polymer physics we are able to model the behavior of such an actin cloud and measure many of its mechanical properties. It provides an actin scaffold capable of deforming non-plastically. At time scale of few seconds it behaves mostly elastically with an elastic modulus of a few Pascal. The Poisson ratio of the actin cloud varies from 0.05 to 0.2 hinting for a sparse structure of loosely entangle filaments forming a meshwork with a typical mes size of 300 to 400 nm.

The filaments at the origin of this loosely entangled network would emanate from the dense actin cortex that can be seen and simulated on actin-beads [Kawska, Carvalho, Manzi, et al. 2012] and the evolution of parameters of this actin cloud are coherent with the preceding studies on biomimetically reconstituted actin cortices. Recently the role of actin network with similar properties as the actin cloud have been described in cells such as *Xenopus* Oocyte [Feric, Brangwynne, 2013]. Poisson ratios of actin networks have been measured in bulk to be higher [Gardel, Valentine, Crocker, et al. 2003] but are not inconsistent with our measurement at lower actin concentration.

The actin cloud provides a novel structure that should be studied further to understand the positioning of organelles in cells and to study which role this sparse actin structure plays in the formation of other actin networks inside cells.

In particular microrheology experiments could be performed on the growing actin cloud in order to further characterize frequency dependence of the mechanical properties of the actin cloud. The effect of cross linking and network branching is crucial for the happening of symmetry breaking on bead system, and

would likely play a role in the structure of the actin cloud. A confined geometry and direct polymerisation on membrane, or the effect of myosin motors might allow to alter the properties of the actin cloud.

All these could be cellular mechanisms to use the actin cloud in order to efficiently form structures needed for its function. Further studies of the actin cloud on biomimetic or *in vivo* system are challenging, but would lead to a better understanding of the mechanics of the cells and its control.

CHAPTER
FOUR

LIPOSOMES DOUBLETS

4.1 Introduction

We have seen that in cells the actin cytoskeleton is a key component to form structures like the actin cortex that serve to transmit forces and gives cells mechanical rigidity. In order to drive shape changes cells regulate the mechanical properties of the sub-micrometer thick actin cortex that is found beneath the membrane [Clark, Dierkes, Paluch, 2013]. The dynamics of the actin cortex drives cell shape changes [Salbreux, Charras, Paluch, 2012] and the presence of the molecular motor myosin 2 plays a fundamental role for the tension of the acto-myosin cortex [Tinevez, Schulze, Salbreux, et al. 2009]. Cortical tension can be measured on cells to vary between 50 and 4000 pN/ μ m depending the activity of actin and myosin. These changes of the cortical tension are also affected by cell-cell adhesions [Maitre, Berthoumieux, Krens, et al. 2012] which have been shown to play a main role in cell sorting.

Recently, such acto-myosin cortices have been reconstructed on cell-sized liposomes [Carvalho, Lemiere, Faqir, et al. 2013] which showed that the attachment of the actin cortex to the membrane plays a crucial role in the behavior and contractility of the acto-myosin network.

In the present study, I collaborated with Kévin Carvalho and Joël Lemière to further extend the previously developed system [Carvalho, Lemiere, Faqir, et al. 2013] with the aim to monitor the cortical tension changes in a biomimetic actin cortex formed on liposomes. My principal contribution was the analysis of the 3D data that was acquired using Spinning Disk Microscopy. For the analysis I developed a novel method to get an precise and unbiased measure of the geometrical parameter.

To determine the role of cortical tension in cells, recent work used cell doublets [Maitre, Berthoumieux, Krens, et al. 2012]. Here we form similar doublets from liposomes around which we polymerize an actin cortex *in vitro* (Fig 4.1). The shape changes of these liposome doublets allow the time dependent monitoring of cortical tension in a non-invasive way. In this project we hence develop a method for the precise acquisition of doublet deformation in order to determine accurately the increase of tension induced by the injection of myosin motor on the preformed actin cortex.

4.2 Experimental description

4.2.1 Formation of liposomes doublets

Liposomes are obtain by electro-formation (cf *Material and methods*) from a mix of EPC and PEG-biotin lipids. The presence of streptavidin in the working buffer allow liposomes to naturally stick together to form

doublets after 15 minutes (Fig 4.1).

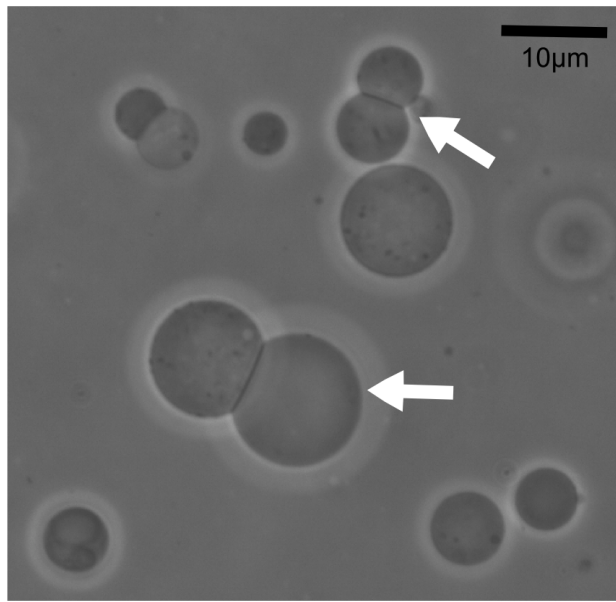


Figure 4.1: Cell-sized liposome doublets. Doublets are indicated by white arrows in the field of view of a phase contrast microscope.

4.2.2 Formation of actin cortex on doublets

Formation of the actin network on doublets is done similar as described recently [Carvalho, Lemiere, Faqir, et al. 2013]. Briefly, actin filaments including biotinylated monomers are stabilized by phalloidin and linked to PEG-Biotin lipids (cf *materials and methods*) via streptavidin that is present in the solution (Fig 4.3). Besides linking the actin to the membrane, it also cross-links the filaments. Such a network has already been characterized recently [Carvalho, Lemiere, Faqir, et al. 2013]. Note that as the actin filaments are only added after the formation of the doublets, the interface between the two liposomes composing the doublets remains free of F-actin (Fig 4.4, 4.2). As the actin added is fluorescent, the absence of actin at the liposome interface can be checked by epifluorescence as it appears dark compared to the rest of the doublet (Fig 4.4).

4.2.3 Visualisation of the interface

To visualise the interface between the liposomes, and to avoid the use of fluorescent lipids that may affect the membrane mechanics [Sandre, Moreaux, BrochardWyart, 1999] the inside buffer of approximately half the liposomes are labeled with 0.9 μ M of sulphorhodamin B (SRB) eventually leading to half of the doublets containing a single fluorescent liposome (Fig 4.4 i and iii).

4.2.4 Geometrical parameters

To study the doublet geometry we model each liposome as well as the interface between them as two spherical caps with their respective center and radius, as sketched in figure 4.5.

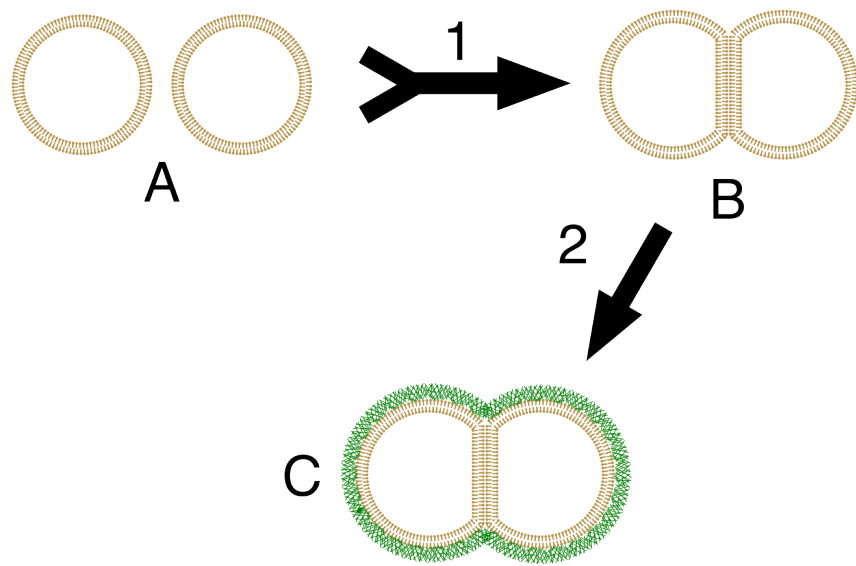


Figure 4.2: Formation of doublets: 1) In the presence of streptavidin, single liposome (A) aggregate into doublets. (B) The addition of biotinylated actin filaments stabilized with phalloidin (2) forms liposome doublets covered with a micrometer-sized actin network (C). The interface between the two liposome is a double lipid bilayer free of actin filaments.

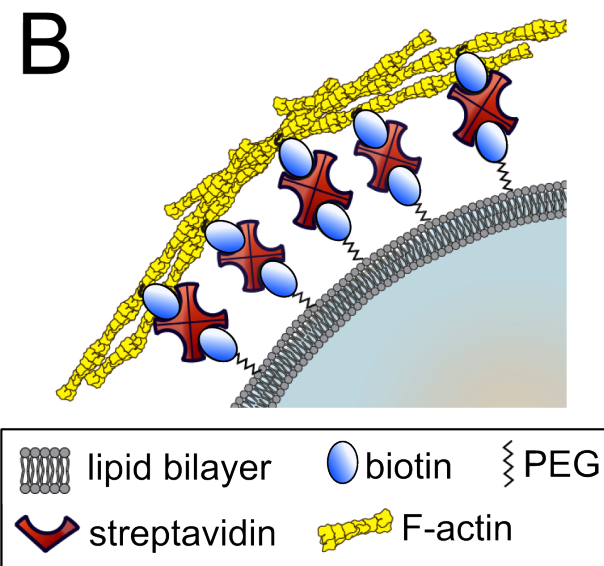


Figure 4.3: Schematic of the stabilized actin cortex at the membrane (proteins not to scale).

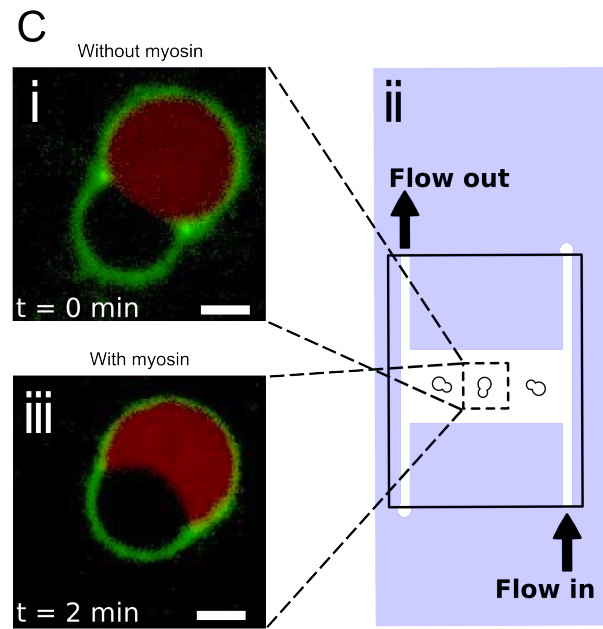


Figure 4.4: i) Flowchamber designed for buffer exchange. Doublets are visualized in the middle horizontal channel of the H shape chamber to avoid movement during the buffer exchange. Spinning disk images of the doublet before i) or after iii) myosin II injection. One liposome contains SRB (red) to visualize the interface of the doublet. The actin cortex is labeled in green. Scale bar 5 μ m.

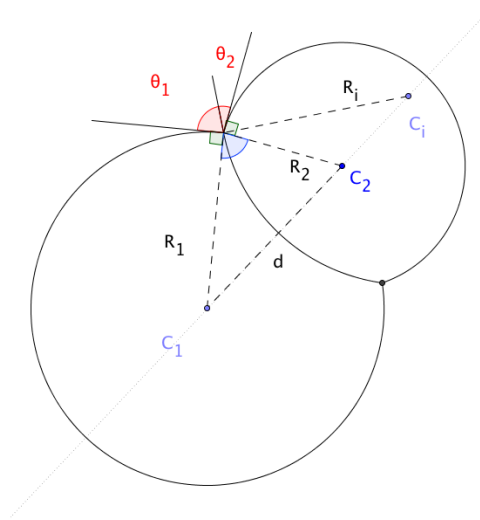


Figure 4.5: Notation of parameters for the doublet model: R_1 , R_2 , R_i are respectively the radius of the liposome 1, the liposome 2 and the interface. d is the distance between the liposome centers. θ_1 and θ_2 are the angles between the tangents of the liposome surface and the tangent to the interface at the contact line. The total contact angle θ is the sum of θ_1 and θ_2 .

The center position in 3D (X,Y,Z) and the radius (R) of the three spherical caps completely determine the doublet geometry, though it is interesting to look at other parameters of the doublets which are :

- the total volume of the liposome doublets V
- the contact angle between the two liposomes
- Each of the “half”-contact angles which are the angle between the interface and each of the liposomes θ_1, θ_2
- The distance between the liposome centers.

4.3 Experimental Observations

4.3.1 Effect of myosin injection

We image the liposomes doublets in an open chamber either in phase contrast and epifluorescence, or spinning disk microscopy in the red (sulphorhodamin) and green (actin) channel.

Muscle Myosin II that forms *bipolars filaments* is carefully injected into the chamber, and leads within minutes to a shape change (Fig 4.6) of the doublets due to the contraction of the actin cortex.

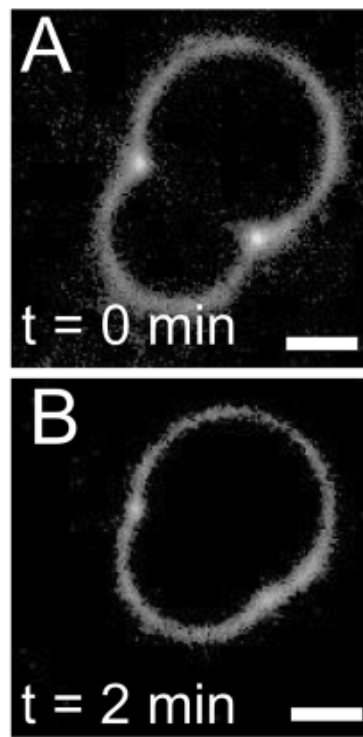


Figure 4.6: Doublets contraction showing green channel (actin): (A) doublet before myosin II injection. (B) doublet during contraction due to myosin II. Time=0 corresponds to myosin II injection. Scalebar is 5 μm

The distance between the liposome centers decreases as the total angle $\theta = \theta_1 + \theta_2$ increases. The contact angle and other parameters of the doublets are obtained by fitting spherical caps onto the 2D epifluorescence

images or on the 3D confocal stack as *described later*. In the absence of myosin, the contact angle θ is measured to be $\theta = 64 \pm 16^\circ$ ($n=18$) whereas in the presence of myosin II (200 nM) we find a value of $\theta = 86 \pm 21^\circ$ ($n=5$). Measurements of the contact angle after myosin II injection are done before the cortex ruptures as characterized in [Carvalho, Lemiere, Faqir, et al. 2013].

4.3.2 Relation between the angles and tension

Each liposome has its respective tension τ_1 , and τ_2 . In the absence of the biomimetic acto-myosin cortex these tensions correspond only to the tension of the liposome membrane. The interface between the two liposomes is formed by two lipid bilayers, and the interfacial tension is composed of two contributions: The tension of the lipid bilayer, noted τ_i , and the adhesion energy per surface unit W due to the biotin-streptavidin-biotin link between the two lipid bilayers. The total tension at the interface can thus be written $\tau_t = \tau_i - W$ [Maitre, Berthoumieux, Krens, et al. 2012].

As the movement of the contact line during the contraction is slow (order of $\mu\text{m}/\text{min}$) compared to pressure equilibration across the doublet, we can consider the contact line between the liposomes and the interface to be at equilibrium. Hence, we can apply Young's equation :

$$\sum_{k \in \text{interfaces}} \tau_k \cdot \vec{t}_k = \vec{0}$$

$$\tau_i \vec{t}_i + \tau_1 \vec{t}_1 + \tau_2 \vec{t}_2 + = \vec{0}$$

In which t_k are the vectors tangent to the interface at the point of contact, as described in figure 4.7

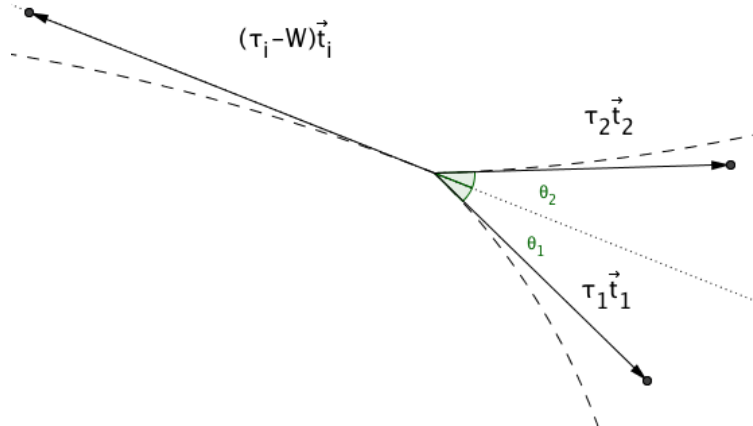


Figure 4.7: Equilibrium of the contact line. Each interface pulls on the line with a force proportional to its tension. As the contact line is at equilibrium the sum of the forces compensate which allow to get a relation between the tensions and the contact angles.

This allows to relate the tension of each of the lipid layers and the angle between them at each instance of the contraction. We can in particular project the result of this equation onto the direction of the contact surface tangent (dotted line on figure 4.7):

$$\tau_i - W = \tau_1 \cos(\theta_1) + \tau_2 \cos(\theta_2) \quad (4.1)$$

And on the direction perpendicular to it :

$$\tau_1 \cdot \sin(\theta_1) = \tau_2 \cdot \sin(\theta_2) \quad (4.2)$$

These equations link the tension to the contact angle both before, during and after the contraction and hence remain correct during the experiment. In the following we will mark the values before the contraction phase by the suffix 0. Thus, for example $\tau_{i,0}$ refers to the tension of the interface before the addition of myosin, and τ_i refers to the tension of the interface at any instant of the contraction.

4.3.3 Contact angle dispersion

The value of the contact angle θ varies across different doublets both before and after the addition of myosin II. This reflects initial variations of tension in $\tau_{i,0}$, $\tau_{1,0}$, and $\tau_{2,0}$ from doublet to doublet. Such variations could be due to a difference in the liposome tension acquired during the different preparations, but also due to a variation of adhesion energy between doublets, or alternatively an effect of tension build-up during the formation of the actin shell. As the dispersion in contact angle is in the same order as the increase in angle upon addition of myosin, a statistical analysis of the contact angle before and during contraction is problematic. Thus to avoid this effect of dispersion, we follow the evolution of θ each individual doublet during time.

4.3.4 Tension of actin-shell

In order to investigate the increase of tension due to the acto-myosin network on liposomes, we first characterise the increase that is only due to the addition of the actin-shell in the absence of myosin. By destroying the F-actin via photo-bleaching ([Fig 4.8](#)) we compare the shape of the same doublets in the presence and absence of the actin-shell. It should be noted that it is established that the actin filaments are destroyed by the bleaching as it frees oxygen radicals that denature the actin monomers. Hence, the bleaching process actually destroys the actin cortex ([vdGucht, Paluch, Plastino, Sykes, 2005]). This investigation showed that the total contact angle changes by $3.4 \pm 2.0^\circ$ ($n=7$) after disruption ([Fig 4.9](#)) of the actin network. Thus we conclude that the change of tension due of the actin-shell is small and negligible compared to the change in tension we see with myosin.

4.4 3D observation

Three dimensional imaging of the doublets is necessary to get the correct contact angle. This requirement comes from the fact that in simple 2D epifluorescence images, the focal plane has to correspond to the equatorial plane of the doublets. If this is not the case, the fit will produce a systematic underestimation of the contact angle. This is especially the case when doublets are of different radii as typically found in our experiments, where the liposomes composing the doublets have an ratio of R_1/R_2 between 1.15 and 1.82.

Time resolved 3D Spinning disk stacks ([Fig 4.10](#) with 3D reconstruction [Fig 4.11](#)) are recorded with a time resolution of less than 5 seconds per stack for an accurate determination of the different parameters of the doublet over time. The analysis reveals: the contact angle θ ([Fig 4.12](#)), the volume of the doublet V ([Fig 4.14](#)) and the distance between liposome centers d ([Fig 4.13](#)). All these parameters are obtain by fitting spherical 3D caps on the 3D stack as explained *in later parts*.

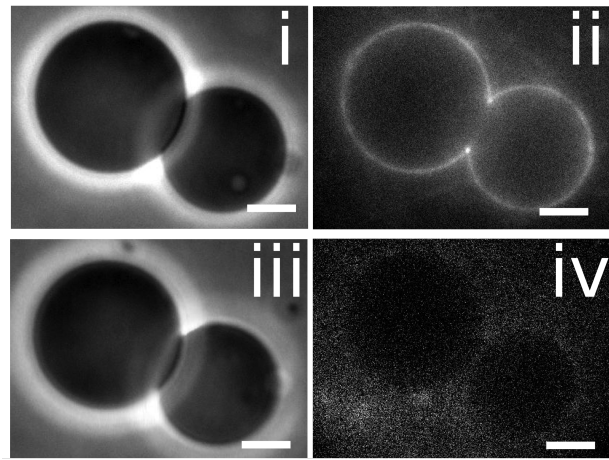


Figure 4.8: Image of an individual doublet coated with fluorescent F-actin before i) ii) and after iii) iv) actin cortex disruption. The actin cortex is visualized by epifluorescence ii) iv) and the doublet by phase contrast i) iii). Scale bar 5 μ m.

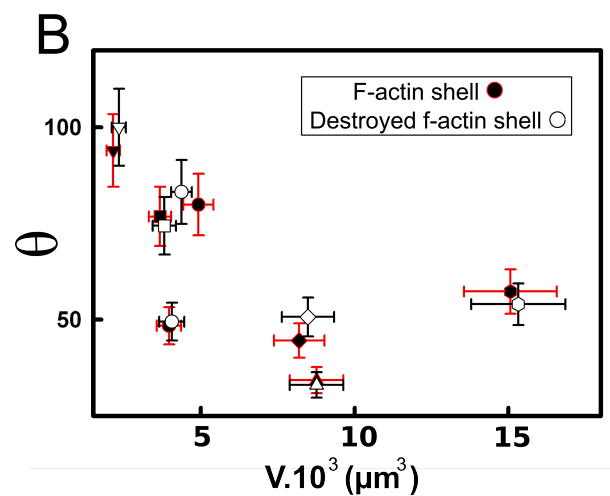


Figure 4.9: Measurement of the contact angle between the two liposomes forming the doublet before (black) and after (white) disruption of the stabilized actin cortex as a function of their volume.

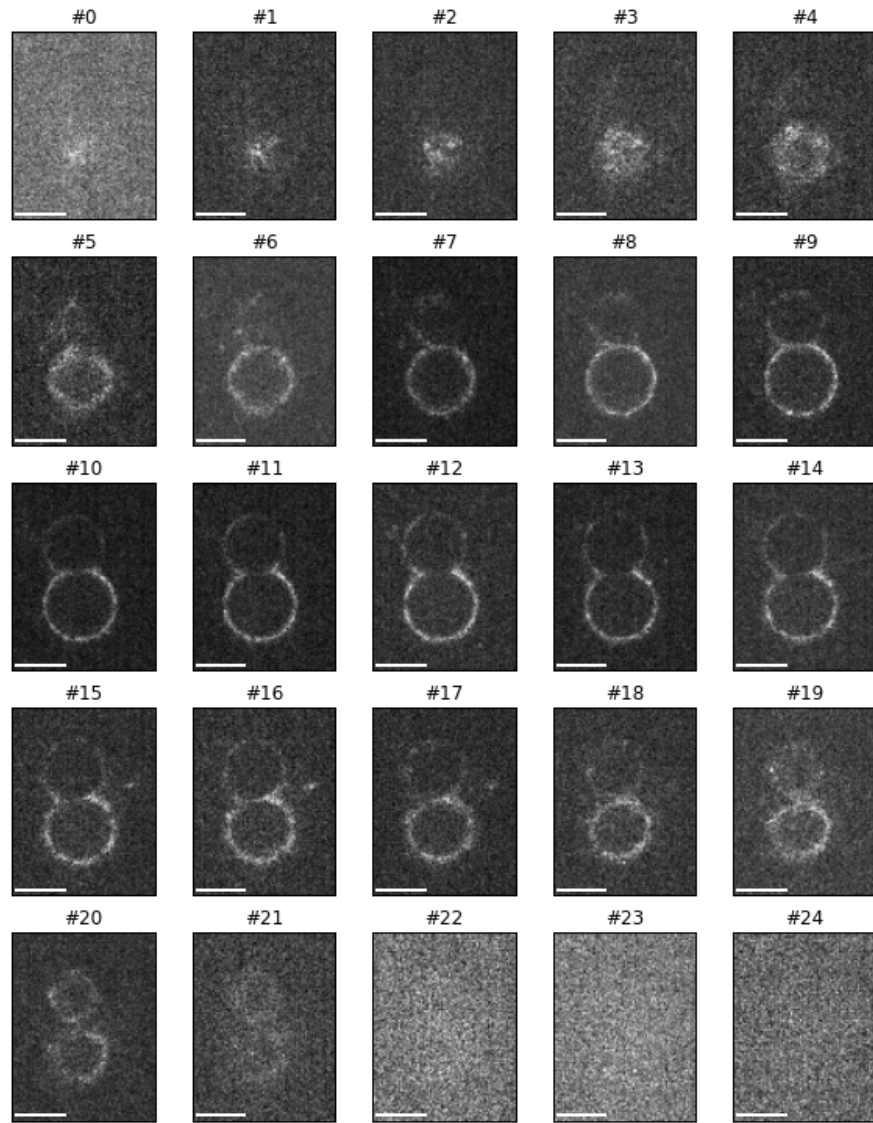


Figure 4.10: Confocal stack of an liposome doublets, actin channel, 3D reconstruction in [Figure 4.11](#). Note that there is no actin at the interface between the liposomes (Frames #11-#14). The distance between each image is $\Delta z = 0.85 \mu\text{m}$.

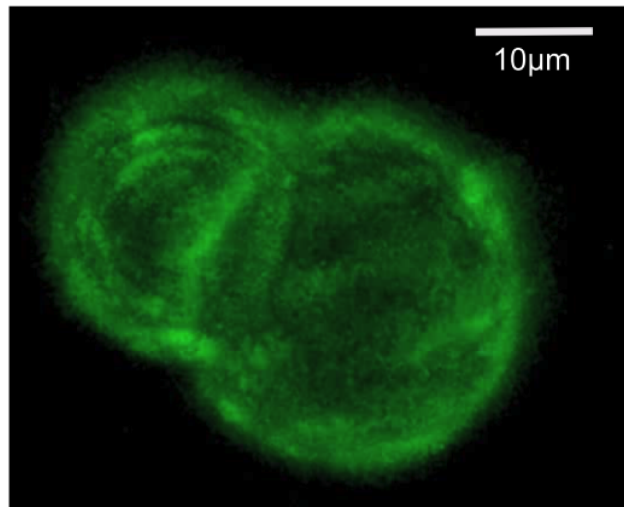


Figure 4.11: 3D reconstruction of a doublet surrounded by actin. The absence of actin on the interface can be seen more easily on [figure 4.10](#).

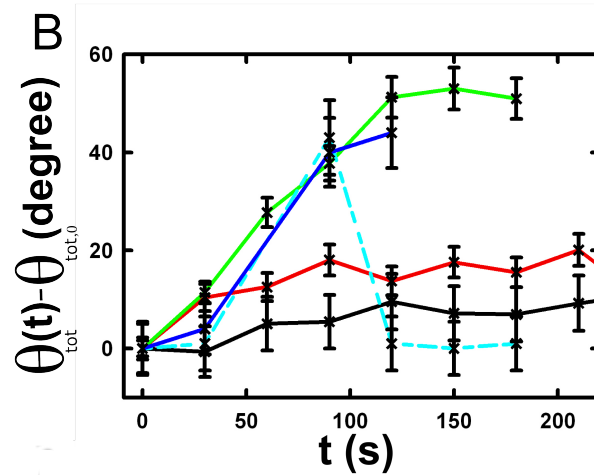


Figure 4.12: Evolution of the contact angle compare to the initial one as a function of time. Each doublet is represented by a different color. The color code corresponds to the doublets shown in figure [4.13](#), [4.14](#) and [4.15](#). A special case is shown in the blue dashed line, where the actin cortex on the doublet ruptured, and the cortex peeled off. The analysis of this case showed that the contact angle after rupture recovers its initial value.

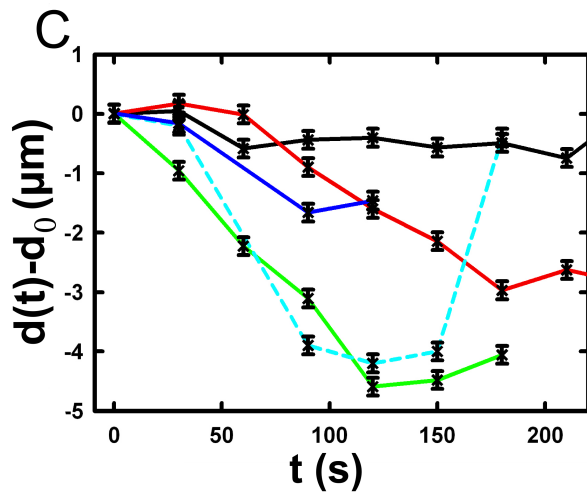


Figure 4.13: Evolution of the distance between the liposome centers over time. Same color code for same doublets as in figure 4.12, 4.14 and 4.15. Again the doublet with the ruptured cortex recovers its initial parameter values.

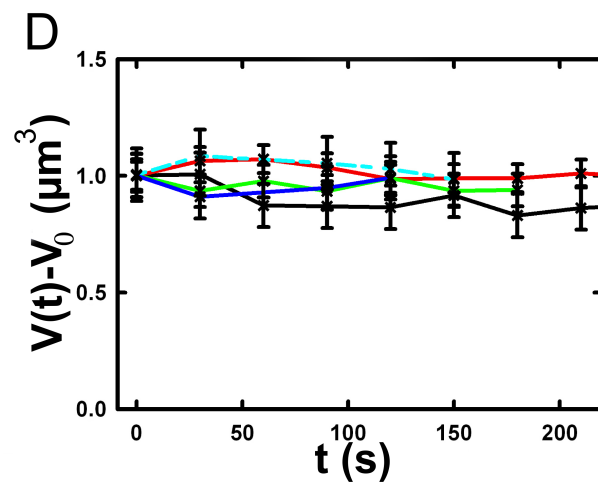


Figure 4.14: Evolution of the volume ratio over time. Same color code for same doublets as in figure 4.12, 4.13 and 4.15.

During contraction triggered by myosin, we observe that the contact angle θ increases while the distance between liposomes center d decreases. During this process the volume remain constant within the 10% error. These result are consistent with the measure of contact angle in freely adhering cell doublet experiments done previously [Maitre, Berthoumieux, Krens, et al. 2012].

4.5 Discussion

4.5.1 Cortical tension is homogeneous for single doublet

Combining equation (4.2) with the finding that $\theta_1 = \theta_2 = \theta/2$ allows to infer the equality of tension on both side of the doublet during all the experiments. We can hence write $\tau_1 = \tau_2 = \tau$. This result is consistent with the fact that actin is distributed continuously all around the liposome doublet. Hence, myosin II minifilaments pull on a continuous shell. In these conditions equation (4.1) simplifies to :

$$\tau_i - W = 2.\tau(t).\cos(\theta(t)/2) \quad (4.3)$$

Where $\tau(t)$ and $\theta(t)$ are the tension and the angle at the time t after myosin injection. Assuming that $\tau_i - W$ may depend on a variability of the initial adhesion between liposomes. Since myosin does not operate at the interface between liposome as it is free from actin, it is reasonable to consider the tension and adhesion energy constant for a given doublets through time $\tau_i - W = \tau_{i,0} - W_0$. Therefore we obtain an expression of the tension $\tau(t)$ during the acto myosin contraction that reads :

$$\begin{aligned} \tau(t) &= \frac{\tau_i - W}{2.\cos(\theta/2)} \\ &= \frac{cst}{2.\cos(\theta/2)} \end{aligned} \quad (4.4)$$

Hence we can evaluate the tension relative to its initial value over time :

$$\frac{\tau(t)}{\tau_0} = \frac{\cos(\theta_0/2)}{\cos(\theta(t)/2)}$$

4.5.2 Relative increase in cortical tension

Interaction of myosin II filaments with a biomimetic actin cortex induces tension build up. The cortical tension, normalized to its initial value, increases and reaches a plateau where $\tau(t) = \tau_{peeling}$ (Fig 4.15) with the same trend as θ . Note that if the acto-myosin shell breaks and peels, the doublet recovers its initial shape (see dashed blue line for d and θ on Fig 4.12, 4.13, 4.14). The average relative tension is found to be $\tau_{peeling}/\tau_0 = 1.56 \pm 0.56$ ($n=5$) in 3D and $\tau_{peeling}/\tau_0 = 1.25 \pm 0.15$ ($n=5$) in epifluorescence, in agreement with discussed expected underestimation of the contact angle in epifluorescence measurements.

4.5.3 Cortical tension increase in doublets and in cells

In cells, cortical tension can be as low as 50 pN/ μ m in fibroblast progenitor cells [Krieg, ArboledaEstudillo, Puech, et al. 2008] and can go up to 4000 pN/ μ m for dictyostelium [Schwarz, Neuhaus, Kistler, et al. 2000]. Surprisingly, when myosin activity is affected, either by drugs or by genetic manipulation, the cortical

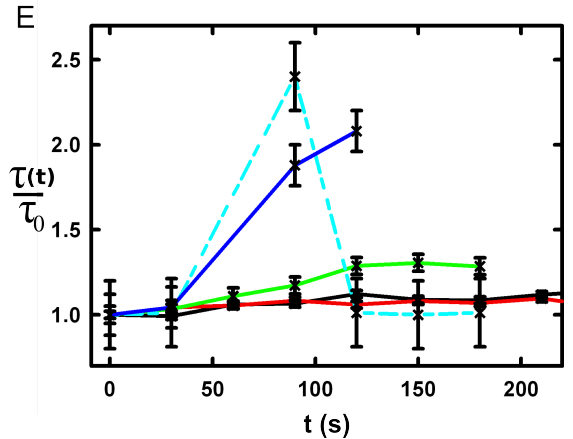


Figure 4.15: Increase of the tension ratio between the tension $\tau(t)$ at time t and the initial one τ_0 . Same color code for same doublets as in figure 4.12, 4.13 and 4.14. The actin cortex rupture in the blue dashed line also presents the highest relative tension increase.

tension only decreases by a factor of about 2. Cells are also observed to round up during division in which an increase of tension by a factor of two is sufficient [Stewart, Helenius, Toyoda, et al. 2011], [Kunda, Pelling, Liu, Baum, 2008]. Our *in vitro* reconstruction is able to reproduce similar changes of cortical tension as we observe a cortical tension increase by a factor of up to 2.4.

4.5.4 Different contributions for cortical tension

Cortical tension is the sum of the membrane tension and the tension due to the acto myosin cortex. We question how the membrane contributes to cortical tension and in our assay we show that may account for approximately 50% of the cortical tension in some cases. In suspended fibroblast cells, membrane tension is estimated to be 10% of the cortical tension [Tinevez, Schulze, Salbreux, et al. 2009]. When polymerisation of actin is stimulated, the cortical tension is multiplied by a factor of 5 showing a strong dependence also with actin dynamics [Tinevez, Schulze, Salbreux, et al. 2009]. Hence the residual tension in cells might be due to actin dynamics which is absent in our experiments. How actin contribute to cortical tension is still an open question that needs to be addressed in the cell geometry. Whereas actin polymerisation outside a liposome has been shown to generate inward pressure, how this can be translated to tension in a different geometry is not yet clear. *In vitro* assay are on their way to mimic actin dynamics in cells [AbuShah, Keren, 2014] and will allow to unveil the mechanism of tension build up by actin dynamics, which is the remaining module that need to be understood. The effect of myosin and of the membrane being clarified in this study.

4.5.5 Conclusion

We provide a biomimetic reconstitution of the tension build up by acto-myosin contractility using liposome doublets. Cortical tension changes are visualized *in situ* over time by analyzing doublet shape changes. This method allows us to directly quantify the relative increase in tension due to myosin, separately from the one due to actin dynamics. Understanding the contraction of composite systems that are rebuilt brick by brick to model a living cell will hopefully lead the way towards for a reconstitution of complex systems like tissues.

4.6 3D fitting

Obtaining the geometrical parameter of doublets remains challenging as in classical phase contrast microscopy and epifluorescence the acquired images only capture a single focal plane of the doublets. This makes the analysis difficult as the observation plane should be the equatorial plane of the doublet.

In order to achieve good precision in the measurements of the contact angle we decided to use confocal microscopy and acquire evenly spaced z-stacks. From these stacks the 3D structure of a doublet was reconstituted. Using the 3D structure of the doublets allows to recover the geometrical parameters and the contact angle.

To determine the geometrical parameter of the doublets we modeled the doublets as two intersecting spheres, determined the expected 3D images and adjusted the parameters of the model to fit the obtained experimental data.

I was responsible for developing a fast and precise method to reliably and automatically recover the geometrical parameters of the liposome doublets based in the image stacks acquired using spinning disk microscopy. In the following part I will develop the principle of this methods and the result on liposomes doublets.

4.6.1 First step: Finding a single liposome

In this part we show the principle that allow us to determine the 8 geometrical parameter that characterise a doublet: 2 centers (X,Y,Z) and 2 radii (R_1 and R_2).

As the principle for finding the geometrical parameter does not differ with the number of dimensions, the presented methods can be applied even in higher dimensions (e.g. deformed ellipsoid liposome, or multi channel imaging). Furthermore, the principles remain the same also in a space with less dimensions, so we will restrict our discussion to a single liposome in a 2D plane (X,Y position of centers and R, radius) hence reducing the parameters to be determined to six instead of eight.

Experimentally, liposomes are observed using fluorescently labeled actin that forms an homogeneous micrometer sized actin shell. In the observation plane, the liposome is a bright ring of given thickness (we will refer to this as the *expected signal*), on top of this image is the experimental noise where the principal noise sources are the presence of fluorescent actin monomers in the buffer solution and electronic noise from the camera CCD. Eventually, the noise in the outside buffer due to monomeric actin can be higher than inside which is free of actin.

The signal from a liposome and the addition of noise can be replicated numerically as seen on [figure 4.16](#).

The *expected signal* can be modeled numerically using several parameters of the system (center and radius of liposome, point spread function of microscope, ...).

To find the correct parameters for the doublets we will numerically correlate the acquired data with the numerical model and search for the correlation that correspond best to the real image. The correlation between the model and the images data can be written.

$$r_{xy} = \frac{\sum_{i=1}^n (x_i - \bar{x})(y_i - \bar{y})}{(n - 1)s_x s_y}$$

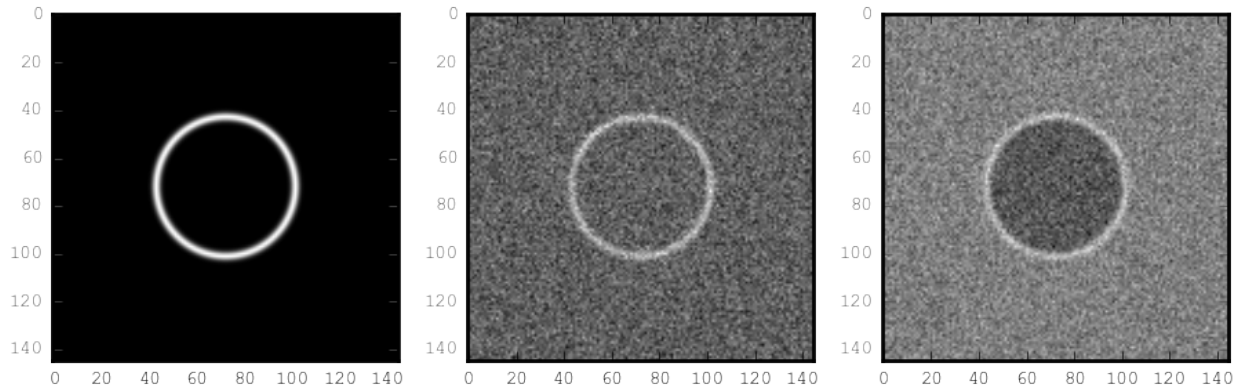


Figure 4.16: Left : A simulation of liposome fluorescent image consisting of an uniform shell or membrane (*expected signal*). Middle: Same Image Adding Gaussian noise. This simulates one plane of a confocal Z-stack. Right: Simulation of liposome with fluorescently labeled actin shell in fluorescent external buffer and non fluorescent inside buffer.

In which x_i are luminosity values of each of the n pixels in the acquired data, y_i are the luminosity of the pixels in the model \bar{x}, \bar{y} correspond to average values over the images, s_x and s_y are the standard deviation of the luminosity values.

As the monomeric fluorescently labeled actin and the electronic noise are dominant in the acquired images, we can assume a uniform noise on top of the *expected signal*. The correlation between the model and the noise is in average uniform.

$$r_{noise,model(params)} = cst$$

And the correlation between the *expected signal* and the model is expected to be maximal for the parameters of the model that equal the real geometrical parameters of the doublets.

$$\arg \max_p (r_{data,model(p)}) = \arg \max_p (r_{expectedSignal,model(p)})$$

In which $(\arg \max_p)$ stands for the argument of the maximum, that is to say, the set of points of the given argument for which the given function attains its maximum value. Thus searching the value of the parameters that maximize the correlation between the model and the data implies finding the geometrical parameters we are interested in.

We can test the ability to do this numerically by generating data, adding noise to it and try to recovering the parameter of the *expected signal*.

By looking at the value of the correlation between the generated data and the model as a function of model parameters, we can check that the correlation value are maximal when the model center value correspond to the *expected signal* center value (Figure 4.17), and when the radius of the model liposome has the same radius in the model correspond to the radius in the generated data (Figure 4.18).

Using minimisation techniques we can search the parameter space of the model and maximise the correlation between the model and the experimental data. We then recover the geometrical parameters of the liposomes. This can be done by efficiently computing the value of the correlation within a few hundreds of points and get access to the liposomes geometrical parameters, here position and radius.

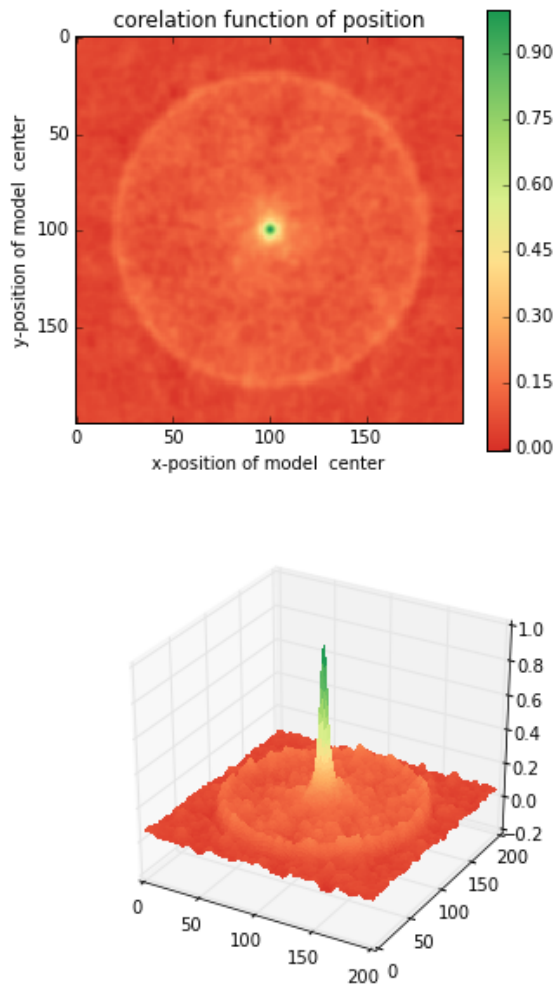


Figure 4.17: Value of the correlation as a function (arbitrary units) of two of the fit parameters. The radius of the liposome in the model is taken as equal to the value of the *expected signal*, and the position of the center is varied in the X and Y direction. The value of the correlation is maximal for the position of the center in the model that equal the center of the *expected signal*. We can see local maxima on the 3D representation that are well below the value of the global maximum. The peak at the global maxima is sharp, hinting that the search of the maxima need relatively good initial parameters (lower than $\sim 1/10$ of liposome radius). The sharpness of the peek point that corresponds to the best fit parameters on experimental data should be robust.

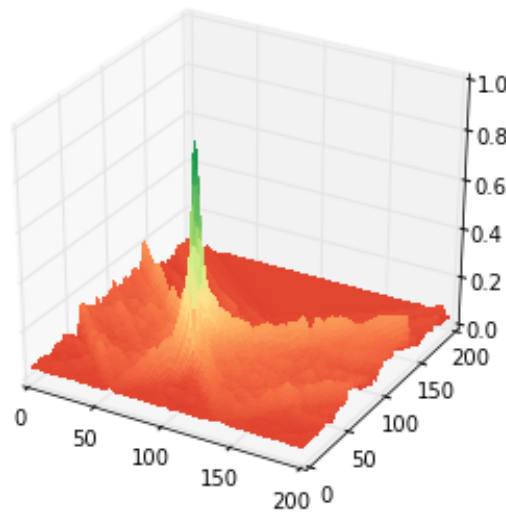
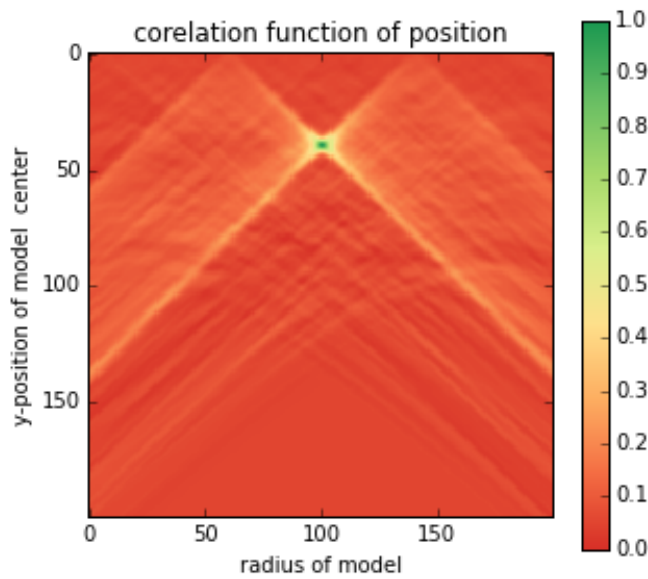


Figure 4.18: Same as figure 4.17 with Y position of the center taken as equal to the expected signal, variating X position of the model and radius of the liposome. The graph shows the same properties as before.

4.6.2 Fitting a doublet

The determination of contact angle on epifluorescence images or phase contrast images often result in an underestimation as the imaging plane is not necessarily one of the doublets equatorial planes. Moreover, most determination of the contact angle on phase contrast and epifluorescence images are done manually [Maitre, Berthoumieux, Krens, et al. 2012] and are subject to experimenter bias as the experimenter draws the tangent lines at the contact point between the liposomes. Thus we decided to develop fitting routines for the acquired 3D confocal stacks. In our case we avoid the usage of fluorescent lipids that could artificially change the tension of the membrane.

As sketched in [Figure 4.2](#), the doublets are covered with a thin micrometer-thick layer of fluorescent actin filaments, which we image by confocal spinning disk microscopy. As the actin-layer is attached to the membrane and the contact angle is defined as the angle between the lipid bilayer, imaging the actin-layer corresponds to the angle between the inner surfaces of the two actin networks present on each liposome.

Thus in order to determine the geometrical parameters of the doublets we need to also model the actin shell. As the liposomes in contact are two spherical caps the uniform actin layer will also form two spherical caps with a given thickness. The total image is thus the union of two spherical caps blurred by the point spread function of the microscope. This can be seen on [figure 4.19](#). We can see on this image that the doublet is here lying on the chamber surface. We checked in this case that the contact surface between the chamber and the doublet did not change during experiments.

(The figures shows tha the doublet is attached to the surface. You might want to discuss this?)

As the contraction of the doublets is rapid, and the recorded 3D stacks contain a large number of frames, it is crucial to be able to compute the model and the correlation in a reasonable time (less than the hour per images). To achieve this besides calculating the model as efficiently as possible one can replace the exact calculation of two spherical cap and the point spread function of the microscope by the union and subtraction of pre calculated spheres followed by a 3D numerical Gaussian blur.

Though the use of numerical technique is not without artifacts. In the case of discret Z-stack that are not sufficiently spaced, the different radii in the fluorescent rings within subsequent stacks can lead to a “ring-artifact” ([Fig 4.21](#)) when using numerical Gaussian blur. In the case of a too pronounced “ring-artifact” a “ghost” spheres can appear around each liposome which can cause the fitting process of the doublets to fall into a local maximum of correlation, thus leading to wrong value of the geometrical parameters.

In our case we have a sufficient number of planes per stack so that the numerical model with the same sample size as the data do not show the ring artefact and have smooth transition near the position of the spherical cap. Though the ring artifact can be eliminated by oversampling/interpolating the model before the numerical Gaussian blur and under sampling afterwards to arrive at the correct number of pixels.

The size of the Gaussian blur can also be adjusted to be higher which will act as a regularisation function for the value of the correlation between the model and the acquired data (cf [Figure 4.22](#)), thus smoothing or eliminating local maxima, but reducing the precision in the position of the maxima.

The value of the correlation between the model and the experimental recorded data can be maximised using already available functions, in particular we used Nelder–Mead simplex as implemented in *scipy.optimize* python library. This gives us the 8 parameters of the doublets. Result of the fits are show in [figure 4.23](#).

Using the fast Cython code ([Seljebotn, 2009]) also allowed to also speed up fitting to a reasonable time: one Z-stack of 3 millions pixels can be fitted in about 40 seconds. Thus allowing the fitting of a full 3D movie of a doublets contraction to be done in less than an hour for 30 to 40 frames.

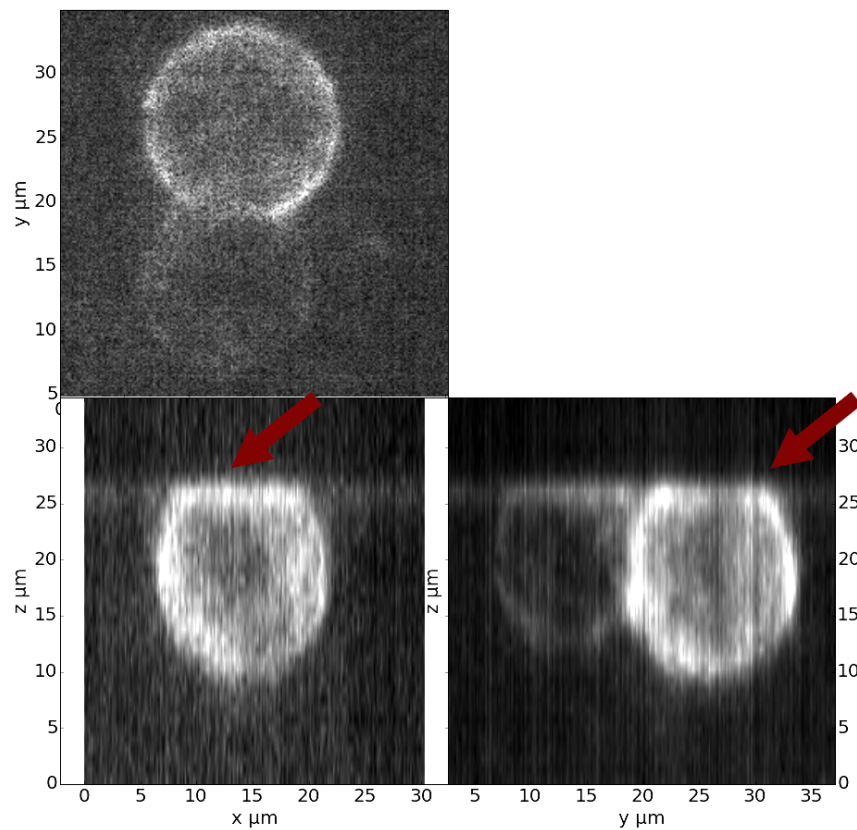


Figure 4.19: Maximum projection along X,Y and Z of recorded stacks, green channel actin. One can see that the liposomes doublets are lying on to the surface of the observation chamber (arrows).

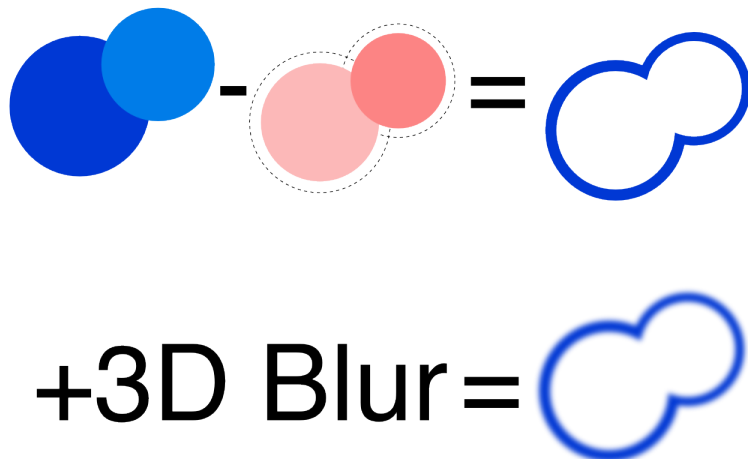


Figure 4.20: Principe of numerically approximating the two spherical caps as intersection of two spheres, followed by a 3D numerical Gaussian blur. The numerical speed-up compared to the exact calculation of the fluorescent density allow to make fits on doublets in minutes instead of hours.

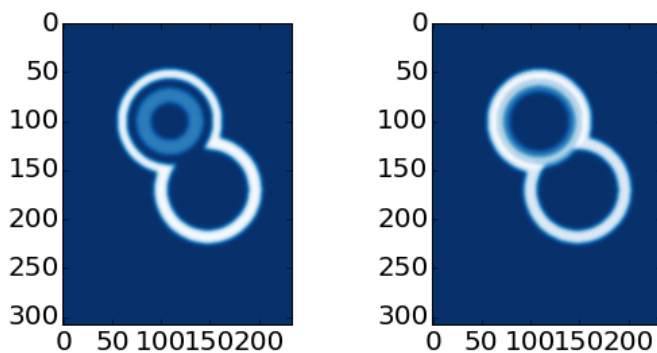


Figure 4.21: Left : One plane of the numerical model with exaggerated ring artifact due to an under sampling of the model in the Z-direction, stacks from “Far” Z leak onto the current Z-plane and form a ring. Right : Same plane of the model with enough sampling plane in the Z-direction do not show the ring artifact. In this case we use a sampling equal to the number of slice than the recorded data. (X,Y in arbitrary units)

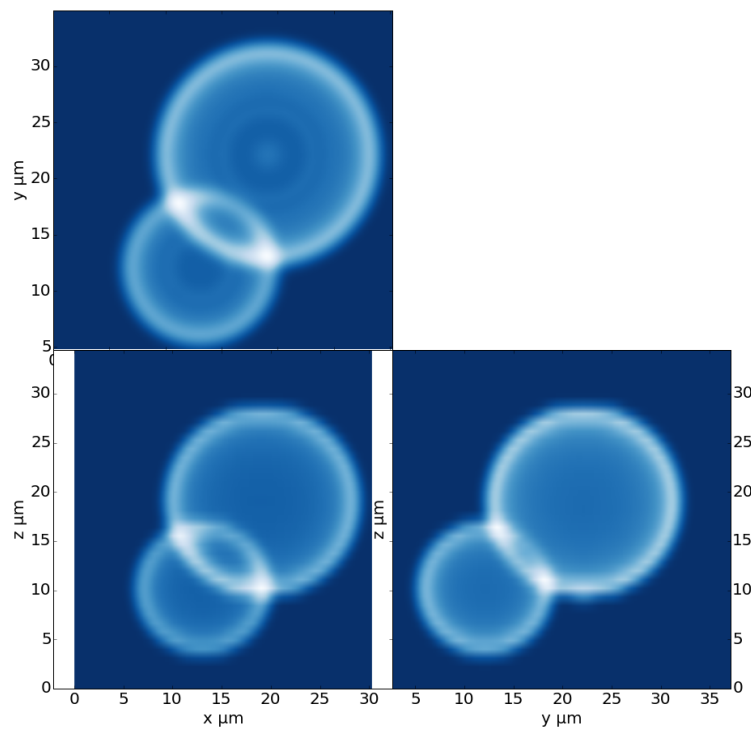


Figure 4.22: Maximum projection along X,Y and Z of numerical model, the “ring” effect can still slightly be seen near the pole of each liposome, but is not sufficient for the fit to be stuck in a local minimum.

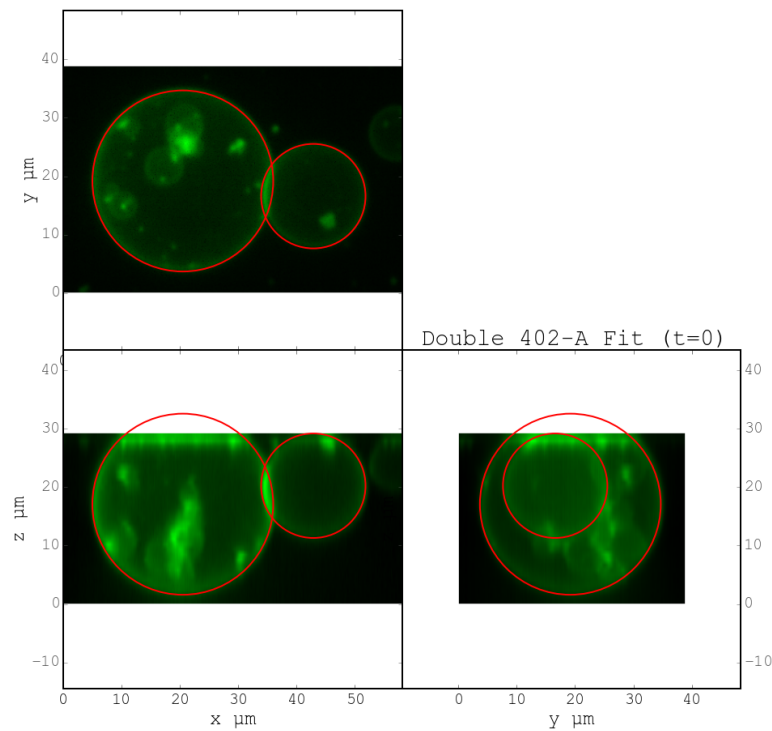


Figure 4.23: Maximum projection of confocal images in the X,Y and Z projection as well as the result of the fits shown as equatorial circles for the three direction of projection.

To ensure robustness of the fits to doublet center displacement during acquisition, the initial parameter of the fit where chosen manually for each first frame of each sequences. The final fit parameters of each frame are reused as initial fit parameter for the subsequent frame.

In order to test robustness of the fit, the initial fit parameters were randomly modified by an amount of +/- 1 μm , and we checked that the final parameters did not vary.

For a couple of parameters, the values of the correlation function can be plotted to check for the regularity of the function and the absence of local maxima. [Figure 4.24](#) and [figure 4.25](#) show the

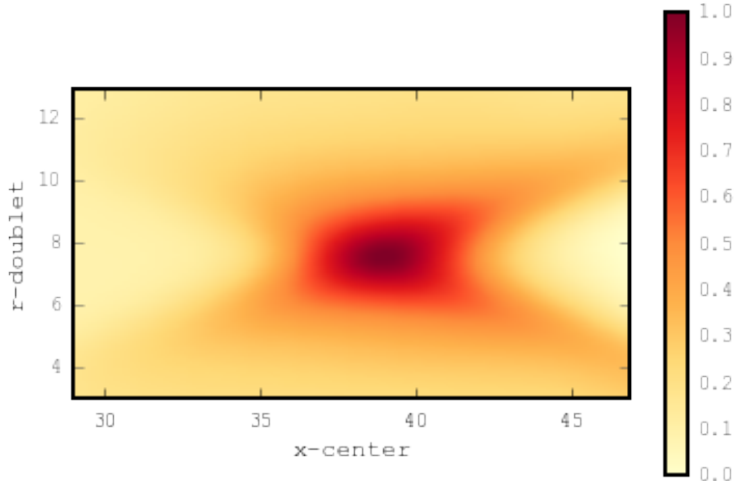


Figure 4.24: Correlation of the model and the data as a function of the center position of one of the model spherical caps along the X axis and the radius of this same spherical cap. Vertical axis in arbitrary unit.

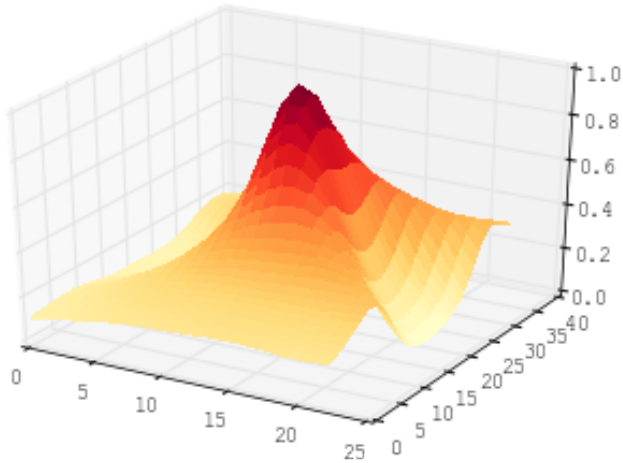


Figure 4.25: 3D representation of the data in [figure 4.24](#), the shape of the function is the same as the simulation done with the *expected signal* in [figure 4.17](#) and [4.18](#)

The correctness of the fit is also checked visually to prevent errors in the procedure. The fit was found to be always accurate and coherent with manual measurements of contact angle. When the red channel was

also present and liposomes contained sulphorhodamin, fits where additionally visually checked by using maximum projection of the red channel. (Cf Fig 4.26).

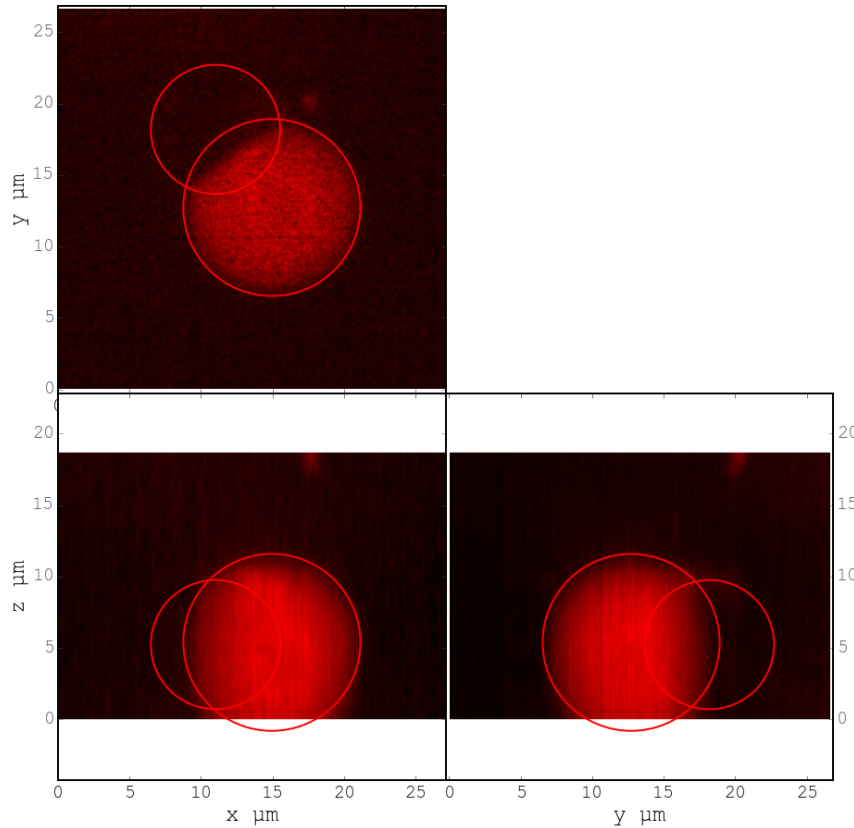


Figure 4.26: Maximum projection of the red channel (*sulphorhodamin*) and the fitted parameter for the doublet.

4.6.3 Discussion

In this part we show that by modeling the liposome doublet and using fluorescently labeled actin we are able to develop a technique that automatically and robustly determine the geometrical properties of the liposome doublets.

We note that the red fluorescent dye present in the inside buffer of the liposome could be used conjointly to the green channel in order to improve the quality of the fit, though this would require the extra parameters of the interface radius. As the computation time needed to fit the doublets increase rapidly with the number of parameter, this solution was found to be impractical. Moreover, the curvature of the interface being relatively small and the difference between the curved interface and a flat plane being close to the optical resolution, we the fits risk to become unstable. The use of fluorescently labeled lipids for the liposome membrane also suffers from the same issues of extra parameter if one want to recover the position of the interface.

4.6.4 Conclusion

We developed a robust and automated method to determine the geometrical parameters of liposome doublets. This allows to determine robustly the geometrical parameters of liposome doublets without experimenter measurement biases due to the selection of the illumination plane, resolution of optics and luminosity scale.

We have seen that liposome doublets with reconstituted acto-myosin cortices are a biomimetic system that allows to measure the changes in cortical tension with time. 3D fitting helped to quantify the tension by obtaining the corresponding contact angles.

Observing the contraction of multiple liposomes doublets simultaneously and the ability to automatically determine the geometrical parameters allows more sample to be collected. Faster and more reliable data acquisition on actin network contractions will allow for a better understanding of the effect of actin network *in vitro* which also pave the way to reconstitution of more complex system.

ACTIVITY IN OOCYTE CYTOPLASM

5.1 Introduction

Mouse oocyte are big spherical cell with a diameter in the order of 80 µm. It has been shown that the spindle positioning during meiotic division of oocyte is dependant of an actin meshwork present in the cell [Schuh, Ellenberg, 2008]. This actin meshwork is regulated by endogenous vesicle which dynamic is myosin-Vb dependant [Holubcova, Howard, Schuh, 2013]. In a collaboration with Marie-Hélène Verhlac and Maria Almonacid in Collège de France, we designed a way to measure cytoplasmic activity in mouse oocyte.

Figure 5.1 shows a mouse oocyte where the nucleus can be seen positioned at the center of the cell.

5.2 OOcytes

As oocyte meshwork in oocyte is controlled by the activity of formins than drive actin polymerisation and Myosins Vb that controlled the dynamism of the vesicle in the meshwork, we decided to develop the analysis in 3 type oocytes. Wild types oocyte, oocyte prelevé on Formin 2 invalidated female that lack the actin meshwork and oocytes injected with the dominant-negative tail of Myosin Vb (Fig 5.2)

5.3 Measure of activity

The diffusion of actin positive vesicle ta can be seen during oocyte meiosis is less important in Formin -/- and MyosinVb-tails oocytes than in Wild type. While particle tracking with the vesicle present in oocyte is possible, it is a complex process especially with the diffusion of vesicle outside the focal plane of the microscope. In order to measure the activity we thus decided to investigate the variations of the bright field images in mouse oocyte.

We can compute the difference between region of interest (ROI) of images as a function of time to see how fast the bright field image changes. We can compare the result for wild type (Fig 5.3), Formin Knockout (Fig 5.5) and MyosinVb dominant negative tail (Fig 5.4).

A quantitative measurement of the difference of the images is the autocorrelation of these thought time. The

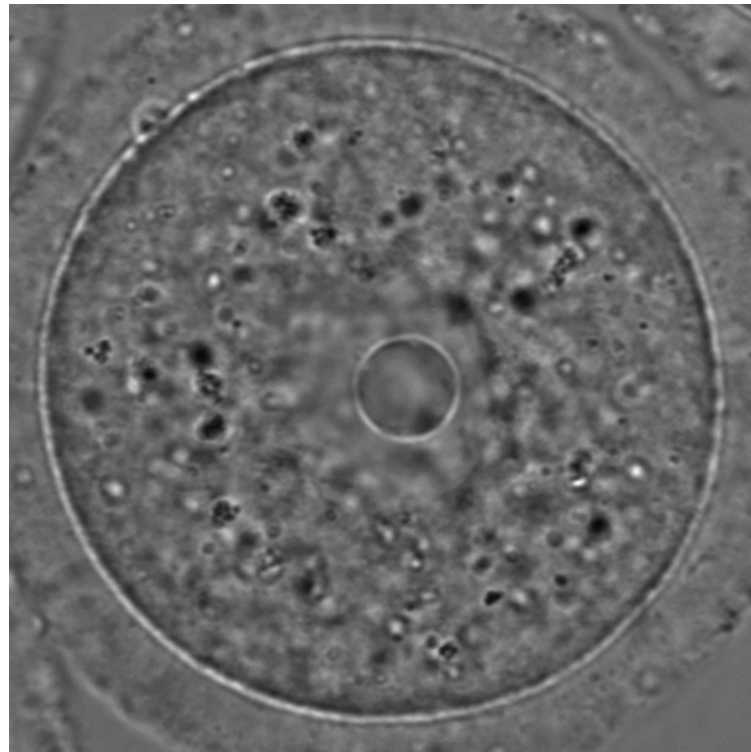


Figure 5.1: Bright field image of a mouse oocyte before meiosis. Cell diameter is of $80\mu\text{m}$. The nucleus can be clearly seen at the center of the cell. The nucleus is positioned at the center of the oocyte during Meiosis I by the help of the actin network. The positioning is a crucial factor for the normal division of the oocyte. Oocytes are a good reference system by their symmetry and their sufficient size that help measuring spatial variation of mechanical properties. Image Credit to Maria Almonacid from Collège de France.

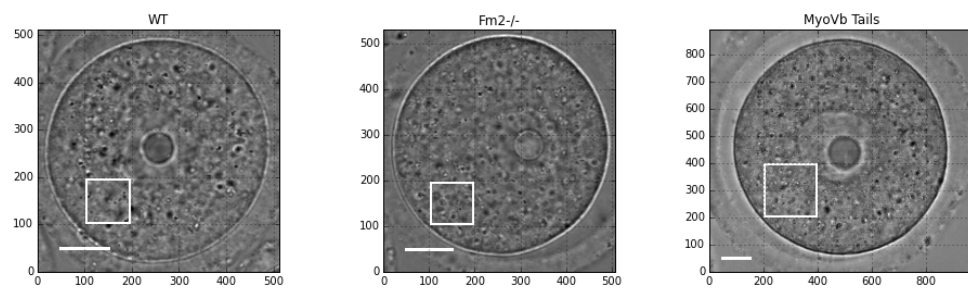


Figure 5.2: Bright field image microscopy of the 3 kinds of oocyte (Credit to Maria Almonacid, Collège de France). WT) Image of Wild Type Oocyte, Scalebar is $20\mu\text{m}$. Fmn2-/-) Oocytes extracted from females with invalidated Formin 2, theses oocytes lack the actin meshwork. MyosinVb Tails) Oocyte injected with a Myosin Vb dominant negative tail have a less actin vesicle population.

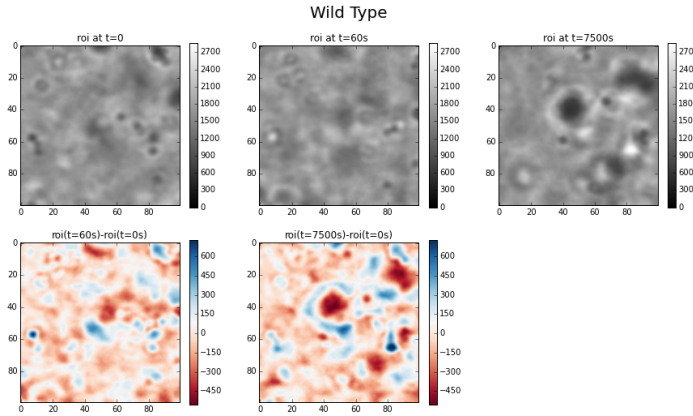


Figure 5.3: Bright field images of Wild type mouse oocyte at $t=0$, $t=1m$ et $t=174m$ as well at the difference between $t=1m$, $t=174m$ and initial image. Blue indicate that the later image is brighter than the original one and red indicate that it is darker. For wild type oocyte, we can see that the scale difference between images is similar for a Δt of 1 minute and 174 minute. Region show is the same as indicated in figure 5.2.

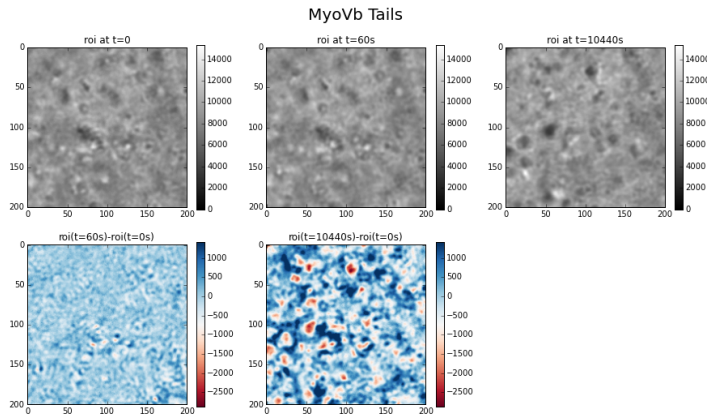


Figure 5.4: Bright field images of MyoVb tails mouse oocyte at $t=0$, $t=1m$ et $t=174m$ as well at the difference between $t=1m$, $t=174m$ and initial image. Blue indicate that the later image is brighter than the original one and red indicate that it is darker. We can see that the difference between images is much stronger after several hours (174min) than after a minute, unlike in Figure 5.3. Region show is the same as indicated in figure 5.2.

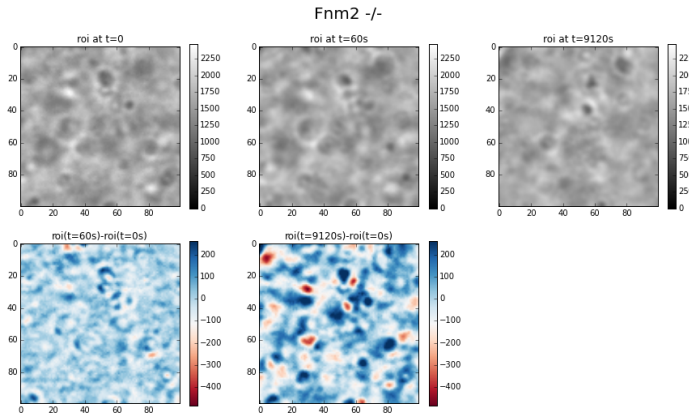


Figure 5.5: Bright field images of *Fmn2*^{-/-} mouse oocyte at $t=0$, $t=1m$ et $t=174m$ as well at the difference between $t=1m$, $t=174m$ and initial image. Blue indicate that the later image is brighter than the original one and red indicate that it is darker. We can see that the difference between images is much stronger after several hours (174min) than after a minute, unlike in [Figure 5.3](#). Region show is the same as indicated in [figure 5.2](#).

correlation of two images x and y of same dimension is defined as :

$$r_{xy} = \frac{\sum_{i=1}^n (x_i - \bar{x})(y_i - \bar{y})}{(n - 1)s_x s_y}$$

In which x_i and y_i are luminosity values of each of the n pixels in \bar{x}, \bar{y} correspond to average values over the images, s_x and s_y are the standard deviation of the luminosity values.

We can compare the decrease of correlation with time depending on the type of oocyte. In order to extract a single value that represent the activity, we can phenomenologically fit the correlation as a function of time with a decaying exponential with an offset :

$$r(t) = (1 - off).e^{(-t/\tau)} + off \quad (5.1)$$

In which t is time, and τ is the characteristic time of correlation decay. The offset off represent the value of the correlation at infinite time to take into account artifact in the chosen region of interest, and defect in the image that will not decorrelate through time.

Example of the result of calculating the correlation through time, and fitting a decaying exponential can be seen on [figure 5.6](#)

We see the value of the characteristic time increases with when we disrupt the actin network or the source of its dynamism by inactivating Myosin Vb. We can then use the inverse of τ as an indicator of activity.

Once we have define the activity of a region of the cytoplasm of the cell, we can repeat the measurement on different area of the cytoplasm, and we can reproduce a map of the activity in the cell as a function of the position ([Fig 5.7](#)).

The measure of the correlation characteristic decay time can also be done on a time sliding widows. This allows for the determination of activity of a particular area of the cytoplasm with time.

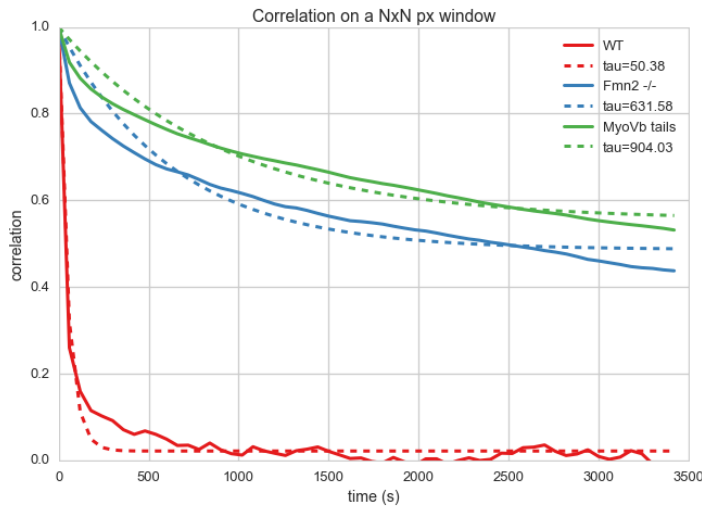


Figure 5.6: Decreasing of autocorrelation off images (solid line) through time, with exponential decay fit (dotted lines) as in (5.1), and value of the characteristic decay time τ as legend. We can see that the correlation of the images decrease much faster in wild type oocyte (red curves, $\tau \sim \text{minute}$) than in Formin knockout (blue lines $\tau > \text{hour}$) that lack the actin meshwork, or than the myosin Vb tails dominant negative (green $\tau > \text{hour}$)

5.4 Conclusion

In this part we developed a methods that allow to determine the cytoplasmic activity. Tis methods also allow to determine the variation of this cytoplasmic activity with space and time. This methods is the study of oocyte as it allows to probe timescale from the second to the hour which is in the order of the relevant timescale for oocyte maturation of a few hours. It is also complementary to techniques like micro rheology that have difficulties probing timescale beyond tens of seconds due to thermal drift and cell movements, but reach much shorter timescale.

The use of this technique is currently under investigation at Collège de France by Marie-Hélène Verhlauc and Maria Almonacid. It is used to measure the activity of actin network in oocyte and determine their effect on the meiosis of mouse oocyte.

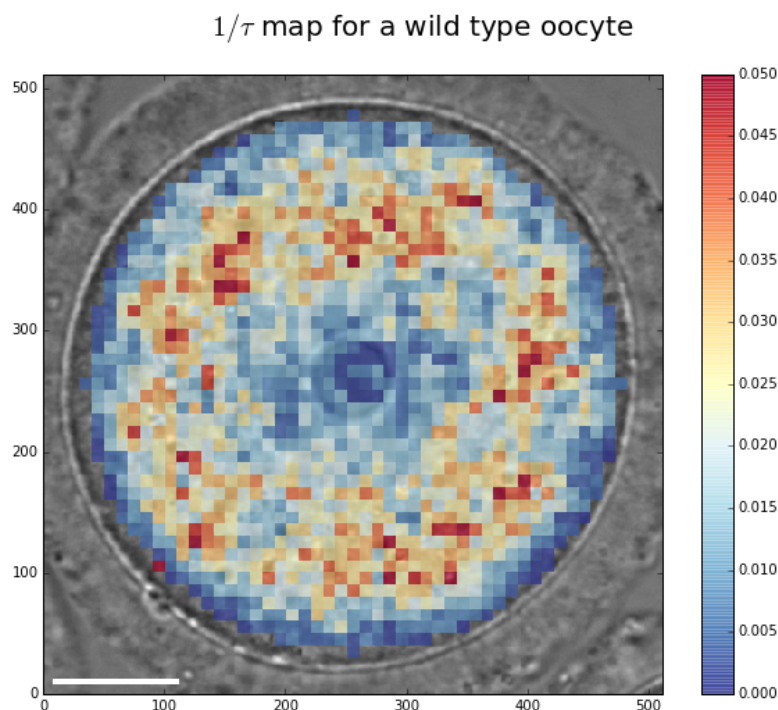


Figure 5.7: Activity for different region of 10 by 10 pixels of a wild type oocyte. Value of $1/\tau$ plotted as color square overlay on to of the analysed bright field image. Example for an of a wild type oocyte. Scale bar is 20 μm . We can see that the activity is near the nucleus is lower (blue) than in the middle of the cytoplasm.

CHAPTER SIX

CONCLUSION

During my PhD I have investigated the mechanics of actin network as found in cells.

In the first part, the reconstitution of biomimetic cortices on polystyrene beads allowed to see that from the thin cortex emanates actin filaments. We determined that the mechanical effect of these actin filament can be perceived 10 to 15 μm from the bead surface well beyond the surface of the reconstituted actin cortex ($\sim 1\mu\text{m}$). The actin cloud formed by these filament appear to be mostly elastic at the time scale of tens of second, and have a elasticity a few pascal, several order of magnitude smaller than the actin gel visible on the surface of the beads. Nonetheless, this actin network appear to be able to sustain forces sufficient to move organelles and seem coherent with several observation made *in-vivo* in cells.

We also studied the properties change of this actin cloud with biochemical condition, and in particular with the concentration of Capping Protein. Using polymer physics, we are able to derive information about the structure of the network, like mesh-size and filaments length. We show that the evolution of the models parameter with the concentration of Capping protein are coherent with previously observed phenomena: The distance offset δ in our model correspond to the measured gels thickness by the position of the half fluorescence maximum.

Our description thus extend the current knowledge of reconstituted actin cortices. It show that beyond a simple dense gels that form on membrane, is a transition to soft structure with highlight different properties. These properties have direct impact on the cells mechanics and could be directly involved in the positioning of organelles in cells.

The mechanical properties of cells and of the actin cortex is not driven only by the dynamics of actin polymerisation. The effect of molecular motors is crucial to understand the change in acto-myosin cortices tension.

In the second part of my PhD I thus focused on the measurement of increase of cortical tension. In order to address the question of evolution of cortical tension with time, we developed a new biomimetic system. This system composed of liposomes doublets allow by 3D imaging and the tracking of geometrical parameter through time to measure the relative increase of the cortex tension with a high time resolution. We also developed an automated methods to measure the geometrical parameters of liposomes doublets to obtain accurate and robust measurement of contact angle independent from experimenter bias. This non invasive measurement methods is a step toward the better understanding of the effect of myosin motors on the cortical tension in cells, and its consequences on cell motility.

The mechanic and dynamic of actin network is decisive for cell fate. In the case of mouse oocytes it is necessary for the correct positioning of different structure of the cells like the mitotic spindle and the nucleus during the meiosis. Without the network formed by actin, or its dynamism due to myosins, the oocyte never achieve complete meiosis leading to non viable cells.

Actin Gels dynamics,

It is on such a system that is based the third part of my PhD. In a collaboration with Collège de France, we used image analysis as a complementary technique to determine the evolution of cytoplasmic activity. In particular we looked at the measure of autocorrelation of bright field images of mouse oocyte. We investigated the change of autocorrelation characteristic decay time with the alteration of protein expression in oocyte and showed that it was strongly dependent on the presence of the actin network and its dynamism due to myosin. The method developed also allow to determine the temporal and spatial change in activity in mouse oocyte actin network. It thus provide a simple methods that hints for change in network dynamics in live cell. This will allow a better understanding of the different phenomenon at the origin of organelles positioning in cells and the role of actin networks.

BIBLIOGRAPHY

- [Alberts, Johnson, Lewis, et al. 2008] B Alberts, A Johnson, J Lewis, M Raff, K Roberts, and P And Walter. *Molecular Biology of the Cell*. volume 54. Garland, 2008. URL: <http://discovery.ucl.ac.uk/109973/>.
- [Angelova, Dimitrov, 1986] Miglena I. Angelova and Dimiter S. Dimitrov. Liposome electroformation. *Faraday Discussions of the Chemical Society*, 81:303, 1986. URL: <http://xlink.rsc.org/?DOI=dc9868100303>, doi:10.1039/dc9868100303.
- [Azoury, Lee, Georget, et al. 2011] Jessica Azoury, Karen Wingman Lee, Virginie Georget, Pascale Hikal, and Marie-Hélène Verlhac. Symmetry breaking in mouse oocytes requires transient F-actin meshwork destabilization.. *Development (Cambridge, England)*, 138(14):2903–8, July 2011. URL: <http://dev.biologists.org/content/138/14/2903.long>, doi:10.1242/dev.060269.
- [BernheimGroswasser, Wiesner, Golsteyn, et al. 2002] Anne Bernheim-Groswasser, Sébastien Wiesner, Roy M. Golsteyn, Marie-France Carlier, and Cécile Sykes. The dynamics of actin-based motility depend on surface parameters. *Nature*, 417(6886):308–311, May 2002. URL: <http://dx.doi.org/10.1038/417308a> <http://www.nature.com/nature/journal/v417/n6886/full/417308a.html>, doi:10.1038/417308a.
- [Berridge, 2012] Michael J. Berridge. Cell Signalling Biology: Module 4 - Sensors and Effectors. 2012. doi:10.1042/csb0001004.
- [Bornschlogl, 2013] Thomas Bornschlogl. How filopodia pull: what we know about the mechanics and dynamics of filopodia.. *Cytoskeleton (Hoboken, N.J.)*, 70(10):590–603, October 2013. URL: <http://www.ncbi.nlm.nih.gov/pubmed/23959922>, doi:10.1002/cm.21130.
- [Buss, KendrickJones, 2008] Folma Buss and John Kendrick-Jones. How are the cellular functions of myosin VI regulated within the cell?. *Biochemical and biophysical research communications*, 369(1):165–175, April 2008. URL: <http://www.sciencedirect.com/science/article/pii/S0006291X07025508>, doi:10.1016/j.bbrc.2007.11.150.
- [Carlier, Laurent, Santolini, et al. 1997] M F Carlier, V Laurent, J Santolini, R Melki, D Didry, G X Xia, Y Hong, N H Chua, and D Pantaloni. Actin depolymerizing factor (ADF/cofilin) enhances the rate of filament turnover: implication in actin-based motility.. *The Journal of cell biology*, 136(6):1307–22, March 1997. URL: <http://www.ncbi.nlm.nih.gov/article/fcgi?artid=2132522&tool=pmcentrez&rendertype=abstract>.
- [Carvalho, Lemiere, Faqir, et al. 2013] Kevin Carvalho, Joël Lemière, Fahima Faqir, John Manzi, Laurent Blanchoin, Julie Plastino, Timo Betz, and Cécile Sykes. Actin polymerization or myosin con-

- traction: two ways to build up cortical tension for symmetry breaking.. *Philosophical transactions of the Royal Society of London. Series B, Biological sciences*, 368(1629):20130005, January 2013. URL: <http://www.ncbi.nlm.nih.gov/pubmed/24062578>, doi:10.1098/rstb.2013.0005.
- [Carvalho, Tsai, Lees, et al. 2013] Kevin Carvalho, Feng-Ching Tsai, Edouard Lees, Raphaël Voituriez, Gijsje H Koenderink, and Cecile Sykes. Cell-sized liposomes reveal how actomyosin cortical tension drives shape change.. *Proceedings of the National Academy of Sciences of the United States of America*, 110(41):16456–61, October 2013. URL: <http://www.pnas.org/content/110/41/16456> <http://www.ncbi.nlm.nih.gov/article/fcgi?artid=3799374&tool=pmcentrez&rendertype=abstract>, doi:10.1073/pnas.1221524110.
- [Chaigne, Campillo, Gov, et al. 2013] Agathe Chaigne, Clément Campillo, Nir S Gov, Raphaël Voituriez, Jessica Azoury, Claudia Umaña-Díaz, María Almonacid, Isabelle Queguiner, Pierre Nassoy, Cécile Sykes, Marie-Hélène Verlhac, and Marie-Emilie Terret. A soft cortex is essential for asymmetric spindle positioning in mouse oocytes.. *Nature cell biology*, 15(8):958–66, August 2013. URL: http://www.nature.com/ncb/journal/v15/n8/fig_tab/ncb2799_F2.html http://www.readcube.com/articles/10.1038/ncb2799?utm_campaign=readcube_access&utm_source=nature.com&utm_medium=referral&utm_content=article_info, doi:10.1038/ncb2799.
- [Charras, Paluch, 2008] Guillaume Charras and Ewa Paluch. Blebs lead the way: how to migrate without lamellipodia.. *Nature reviews. Molecular cell biology*, 9(9):730–6, September 2008. URL: <http://dx.doi.org/10.1038/nrm2453> <http://www.ncbi.nlm.nih.gov/pubmed/18628785>, doi:10.1038/nrm2453.
- [Clark, Dierkes, Paluch, 2013] Andrew G. Clark, Kai Dierkes, and Ewa K. Paluch. Monitoring actin cortex thickness in live cells.. *Biophysical journal*, 105(3):570–80, August 2013. URL: <http://www.ncbi.nlm.nih.gov/pubmed/23931305>, doi:10.1016/j.bpj.2013.05.057.
- [Dabiri, Sanger, Portnoy, Southwick, 1990] G A Dabiri, J M Sanger, D A Portnoy, and F S Southwick. Listeria monocytogenes moves rapidly through the host-cell cytoplasm by inducing directional actin assembly.. *Proceedings of the National Academy of Sciences of the United States of America*, 87(16):6068–72, August 1990. URL: <http://www.ncbi.nlm.nih.gov/article/fcgi?artid=54473&tool=pmcentrez&rendertype=abstract>, doi:10.1073/pnas.87.16.6068.
- [Engler, Sen, Sweeney, Discher, 2006] Adam J. Engler, Shamik Sen, H. Lee Sweeney, and Dennis E. Discher. Matrix elasticity directs stem cell lineage specification.. *Cell*, 126(4):677–89, August 2006. URL: <http://www.ncbi.nlm.nih.gov/pubmed/16923388>, doi:10.1016/j.cell.2006.06.044.
- [Faix, Rottner, 2006] Jan Faix and Clemens Rottner. The making of filopodia.. *Current opinion in cell biology*, 18(1):18–25, February 2006. URL: <http://www.sciencedirect.com/science/article/pii/S095506740500178X>, doi:10.1016/j.ceb.2005.11.002.
- [Feric, Brangwynne, 2013] Marina Feric and Clifford P Brangwynne. A nuclear F-actin scaffold stabilizes ribonucleoprotein droplets against gravity in large cells. *Nature Cell Biology*, 15:1253–1259, 2013. URL: <http://dx.doi.org/10.1038/ncb2830>, doi:10.1038/ncb2830.
- [Fletcher, Mullins, 2010] Daniel A Fletcher and R Dyche Mullins. Cell mechanics and the cytoskeleton.. *Nature*, 463(7280):485–92, January 2010. URL: <http://dx.doi.org/10.1038/nature08908> <http://www.ncbi.nlm.nih.gov/article/fcgi?artid=2851742&tool=pmcentrez&rendertype=abstract>, doi:10.1038/nature08908.

- [Gardel, Valentine, Crocker, et al. 2003] M. L Gardel, M. T Valentine, J. C Crocker, A. R Bausch, and D. A Weitz. Microrheology of entangled F-actin solutions.. *Physical review letters*, 91(15):158302, October 2003. URL: <http://www.ncbi.nlm.nih.gov/pubmed/14611506> <http://link.aps.org/doi/10.1103/PhysRevLett.91.158302>, doi:10.1103/PhysRevLett.91.158302.
- [Goley, Welch, 2006] Erin D Goley and Matthew D Welch. The ARP2/3 complex: an actin nucleator comes of age.. *Nature reviews. Molecular cell biology*, 7(10):713–26, October 2006. URL: <http://dx.doi.org/10.1038/nrm2026>, doi:10.1038/nrm2026.
- [Hartman, Spudich, 2012] M. A. Hartman and J. A. Spudich. The myosin superfamily at a glance. *Journal of Cell Science*, 125(7):1627–1632, May 2012. URL: <http://jcs.biologists.org/content/125/7/1627.full> <http://jcs.biologists.org/cgi/doi/10.1242/jcs.094300>, doi:10.1242/jcs.094300.
- [Helfrich, 1973] W Helfrich. Elastic properties of lipid bilayers: theory and possible experiments.. *Zeitschrift für Naturforschung. Teil C: Biochemie, Biophysik, Biologie, Virologie*, 28(11):693–703, 1973. URL: <http://www.ncbi.nlm.nih.gov/pubmed/4273690>.
- [Holubcova, Howard, Schuh, 2013] Zuzana Holubcová, Gillian Howard, and Melina Schuh. Vesicles modulate an actin network for asymmetric spindle positioning.. *Nature cell biology*, 15(8):937–47, August 2013. URL: <http://www.pubmedcentral.nih.gov/articlerender.fcgi?artid=3797517&tool=pmcentrez&rendertype=abstract>, doi:10.1038/ncb2802.
- [Huelsmann, Ylanne, Brown, 2013] Sven Huelsmann, Jari Ylänne, and Nicholas H Brown. Filopodia-like actin cables position nuclei in association with perinuclear actin in Drosophila nurse cells.. *Developmental cell*, 26(6):604–15, September 2013. URL: <http://www.pubmedcentral.nih.gov/articlerender.fcgi?artid=3791400&tool=pmcentrez&rendertype=abstract>, doi:10.1016/j.devcel.2013.08.014.
- [Isambert, Maggs, 1996] H. Isambert and A. C. Maggs. Dynamics and Rheology of Actin Solutions. *Macromolecules*, 29(3):1036–1040, January 1996. URL: <http://dx.doi.org/10.1021/ma946418x> <http://pubs.acs.org/doi/abs/10.1021/ma946418x> <http://pubs.acs.org/doi/full/10.1021/ma946418x> <http://pubs.acs.org/doi/pdf/10.1021/ma946418x>, doi:10.1021/ma946418x.
- [Isambert, Venier, Maggs, et al. 1995] H. Isambert, P. Venier, A. Maggs, A. Fattoum, R. Kassab, D. Pantaloni, and M. Carlier. Flexibility of actin filaments derived from thermal fluctuations. Effect of bound nucleotide, phalloidin, and muscle regulatory proteins. *Journal of Biological Chemistry*, 270(19):11437–11444, May 1995. URL: <http://www.jbc.org/content/270/19/11437.short>, doi:10.1074/jbc.270.19.11437.
- [Iwabuchi, Takagi, 2010] Kosei Iwabuchi and Shingo Takagi. Actin-based mechanisms for light-dependent intracellular positioning of nuclei and chloroplasts in Arabidopsis.. *Plant signaling & behavior*, 5(8):1010–3, August 2010. URL: <http://www.plantphysiol.org/content/152/3/1309>, doi:10.1104/pp.109.149526.
- [Jaalouk, Lammerding, 2009] Diana E Jaalouk and Jan Lammerding. Mechanotransduction gone awry.. *Nature reviews. Molecular cell biology*, 10(1):63–73, January 2009. URL: <http://www.pubmedcentral.nih.gov/articlerender.fcgi?artid=2668954&tool=pmcentrez&rendertype=abstract>, doi:10.1038/nrm2597.
- [Jahnel, Behrndt, Jannasch, et al. 2011] Marcus Jahnel, Martin Behrndt, Anita Jannasch, Erik Schäffer, and Stephan W. Grill. Measuring the complete force field of an optical trap.

Optics Letters, 36(7):1260–1262, April 2011. URL: <http://ol.osa.org/abstract.cfm?URI=ol-36-7-1260> http://www.opticsinfobase.org/DirectPDFAccess/76D790BC-EEE1-F229-0BB6465895770C07__211408.pdf?da=1&id=211408&seq=0&mobile=no
http://www.opticsinfobase.org/DirectPDFAccess/76F33103-E64B-6A63-1BD7BF1ECC155C__211408.pdf?da=1&id=211408&seq=0&mobile=no
<http://www.opticsinfobase.org/ol/abstract.cfm?URI=ol-36-7-1260>, doi:10.1364/OL.36.001260.

[Kawska, Carvalho, Manzi, et al. 2012] Agnieszka Kawska, Kévin Carvalho, John Manzi, Rajaa Boujemaa-Paterski, Laurent Blanchoin, Jean-Louis Martiel, and Cécile Sykes. How actin network dynamics control the onset of actin-based motility.. *Proceedings of the National Academy of Sciences of the United States of America*, 109(36):14440–5, September 2012. URL: <http://www.pnas.org/content/109/36/14440.short>, doi:10.1073/pnas.1117096109.

[Krieg, ArboledaEstudillo, Puech, et al. 2008] M Krieg, Y Arboleda-Estudillo, P-H Puech, J Käfer, F Graner, D J Müller, and C-P Heisenberg. Tensile forces govern germ-layer organization in zebrafish.. *Nature cell biology*, 10(4):429–36, April 2008. URL: <http://dx.doi.org/10.1038/ncb1705>, doi:10.1038/ncb1705.

[Kruse, Joanny, Julicher, et al. 2005] Karsten Kruse, J F Joanny, Frank Jülicher, J Prost, and K Sekimoto. Generic theory of active polar gels: a paradigm for cytoskeletal dynamics.. *The European physical journal. E, Soft matter*, 16(1):5–16, January 2005. URL: <http://link.springer.com/article/10.1140/epje/e2005-00002-5> <http://www.ncbi.nlm.nih.gov/pubmed/15688136>, doi:10.1140/epje/e2005-00002-5.

[Kunda, Pelling, Liu, Baum, 2008] Patricia Kunda, Andrew E Pelling, Tao Liu, and Buzz Baum. Moesin controls cortical rigidity, cell rounding, and spindle morphogenesis during mitosis.. *Current biology : CB*, 18(2):91–101, January 2008. URL: <http://www.ncbi.nlm.nih.gov/pubmed/18207738>, doi:10.1016/j.cub.2007.12.051.

[Liverpool, 2006] Tanniemola B Liverpool. Active gels: where polymer physics meets cytoskeletal dynamics.. *Philosophical transactions. Series A, Mathematical, physical, and engineering sciences*, 364(1849):3335–55, December 2006. URL: <http://www.ncbi.nlm.nih.gov/pubmed/17090463>, doi:10.1098/rsta.2006.1897.

[Loisel, Boujemaa, Pantaloni, Carlier, 1999] T P Loisel, R Boujemaa, D Pantaloni, and M F Carlier. Reconstruction of actin-based motility of Listeria and Shigella using pure proteins.. *Nature*, 401(6753):613–6, October 1999. URL: <http://www.ncbi.nlm.nih.gov/pubmed/10524632>, doi:10.1038/44183.

[Lenart, Bacher, Daigle, et al. 2005] Péter Lénárt, Christian P Bacher, Nathalie Daigle, Arthur R Hand, Roland Eils, Mark Terasaki, and Jan Ellenberg. A contractile nuclear actin network drives chromosome congression in oocytes.. *Nature*, 436:812–818, 2005. doi:10.1038/nature03810.

[Machesky, Mullins, Higgs, et al. 1999] L. M. Machesky, R. D. Mullins, H. N. Higgs, D. A. Kaiser, L. Blanchoin, R. C. May, M. E. Hall, and T. D. Pollard. Scar, a WASp-related protein, activates nucleation of actin filaments by the Arp2/3 complex. *Proceedings of the National Academy of Sciences*, 96(7):3739–3744, March 1999. URL: <http://www.pnas.org/content/96/7/3739.full>, doi:10.1073/pnas.96.7.3739.

[MacKintosh, Kas, Janmey, 1995] F. MacKintosh, J. Käs, and P. Janmey. Elasticity of Semiflexible Biopolymer Networks. *Physical Review Letters*, 75(24):4425–4428, December 1995. URL: <http://link.aps.org/doi/10.1103/PhysRevLett.75.4425>, doi:10.1103/PhysRevLett.75.4425.

- [Mahaffy, Park, Gerde, et al. 2004] R E Mahaffy, S Park, E Gerde, J Käs, and C K Shih. Quantitative analysis of the viscoelastic properties of thin regions of fibroblasts using atomic force microscopy.. *Biophysical journal*, 86(3):1777–93, March 2004. URL: <http://www.ncbi.nlm.nih.gov/pmc/articles/PMC1304012/>&tool=pmcentrez&rendertype=abstract, doi:10.1016/S0006-3495(04)74245-9.
- [Maitre, Berthoumieux, Krens, et al. 2012] Jean-Léon Maitre, Hélène Berthoumieux, Simon Frederik Gabriel Krens, Guillaume Salbreux, Frank Jülicher, Ewa Paluch, and Carl-Philipp Heisenberg. Adhesion functions in cell sorting by mechanically coupling the cortices of adhering cells.. *Science (New York, N.Y.)*, 338(6104):253–6, October 2012. URL: <http://www.ncbi.nlm.nih.gov/pmc/articles/PMC3386104/> long <http://www.ncbi.nlm.nih.gov/pmc/articles/PMC3386104/> http://www.ncbi.nlm.nih.gov/pmc/articles/PMC3386104/abstract, doi:10.1126/science.1225399.
- [Marcy, Prost, Carlier, Sykes, 2004] Yann Marcy, Jacques Prost, Marie-France Carlier, and Cécile Sykes. Forces generated during actin-based propulsion: a direct measurement by micromanipulation.. *Proceedings of the National Academy of Sciences of the United States of America*, 101(16):5992–7, April 2004. URL: <http://www.ncbi.nlm.nih.gov/pmc/articles/PMC395911/>&tool=pmcentrez&rendertype=abstract, <http://www.ncbi.nlm.nih.gov/pmc/articles/PMC395911/> full <http://www.ncbi.nlm.nih.gov/pmc/articles/PMC395911/> full.pdf <http://www.ncbi.nlm.nih.gov/pmc/articles/PMC395911/>&tool=pmcentrez&rendertype=abstract, doi:10.1073/pnas.0307704101.
- [McCullough, Grintsevich, Chen, et al. 2011] Brannon R. McCullough, Elena E. Grintsevich, Christine K. Chen, Hyeran Kang, Alan L. Hutchison, Arnon Henn, Wenxiang Cao, Cristian Suarez, Jean Louis Martiel, Laurent Blanchoin, Emil Reisler, and Enrique M. De La Cruz. Cofilin-linked changes in actin filament flexibility promote severing. *Biophysical Journal*, 101:151–159, 2011. doi:10.1016/j.bpj.2011.05.049.
- [Mizuno, Tardin, Schmidt, Mackintosh, 2007] Daisuke Mizuno, Catherine Tardin, C. F. Schmidt, and F C Mackintosh. Nonequilibrium mechanics of active cytoskeletal networks.. *Science (New York, N.Y.)*, 315(5810):370–3, January 2007. URL: <http://www.ncbi.nlm.nih.gov/pmc/articles/PMC1723494/>&tool=pmcentrez&rendertype=abstract, <http://www.ncbi.nlm.nih.gov/pmc/articles/PMC1723494/>.short <http://www.ncbi.nlm.nih.gov/pmc/articles/PMC1723494/>, doi:10.1126/science.1134404.
- [Morone, Fujiwara, Murase, et al. 2006] Nobuhiro Morone, Takahiro Fujiwara, Kotono Murase, Rinshi S Kasai, Hiroshi Ike, Shigeki Yuasa, Jiro Usukura, and Akihiro Kusumi. Three-dimensional reconstruction of the membrane skeleton at the plasma membrane interface by electron tomography.. *The Journal of cell biology*, 174(6):851–62, September 2006. URL: <http://www.ncbi.nlm.nih.gov/pmc/articles/PMC1746851/>&tool=pmcentrez&rendertype=abstract, <http://www.ncbi.nlm.nih.gov/pmc/articles/PMC1746851/>.long, doi:10.1083/jcb.200606007.
- [Morse, 1998a] David C Morse. Viscoelasticity of concentrated isotropic solutions of semi-flexible polymers. 2. Linear response. *Macromolecules*, 9297(98):7044–7067, 1998. URL: <http://pubs.acs.org/doi/abs/10.1021/ma980304u>.
- [Morse, 1998b] David C. Morse. Viscoelasticity of Concentrated Isotropic Solutions of Semi-flexible Polymers. 1. Model and Stress Tensor. *Macromolecules*, 31(20):7030–7043, October 1998. URL: <http://pubs.acs.org/doi/abs/10.1021/ma9803032> <http://dx.doi.org/10.1021/ma9803032>, doi:10.1021/ma9803032.
- [Nieminens, Knöner, Heckenberg, RubinszteinDunlop, 2007] Timo Nieminens, A Gregor Knöner, Norman R Heckenberg, and Halina Rubinsztein-Dunlop. Physics

- of optical tweezers.. *Methods in cell biology*, 82:207–36, January 2007. URL: <http://www.sciencedirect.com/science/article/pii/S0091679X06820066>, doi:10.1016/S0091-679X(06)82006-6.
- [Noguera, 2012] Philippe Noguera. *Etude du rôle de la protéine VASP dans la dynamique et la mécanique des réseaux d'actine avec un système biomimétique de la motilité cellulaire*. PhD thesis, Paris 7, September 2012. URL: <http://tel.archives-ouvertes.fr/tel-00834288>.
- [Parekh, Chaudhuri, Theriot, Fletcher, 2005] Sapun H Parekh, Ovijit Chaudhuri, Julie A Theriot, and Daniel A Fletcher. Loading history determines the velocity of actin-network growth.. *Nature cell biology*, 7(12):1219–23, December 2005. URL: <http://www.nature.com/gate1.inist.fr/ncb/journal/v7/n12/full/ncb1336.html> <http://www.ncbi.nlm.nih.gov/pubmed/16299496>, doi:10.1038/ncb1336.
- [Plastino, Sykes, 2005] Julie Plastino and Cécile Sykes. The actin slingshot. *Current Opinion in Cell Biology*, 17(1):62–66, 2005. URL: <http://www.sciencedirect.com/science/article/pii/S0955067404001693>.
- [Pollard, 1986] T D Pollard. Rate constants for the reactions of ATP- and ADP-actin with the ends of actin filaments.. *The Journal of cell biology*, 103(6 Pt 2):2747–54, December 1986. URL: <http://www.ncbi.nlm.nih.gov/article/fcgi?artid=2114620&tool=pmcentrez&rendertype=abstract>, doi:10.1083/jcb.103.6.2747.
- [Pollard, Blanchoin, Mullins, 2000] T D Pollard, L Blanchoin, and R D Mullins. Molecular mechanisms controlling actin filament dynamics in nonmuscle cells.. *Annual review of biophysics and biomolecular structure*, 29:545–76, January 2000. URL: <http://www.ncbi.nlm.nih.gov/pubmed/10940259>, doi:10.1146/annurev.biophys.29.1.545.
- [Pollard, Borisy, 2003] Thomas D. Pollard and Gary G. Borisy. Cellular motility driven by assembly and disassembly of actin filaments.. *Cell*, 112(4):453–65, February 2003. URL: <http://linkinghub.elsevier.com/retrieve/pii/S009286740300120X> <http://www.ncbi.nlm.nih.gov/pubmed/12600310>, doi:10.1016/S0092-8674(03)00120-X.
- [Pontani, vdGucht, Salbreux, et al. 2009] Léa-Laetitia Pontani, Jasper van der Gucht, Guillaume Salbreux, Julien Heuvingh, Jean-François Joanny, and Cécile Sykes. Reconstruction of an Actin Cortex Inside a Liposome. *Biophysical Journal*, 96(1):192–198, January 2009. URL: <http://www.ncbi.nlm.nih.gov/article/B94RW-4VC7NYF-P/2/68db024edc5376193f140b634a1e5111> [http://www.ncbi.nlm.nih.gov/biophysj/abstract/S0006-3495\(08\)00038-6](http://www.ncbi.nlm.nih.gov/biophysj/abstract/S0006-3495(08)00038-6) http://www.ncbi.nlm.nih.gov/science?_ob=ArticleURL&_udi=B94RW-4VC7NYF-P&_user=5323486&_coverDate=01%2F07%2F2009&_rdoc=1&_fmt=high&_orig=gateway&_origin=fulltext&_listType=fullText http://www.ncbi.nlm.nih.gov/science?_ob=MIImg&_i, doi:10.1016/j.bpj.2008.09.029.
- [Pring, Evangelista, Boone, et al. 2003] Martin Pring, Marie Evangelista, Charles Boone, Changsong Yang, and Sally H Zigmund. Mechanism of formin-induced nucleation of actin filaments.. *Biochemistry*, 42(2):486–96, January 2003. URL: <http://dx.doi.org/10.1021/bi026520j>, doi:10.1021/bi026520j.
- [Pruyne, Evangelista, Yang, et al. 2002] David Pruyne, Marie Evangelista, Changsong Yang, Erfei Bi, Sally Zigmund, Anthony Bretscher, and Charles Boone. Role of formins in actin assembly: nucleation and barbed-end association.. *Science (New York, N.Y.)*, 297(5581):612–5, July 2002. URL: <http://www.sciencemag.org/content/297/5581/612.abstract>, doi:10.1126/science.1072309.
- [Pujol, dRoure, Fermigier, Heuvingh, 2012] Thomas Pujol, Olivia du Roure, Marc Fermigier, and Julien Heuvingh. Impact of branching on the elasticity of actin networks.. *Proceedings of the National Academy of Sciences of the United States of America*, 109(35):14173–7, August 2012. URL: <http://www.ncbi.nlm.nih.gov/pmc/articles/PMC3449356/>, doi:10.1073/pnas.1211733109.

- tional Academy of Sciences of the United States of America, 109(26):10364–9, June 2012. URL: <http://www.pnas.org/content/early/2012/06/05/1121238109>, doi:10.1073/pnas.1121238109.
- [Salbreux, Charras, Paluch, 2012] Guillaume Salbreux, Guillaume Charras, and Ewa Paluch. Actin cortex mechanics and cellular morphogenesis.. *Trends in cell biology*, 22(10):536–45, October 2012. URL: <http://www.sciencedirect.com/science/article/pii/S0962892412001110> <http://www.ncbi.nlm.nih.gov/pubmed/22871642>, doi:10.1016/j.tcb.2012.07.001.
- [Sandre, Moreaux, BrochardWyart, 1999] O Sandre, L Moreaux, and F Brochard-Wyart. Dynamics of transient pores in stretched vesicles.. *Proceedings of the National Academy of Sciences of the United States of America*, 96(19):10591–6, September 1999. URL: <http://www.ncbi.nlm.nih.gov/articlerender.fcgi?artid=17927&tool=pmcentrez&rendertype=abstract>.
- [Schafer, 2004] Dorothy A Schafer. Cell biology: barbed ends rule.. *Nature*, 430(7001):734–5, August 2004. URL: <http://www.nature.com.rproxy.sc.univ-paris-diderot.fr/nature/journal/v430/n7001/full/430734a.html>, doi:10.1038/430734a.
- [Schuh, Ellenberg, 2008] Melina Schuh and Jan Ellenberg. A new model for asymmetric spindle positioning in mouse oocytes.. *Current biology : CB*, 18(24):1986–92, December 2008. URL: <http://www.ncbi.nlm.nih.gov/pubmed/19062278>, doi:10.1016/j.cub.2008.11.022.
- [Schwarz, Neuhaus, Kistler, et al. 2000] E C Schwarz, E M Neuhaus, C Kistler, A W Henkel, and T Soldati. Dictyostelium myosin IK is involved in the maintenance of cortical tension and affects motility and phagocytosis.. *Journal of cell science*, 113 (Pt 4):621–33, February 2000. URL: <http://www.ncbi.nlm.nih.gov/pubmed/10652255>.
- [Seljebotn, 2009] Dag Sverre Seljebotn. Proceedings of the Python in Science Conference (SciPy): Fast numerical computations with Cython. 2009. URL: http://conference.scipy.org/proceedings/SciPy2009/paper_2/.
- [Semmrich, Larsen, Bausch, 2008] Christine Semmrich, Ryan J. Larsen, and Andreas R. Bausch. Nonlinear mechanics of entangled F-actin solutions. *Soft Matter*, 4(8):1675, 2008. URL: <http://xlink.rsc.org/?DOI=b800989a>, doi:10.1039/b800989a.
- [Soeno, Abe, Kimura, et al. 1998] Y Soeno, H Abe, S Kimura, K Maruyama, and T Obinata. Generation of functional beta-actinin (CapZ) in an *E. coli* expression system.. *Journal of muscle research and cell motility*, 19(6):639–46, August 1998. URL: <http://www.ncbi.nlm.nih.gov/pubmed/9742448>.
- [Stewart, Helenius, Toyoda, et al. 2011] Martin P Stewart, Jonne Helenius, Yusuke Toyoda, Subramanian P Ramanathan, Daniel J Muller, and Anthony A Hyman. Hydrostatic pressure and the actomyosin cortex drive mitotic cell rounding.. *Nature*, 469(7329):226–30, January 2011. URL: <http://dx.doi.org/10.1038/nature09642> <http://www.ncbi.nlm.nih.gov/pubmed/21196934>, doi:10.1038/nature09642.
- [Sturmer, Baumann, Walz, 1995] K Stürmer, O Baumann, and B Walz. Actin-dependent light-induced translocation of mitochondria and ER cisternae in the photoreceptor cells of the locust *Schistocerca gregaria*.. *Journal of cell science*, 108 (Pt 6):2273–2283, 1995.
- [Thoumine, Ott, 1997] O Thoumine and A Ott. Time scale dependent viscoelastic and contractile regimes in fibroblasts probed by microplate manipulation.. *Journal of cell science*, 110 (Pt 1):2109–16, September 1997. URL: <http://www.ncbi.nlm.nih.gov/pubmed/9378761>.
- [Tinevez, Schulze, Salbreux, et al. 2009] Jean-Yves Tinevez, Ulrike Schulze, Guillaume Salbreux, Julia Roensch, Jean-Francois Joanny, and Ewa Paluch. Role of cortical tension in bleb growth. *Proceedings*

- of the National Academy of Sciences of the United States of America*, 106(44):18581–18586, November 2009. URL: <http://www.ncbi.nlm.nih.gov/pmc/articles/PMC2765453/> <http://www.ncbi.nlm.nih.gov/pmc/articles/PMC2765453/pdf/zpq04409018581.pdf>, doi:10.1073/pnas.0903353106.
- [Valiron, Caudron, Job, 2001] O. Valiron, N. Caudron, and D. Job. Microtubule dynamics. *Cellular and Molecular Life Sciences*, 58(14):2069–2084, December 2001. URL: <http://link.springer.com/10.1007/PL00000837>, doi:10.1007/PL00000837.
- [vdGucht, Paluch, Plastino, Sykes, 2005] Jasper van der Gucht, Ewa Paluch, Julie Plastino, and Cécile Sykes. Stress release drives symmetry breaking for actin-based movement. *Proceedings of the National Academy of Sciences of the United States of America*, 102(22):7847 –7852, May 2005. URL: <http://www.pnas.org/content/102/22/7847.abstract> <http://www.pnas.org/content/102/22/7847.full.pdf> <http://www.pnas.org/content/102/22/7847.short>, doi:10.1073/pnas.0502121102.
- [Vasilev, Chun, Gragnaniello, et al. 2012] Filip Vasilev, Jong T. Chun, Giovanni Gragnaniello, Ezio Garante, and Luigia Santella. Effects of ionomycin on egg activation and early development in starfish.. *PloS one*, 7(6):e39231, January 2012. URL: <http://www.pubmedcentral.nih.gov/articlerender.fcgi?artid=3377674&tool=pmcentrez&rendertype=abstract>, doi:10.1371/journal.pone.0039231.
- [Vermeulen, vMameren, Stienen, et al. 2006] Karen C Vermeulen, Joost van Mameren, Ger J. M Stienen, Erwin J. G Peterman, Gijs J. L Wuite, and Christoph F Schmidt. Calibrating bead displacements in optical tweezers using acousto-optic deflectors. *Review of Scientific Instruments*, 77(1):013704, January 2006. URL: http://rsi.aip.org/resource/1/rsinak/v77/i1/p013704_s1?isAuthorized=no <http://scitation.aip.org/content/aip/journal/rsi/77/1/10.1063/1.2165568>, doi:10.1063/1.2165568.
- [Yao, Becker, Broedersz, et al. 2011] Norman Y Yao, Daniel J Becker, Chase P Broedersz, Martin Depken, Frederick C Mackintosh, Martin R Pollak, and David A Weitz. Nonlinear viscoelasticity of actin transiently cross-linked with mutant α -actinin-4.. *Journal of molecular biology*, 411(5):1062–71, September 2011. URL: <http://www.sciencedirect.com/science/article/pii/S0022283611007376>, doi:10.1016/j.jmb.2011.06.049.
- [Yarmola, Bubb, 2009] Elena G Yarmola and Michael R Bubb. How depolymerization can promote polymerization: the case of actin and profilin.. *BioEssays : news and reviews in molecular, cellular and developmental biology*, 31(11):1150–60, November 2009. URL: <http://www.ncbi.nlm.nih.gov/pubmed/19795407>, doi:10.1002/bies.200900049.
- [AbuShah, Keren, 2014] E. Abu Shah and K. Keren. Symmetry breaking in reconstituted actin cortices. *eLife*, 3:e01433–e01433, April 2014. URL: <http://elifesciences.org/content/3/e01433.abstract>, doi:10.7554/eLife.01433.
- [DosRemedios, Chhabra, Kekic, et al. 2003] C G Dos Remedios, D Chhabra, M Kekic, I V Dedova, M Tsubakihara, D A Berry, and N J Nosworthy. Actin binding proteins: regulation of cytoskeletal microfilaments.. *Physiological reviews*, 83(2):433–73, April 2003. URL: <http://www.ncbi.nlm.nih.gov/pubmed/12663865>, doi:10.1152/physrev.00026.2002.
- [SoareseSilva, Depken, Stuhrmann, et al. 2011] Marina Soares e Silva, Martin Depken, Björn Stuhrmann, Marijn Korsten, Fred C MacKintosh, and Gijsje H Koenderink. Active multistage coarsening of actin networks driven by myosin motors.. *Proceedings of the National Academy of Sciences of the United States of America*, 108(23):9408–13, June 2011. URL: <http://www.pnas.org/content/108/23/9408>, doi:10.1073/pnas.1016616108.